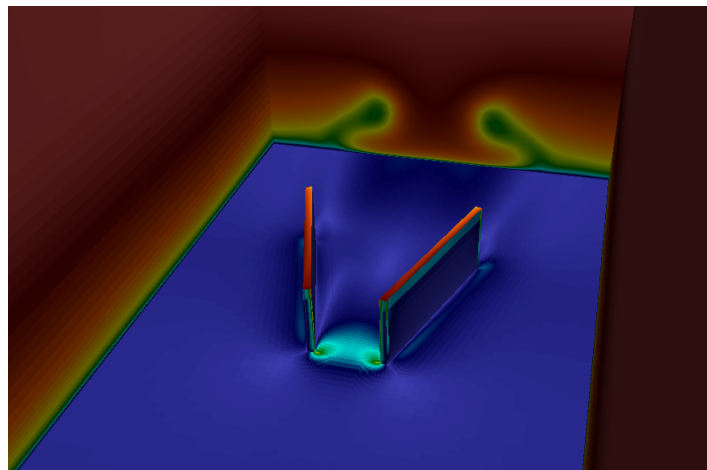


Master of Science Thesis

Implementation and Analysis of a Semi-Empirical Vortex Generator Model in OpenFOAM

Ana Sofia Moreira Ribeiro

January 26, 2017



Implementation and Analysis of a Semi-Empirical Vortex Generator Model in OpenFOAM

Master of Science Thesis

For obtaining the degree of Master of Science in Aerospace Engineering
at Delft University of Technology

Ana Sofia Moreira Ribeiro

January 26, 2017



Delft University of Technology

Copyright © Aerospace Engineering, Delft University of Technology
All rights reserved.

DELFT UNIVERSITY OF TECHNOLOGY
DEPARTMENT OF AERODYNAMICS

The undersigned hereby certify that they have read and recommend to the Faculty of Aerospace Engineering for acceptance the thesis entitled “**Implementation and Analysis of a Semi-Empirical Vortex Generator Model in OpenFOAM**” by **Ana Sofia Moreira Ribeiro** in fulfillment of the requirements for the degree of **Master of Science**.

Dated: January 26, 2017

Supervisors:

Dr. ir. S. J. Hulshoff

Ir. L. Florentie

Dr. ir. B. W. Oudheusden

Dr. ir. A. H. van Zuijlen

Dr. ir. C. J. Simao Ferreira

Abstract

Passive vortex generators (VGs) are small plate-devices that are placed on the top of wings, in an array configuration, in order to delay or event prevent stall. Due to their small size, when compared to the wing, a highly refined mesh is required to accurately simulate the flow behaviour downstream the VG location. As a consequence, the computational time required for a high fidelity 3D computational simulations is very large. In recent years, there have been efforts to create models that allow the computation of the VGs effect without grid them. Reducing this way the computational effort.

During this thesis a semi-empirical model, the Wendt model, was implemented in OpenFOAM and later analysed and compared with gridded VG simulations. The Wendt model is used to predict the vortex circulation and peak vorticity. These entities are then used to calculate the vortex velocity profile at a certain position downstream the VG location. In this projects besides the predictive capabilities of the model, it was tested the hypothesis that to mimic the flow behaviour of a gridded VG simulation, it is enough to impose a vortex velocity profile at a certain position downstream the VG location.

It was seen that the Wendt model is able to predict reasonably well peak vorticity and circulation on the tested parameter range, but for higher values of freestream velocities and lower values of height-to-boundary-layer-thickness-ratio and \mathcal{R} . Furthermore it was seen that, although the implemented model produce inconsistent flow results, the implementation made can be used for that propose. With the correct vortex circulation, peak vorticity and vortex position inputs, it is possible to mimic the correct vortex development as well as the correct flow behaviour, but only far from the VG location, where the influence of the vanes in the streamwise velocity is no longer relevant.

Acknowledgements

First of all, I would like to thank my parents for all the sacrifices they do for me, for making my education their priority, for all the trust, support and love. My mom for always being there and my dad for being my guide.

Secondly I would like to thank my supervisors. To ir. Liesbeth Florentie for always being ready to help me, for all the patience and for pushing forward the work. To Dr.ir. Steve Hulshoff for transmitting all his enthusiasm and knowledge and for the most helpful feedback I could ask.

I would also like to thank to my fellow colleagues with whom I shared many hours of hard work but more importantly, many hours of happiness. In special to Rajat Habbare, Jordi Casacuberta, Delphine De Tavernier and Sebastien Callens.

Furthermore I would like to express my deeply gratitude to my friends. Those I growth with, those who shaped me, those who were, are, and will always be there, those who make my world a happier place: Ruben Costa, Rafael Esteves, Joana Martins, Melodie Carvalho, Sofia Barros, Laura Almeida, Ines Ribeiro, Rita Neves and Emanuel Ferreira. And to Marta Verdugo and Miguel Dias who are brothers to me.

Last, but not least, I would like to thank my family, for the unconditional support, love and companion. But also, very surprisingly to my brother, the person I missed most.

Delft, The Netherlands
January 26, 2017

Ana Sofia Ribeiro

Table of Contents

Abstract	v
Acknowledgements	vii
List of Figures	xiii
List of Tables	xvii
Nomenclature	xix
I Introduction	1
1 Introduction	3
1.1 Passive Vortex Generators	3
1.2 Vortex Generators Models	4
1.3 Flow Parameters under Analysis	5
1.4 Research Questions	6
1.5 Associated Goals	7
1.6 Layout	8

II Existing Semi-Empirical Models	9
2 Semi-Empirical Models	11
2.1 Wendt Model	12
2.1.1 Parametric Study	12
2.1.2 Circulation	13
2.1.3 Peak Vorticity	13
2.2 Bray Model	15
2.2.1 Parametric Study	15
2.2.2 Circulation	17
2.2.3 Peak Vorticity	17
2.3 May Model	18
3 Possible Implementations of Semi-Empirical Models in FNS Solvers	19
3.1 Dudek Implementation	20
3.2 May Implementation	20
III Semi-Empirical Model Implementation	21
4 Comparison Between Wendt and Bray Models	23
5 Wendt Model Implementation	31
5.1 Implementation Procedure	31
5.2 Verification Procedure	35
IV Analysis of the Wendt Model	39
6 Analysis of the Wendt Model	41
6.1 Test Cases	41

6.1.1	Computational Strategy	42
6.1.2	Mesh Details	43
6.2	Comparison between the Wendt Model and the Gridded VG Simulations	48
6.2.1	Case 1	48
6.2.2	Case 2	52
6.2.3	Case 3	55
6.3	Effect of the Mirror Vortices	58
7 Model Behaviour with Calibrated Inputs		63
7.1	Vortex Circulation and Peak Vorticity Calibration	63
7.2	Vortex Position Calibration	69
7.3	Peak Vorticity Estimation	70
V Conclusion		71
8 Conclusion		73
8.1	Conclusions	73
8.2	Recommendations	75
Bibliography		77
A Wendt Parametric Study Results		79
B Bray Parametric Study Results		81
C Implementation of Empirical Models with Source Term		85
D Induced Velocities Code		87
E myFixedJump Boundary Condition Code		93
E.1	<i>myJumpCyclic</i> Main	93
E.2	<i>myFixedJump</i> Main	95

List of Figures

1.1	Counter-rotating common-flow-down configuration, [Stillfried et al. (2010)]	4
1.2	Co-rotating configuration, [Stillfried et al. (2010)]	4
1.3	Vortex Generator Models	5
2.1	Definition of the coordinate system. Modified image from Törnblom and Johansson (2007).	11
2.2	Velocity ratio definition, [Wendt (2001)].	14
4.1	Circulation with varying VG angle of attack	26
4.2	Peak vorticity with varying VG angle of attack.	26
4.3	Circulation with varying freestream velocity.	26
4.4	Peak vorticity with varying freestream velocity.	26
4.5	Circulation with varying VG aspect ratio. $\frac{h}{\delta} = 0.29$	27
4.6	Peak vorticity with varying VG aspect ratio. $\frac{h}{\delta} = 0.29$	27
4.7	Circulation with varying VG aspect ratio. $\frac{h}{\delta} = 0.57$	27
4.8	Peak vorticity with varying VG aspect ratio. $\frac{h}{\delta} = 0.57$	27
4.9	Circulation with varying VG aspect ratio. $\frac{h}{\delta} = 0.86$	27
4.10	Peak vorticity with varying VG aspect ratio. $\frac{h}{\delta} = 0.86$	27
4.11	Circulation with varying VG aspect ratio. $\frac{h}{\delta} = 1.14$	28
4.12	Peak vorticity with varying VG aspect ratio. $\frac{h}{\delta} = 1.14$	28

4.13	Circulation with varying h/δ . $\mathcal{R} = 0.64$	28
4.14	Peak vorticity with varying h/δ . $\mathcal{R} = 0.64$	28
4.15	Circulation with varying h/δ . $\mathcal{R} = 1.53$	28
4.16	Peak vorticity with varying h/δ . $\mathcal{R} = 1.53$	28
4.17	Circulation with varying h/δ . $\mathcal{R} = 3.06$	29
4.18	Peak vorticity with varying h/δ . $\mathcal{R} = 3.06$	29
4.19	Circulation with VG angle of attack. $\frac{h}{\delta} = 1.639$, $\frac{\Delta x}{c} = 1.176$	30
4.20	Circulation with VG angle of attack. $\frac{h}{\delta} = 1.277$, $\frac{\Delta x}{c} = 1.509$	30
5.1	Flow chart of induced velocities code	32
5.2	Vortex array with N real and mirror images and with cell i . Modified imaged from von Stillfried (2012).	33
5.3	Simplified OpenFOAM class diagram	33
5.4	Example of velocity boundary condition file with vortex imposed on the patch "vortex_left"	34
5.5	Fine computational grid behind the VG used in the gridded VG and Wendt model simulations performed by Dudek (2006).	35
5.6	Fine computational grid used in the pipe flow simulation.	36
5.7	Peak vorticity comparison between Dudek implementation, author implementation and experimental results	36
5.8	Dudek velocity contours (top) compared with writer velocity contours (bottom) at different streamwise stations.	37
6.1	Bottom view of a coarse mesh with gridded VG.	43
6.2	Front view of a coarse mesh downstream the VG position.	43
6.3	Mesh study case 1, gridded VG: Circulation with streamwise position.	44
6.4	Mesh study case 1, gridded VG: Peak vorticity with streamwise position.	44
6.5	Mesh study case 1, gridded VG: Shape factor at $d = \Delta x/c = 1, 3, 5, 10, 15$	45
6.6	Mesh study case 1, Wendt model: Circulation with streamwise position.	45
6.7	Mesh study case 1, Wendt model: Peak vorticity with streamwise position.	45

6.8	Mesh study case 1, Wendt VG: Shape factor at $d = \Delta x/c = 1, 3, 5, 10, 15$	46
6.9	Mesh study case 3, Wendt model: Circulation with streamwise position.	47
6.10	Mesh study case 3, Wendt model: Peak vorticity with streamwise position.	47
6.11	Mesh study case 3, Wendt model: Shape factor at $d = \Delta x/c = 1, 3, 5, 10, 15$	47
6.12	Case 1: Vortex circulation with streamwise position.	49
6.13	Case 1: Peak vorticity with streamwise position.	49
6.14	Case 1: Vortex radius with streamwise position.	49
6.15	Case 1: Vorticity field, $\omega_x U_\infty/h$, at $d = \Delta x/c = 1, 3, 5, 10, 15$. On the top the gridded VG vorticity, on the bottom the Wendt model vorticity.	50
6.16	Case 1: U_x/U_∞ contour at $d = \Delta x/c = 1, 3, 5, 10, 15$. On the top the gridded VG velocity field, on the bottom the Wendt model velocity field.	51
6.17	Case 1: Shape factor at $d = \Delta x/c = 1, 3, 5, 10, 15$	52
6.18	Case 2: Vortex circulation with streamwise position.	53
6.19	Case 2: Peak vorticity with streamwise position.	53
6.20	Case 2: Vortex radius with streamwise position.	54
6.21	Case 2: Vorticity field, $\omega_x U_\infty/h$, at $d = \Delta x/c = 1, 3, 5, 10, 15$. On the top the gridded VG vorticity, on the bottom the Wendt model vorticity.	54
6.22	Case 2: Streamwise velocity field, $\frac{U_x}{U_\infty}$, at $d = \Delta x/c = 1, 3, 5, 10, 15$. On the top the gridded VG vorticity, on the bottom the Wendt model vorticity.	55
6.23	Case 2: Shape factor at $\Delta x/c = 1, 3, 5, 10, 15$	55
6.24	Case 3: Circulation with streamwise position.	56
6.25	Case 3: Peak vorticity with streamwise position.	56
6.26	Case 3: Vortex radius with streamwise position.	56
6.27	Case 3: Vorticity field, $\omega_x U_\infty/h$, at $d = \Delta x/c = 1, 3, 5, 10, 15$. On the top the gridded VG vorticity, on the bottom the Wendt model vorticity.	57
6.28	Case 3: Shape factor at $d = \Delta x/c = 1, 3, 5, 10, 15$	57
6.29	Schematic representation of the real and mirror vortices.	58
6.30	Case 1: $\frac{U_z}{U_\infty}$ profiles with(out) mirror at $d = \Delta x/c = 1, 3, 5, 10, 15$, starting at the top, and $y = 0mm, 3mm, 5mm, 10mm$	59

6.31	Case 3: $\frac{U_y}{U_\infty}$ profiles with(out) mirror at $d = \Delta x/c = 1, 3, 5, 10, 15$, starting at the top, and $y = 0mm, 3mm, 5mm, 10mm$	59
6.32	Case 1: $\frac{U_z}{U_\infty}$ profiles with(out) mirror at $d = \Delta x/c = 1, 3, 5, 10, 15$ and $y = 0mm, 3mm, 5mm, 10mm$	60
6.33	Case 3: $\frac{U_z}{U_\infty}$ profiles with(out) mirror at $d = \Delta x/c = 1, 3, 5, 10, 15$ and $y = 0mm, 3mm, 5mm, 10mm$	60
6.34	Case 1: Circulation with(out) mirror vortices.	61
6.35	Case 3: Circulation with(out) mirror vortices.	61
6.36	Case 1: Peak vorticity with(out) mirror vortices.	61
6.37	Case 3: Peak vorticity with(out) mirror vortices.	61
6.38	Case 1: Shape factor with(out) mirror vortices. $d = \Delta x/c = 1, 3, 5, 10, 15$	62
6.39	Case 3: Shape factor with(out) mirror vortices. $d = \Delta x/c = 1, 3, 5, 10, 15$	62
7.1	Case 1 calibrated: Vortex circulation with streamwise position.	64
7.2	Case 3 calibrated: Vortex circulation with streamwise position.	64
7.3	Case 1 calibrated: Vortex peak vorticity with streamwise position zoomed in.	64
7.4	Case 3 calibrated: Vortex peak vorticity with streamwise position zoomed in.	64
7.5	Case 1 calibrated: Radius with streamwise position.	64
7.6	Case 3 calibrated: Radius with streamwise position.	64
7.7	Case 1 calibrated: Vorticity field, $\omega_x U_\infty/h$, at $d = \Delta x/c = 1, 3, 5, 10, 15$	65
7.8	Case 3 calibrated: Vorticity field, $\omega_x U_\infty/h$, at $d = \Delta x/c = 1, 3, 5, 10, 15$	66
7.9	Case 1 calibrated: Shape factor at $d = \Delta x/c = 1, 3, 5, 10, 15$	66
7.10	Case 3 calibrated: Shape factor at $d = \Delta x/c = 1, 3, 5, 10, 15$	67

List of Tables

2.1	Parameter range used during Wendt (2001) experiments.	12
2.2	Wendt model coefficients.	13
2.3	Parameter range used during Bray (1998) low speed experimental campaign.	16
2.4	Parameters range used during Bray (1998) high speed experimental campaign.	16
2.5	Constants for equation 2.25, from Bray (1998)	18
4.1	Input parameters to compare with Wendt experiment.	24
4.2	Input parameters to the comparison between models using the low speed experimental campaign done by Bray (1998)	29
6.1	Flow characteristics and VG geometry details.	42
6.2	Case 1: Mesh details of the gridded VG simulations and VG model simulations.	44
6.3	Case 3: Mesh details of the gridded VG simulations and Wendt model simulations.	47
6.4	Case 1: Error Analysis.	48
6.5	Case 2: Error Analysis.	53
6.6	Case 3: Error Analysis.	56
7.1	Case 1 calibrated: Error Analysis.	67
7.2	Case 3 calibrated: Error Analysis.	67
A.1	Results from Wendt (2001) parametric study for isolated VGs and VGs tested in full counter-rotating arrays.[Wendt (2001)]	80

- B.1 Low-mach number study results from Bray (1998) parametric study. [Bray (1998)] 83
- B.2 High-mach number study results from Bray (1998) parametric study. [Bray (1998)] 83

Nomenclature

Abbreviations

<i>CF</i>	Characteristic force
<i>CMA</i>	Characteristic moment arm
<i>FNS</i>	Full Navier-Stokes solver
<i>PNS</i>	Parabolized Navier-Stokes solver
CFD	Computational Fluid Dynamics
RANS	Reynolds Averaged Navier Stokes
VG	Vortex generator

Coefficients

C_L	Lift coefficient
C_P	Pressure Coefficient

Greek Symbols

α	Vortex generator angle of attack
χ	Eddy viscosity ratio
δ	Boundary layer thickness
δ^*	Boundary layer displacement thickness
Γ	Vortex circulation
ν	Fluid kinetic viscosity
ω	Vorticity field
ω_{max}	Vortex peak vorticity
ρ	Fluid density
θ	Boundary layer momentum thickness

Latin Symbols

c	Vortex generator chord
D	Distance between vanes
G	Vortex angular momentum
H	Boundary layer shape factor

h	Vortex generator height
L	Trailing edge vortex generator location
l	Flat plate length
Ma	Mach number
R	Vortex radius
Re	Reynolds number
t	Time
u, v, w	Streamwise, horizontal and vertical vortex velocity components
U_x, U_y, U_z	Velocity in streamwise, horizontal and vertical components
x, y, z	Streamwise, horizontal and vertical coordinates

Constants

τ	Prandtl constant
ζ	Velocity ratio in vortex peak vorticity expression in the Wendt model
k_1, k_2, k_3, k_4	Velocity ratio in vortex circulation expression in the Wendt model
k_α, k_M, k_a, k_e	Velocity ratio in vortex peak vorticity expression in the Bray model

Miscellaneous

\mathcal{R}	Vortex generator aspect ratio
U_∞	Freestream velocity
v_x, v_r, v_θ	Streamwise, radial and azimuthal velocity components
x, r, θ	Streamwise, radial and azimuthal coordinates

Part I

Introduction

Chapter 1

Introduction

Passive vortex generators (VGs) are small plate-devices that are located on the top of wings, in an array configuration, in order to delay or event prevent stall. Due to their easy implementation and low cost, they can be seen nowadays in many systems as aircraft engine inlets, aircraft/car wings, wind turbines blades, etc.

The interaction between VGs and the boundary layer is a complex process that must be studied so that VG designs keep improving. However, because the VG vanes are very small, when compared with the surface were these are placed, a highly refined mesh is required in high fidelity 3D computational simulations in order to correctly simulate the effect of the VG on the flow. The necessary time for this type of simulations is therefore very high.

In recent years there have been efforts to create models that allow the computation of VGs without grid them. As a consequence, the mesh size is reduced and so is the computational effort.

1.1 Passive Vortex Generators

The lift on a wing arises from a pressure difference between its top and bottom parts. At the wing tip, where this difference is no longer physically sustained, the fluid will tend to go from the high-pressure zone (bottom) to the low-pressure zone (top). This fluid motion, together with the flow velocity in streamwise direction, induces a vortex at the wing tip.

The same principle applies to passive vortex generators. In figure 1.1 is seen that the vortex generators are small and thin wing-like devices that are placed along the top part of the wing/blade span. The vortex shed by each vane is able to mix the different boundary layer regions: the high-momentum particles, located in the upper part of the boundary layer, will be mixed with low-momentum particles (located in the lower part of the boundary layer). As a consequence of this mixing the lower part of the boundary layer will be energized (low-momentum particles will gain velocity). Particles with higher momentum are able to withstand higher adverse pressure gradient without detach from the surface. And so the fluid

will remain longer attached to the wing surface.

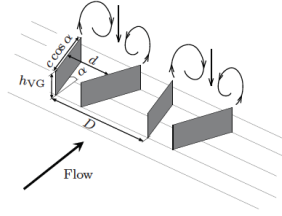


Figure 1.1: Counter-rotating common-flow-down configuration, [Stillfried et al. (2010)]

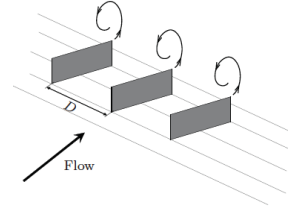


Figure 1.2: Co-rotating configuration, [Stillfried et al. (2010)]

There are two different configurations of passive vortex generators arrays, co-rotating (figure 1.2) and counter-rotating VGs (figure 1.1).

In the co-rotating VGs all the vanes align with each other and each shed vortex has the same orientation. The influence of neighbour vortices on co-rotating arrays is small. On a certain vortex core, the velocity induced by the left vortex will be cancelled with the velocity induced by the right vortex. The exception being, the outer vortices: one will be pushed towards the wall, while the other will be pushed upwards, depending on the vortices orientation [Bray (1998)]. Due to the small influence of neighbour vortices the main decay mechanism is the wall friction.

In the counter-rotating arrays, near the vane, where the influence of the neighbour vortices is small, the main decay mechanism will be the wall friction. Far from the vane, the vortices will tend to pair-up and together lift away from the wall, [Lögberg et al. (2009)]. At this point, due to the large influence of the neighbour vortex, the vorticity will suffer a sudden decay.

1.2 Vortex Generators Models

Ideally, the geometry of the VGs would be introduced in the CFD (computational fluid dynamics) simulations. This however requires the vanes to be gridded, and by that, the number of cells will increase significantly. In order to reduce the mesh size of these computations, some VG models were created. One can identify two large groups of VGs models, see figure 1.3.

The *source term models* aim to mimic the side force produced by the VG vanes. If one introduces this force in the momentum equations - in a volume similar to that of the VG vane - then, the resultant flow will roll-up and a vortex will be created downstream the vane location. [Bender et al. (1999), Jirasek (2005), Fernandez (2013)].

On the other hand, instead of the side force, one can model the *vortex profile*, by either mimicking the vortex vorticity or, more recently, mimicking the Reynolds stresses produced by the vortex.

The vortex vorticity can be calculated by theoretical means as Kunik (1986) and Prandtl (lifting line theory) derived, or by semi-empirical means as Wendt (2001) and Bray (1998) did.

The vortex velocity can then be calculated and added as a velocity-jump-boundary-condition [Dudek (2006)] or as source-term in the momentum equations [May (2001)]. Furthermore Törnblom and Johansson (2007) developed a model in which the Reynolds stresses produced by the vortex are introduced in the Reynolds stress transport equation. This approach is however restricted to 2D simulations.

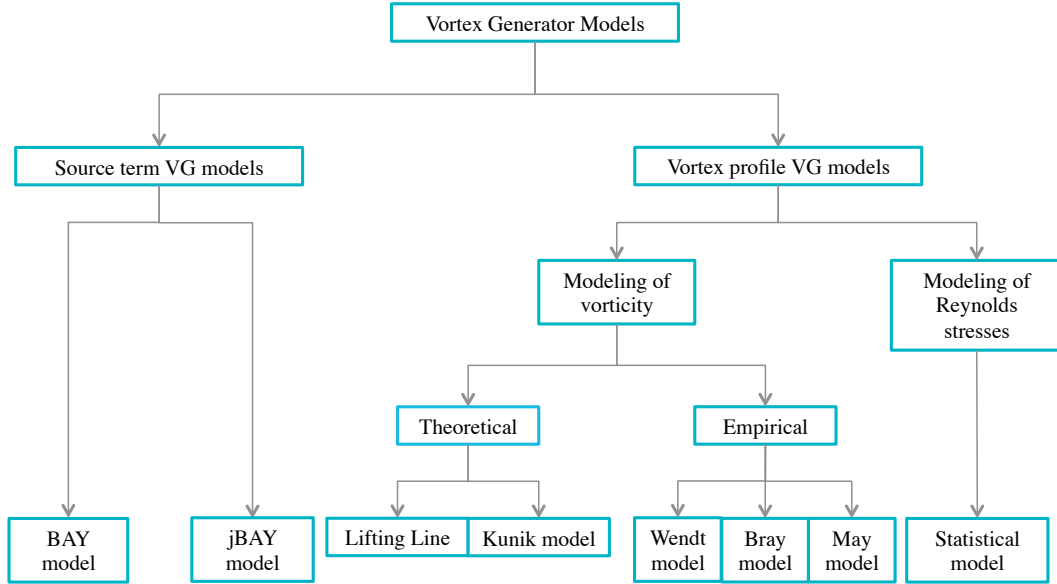


Figure 1.3: Vortex Generator Models

1.3 Flow Parameters under Analysis

Let us now understand which are the most relevant parameters to quantify the flow behaviour of a problem with VGs. An accurate model is the one that at the same time that reduces the computational effort, it is able to mimic the velocity field existing in the gridded VG simulation. Therefore it is imperative to compare the model velocity field with the one from the gridded VG simulations. Due to the spinning motion of the flow due to the vortices, it is more natural to study the velocity rotational around the streamwise axis, calculated as

$$\vec{\omega}_x = \left(\frac{\partial \vec{u}}{\partial x} - \frac{\partial \vec{v}}{\partial y} \right), \quad (1.1)$$

where x , y and z are the streamwise, horizontal and vertical axis and u, v are the velocities in x and y directions respectively. The analysis of the vortex vorticity field is however very qualitative. Nevertheless, to characterize and quantify the vorticity field, one can evaluate:

- **Peak vorticity** (ω_{max}): is defined as the highest vorticity value found in the area that encloses the vortex and indicates its concentration. The higher the peak vorticity, the lower the vortex radius, [Wendt et al. (1995)]. When evaluated along the domain, it also provides a reference for the vortex dissipation.

- **Vortex circulation (Γ):** Is the amount of vorticity found in a certain area and it gives a measure for the vortex strength. It is calculated as following

$$\Gamma = \iint_A \omega dA. \quad (1.2)$$

When evaluated along the domain, it provides a measure for the vortex decay. Along the thesis the area is defined as the one that enclosures vorticity values higher than $0.1\omega_{max}$.

- **Vortex core position (x, y, z):** defined by the point where ω_{max} is found. It measures the vortex location and by that the vortex displacement along the domain.

If the model provides a good estimation for the vorticity field along the domain, then the effect of the VG will be correctly simulated. Notwithstanding, since in the models the vortex is introduced in the simulation by either force, velocity or Reynolds stressed modelling, the physics involved in the creation of the vortex is different from the one find in the gridded VG simulations. Thereafter it is difficult to obtain an accurate vorticity field, specially near the the vanes. As a consequence, it is important to also characterize the interaction between the unperturbed flow and the modelled vortices. Driven by the vortex generators applicability, the parameter that best quantify this interaction is the:

- **Boundary layer shape factor (H):** defined as the ratio between the displacement thickness (δ^*) and the momentum thickness (θ):

$$H = \frac{\delta^*}{\theta} = \frac{\int_0^\delta (1 - \frac{U_x}{U_\infty})}{\int_0^\delta \frac{U_x}{U_\infty} (1 - \frac{U_x}{U_\infty})}, \quad (1.3)$$

where δ is the boundary layer thickness. This entity quantifies the form of the boundary layer velocity profile, and gives an indication for the boundary layer stability. If the boundary layer velocity profile is fuller, the ratio $\frac{U_x}{U_\infty}$ will be high and so the shape factor will be lower. In these conditions, the particles located in the lower parts of the boundary layer present high momentum and the boundary layer can be considerer far from separation.

1.4 Research Questions

The existing analysis on the semi-empirical models is rather limited. Very little is known of these models if not in pipe flows. Besides this, most implementations made in Navier-Stokes codes neglect the circulation and peak vorticity estimation from the semi-empirical models. Instead, the circulation and peak vorticity, required to compute the 2D vortex profile, is found by experimental means. Consequently, only the model implementation is tested rather than the semi-empirical model.

From the existing literature is hard to know how well the semi-empirical models predict the

flow behaviour downstream the vortex generators and in which circumstances they can be applied. The aim of this thesis is to investigate the applicability of the models, and can be expressed in the following research question:

Can the Bray model or the Wendt model be applied in CFD simulations of incompressible airfoil flows to reproduce a similar boundary layer shape factor to the one found in simulations with gridded vortex generators?

To successfully answer the research question, one should study the following:

RQ1 Which semi-empirical model, Bray or Wendt, predicts best the circulation and peak vorticity of a vortex shed by a VG at one chord length downstream VG trailing edge?

RQ2 How well can the best model predict the vortex strength and shape as well as shape factor downstream the VG location? And what are its limits of application?

RQ3 How does the vortex circulation, peak vorticity and position estimation influence the vortex development and the boundary layer shape factor?

RQ4 How important is the peak vorticity prediction to obtain the correct boundary layer shape factor?

With the question **RQ1** it is aimed to compare Wendt and Bray formulations for circulation and peak vorticity. The one that predicts best the vortex profile will serve to analyse the accuracy of the semi-empirical models in different situations, answering **RQ2**. With question **RQ3** and **RQ4** is intended to assess how can the model be improved and which are the most relevant parameters (vortex circulation, peak vorticity or position) to obtain the correct flow behaviour.

1.5 Associated Goals

1. To test which semi-empirical model produces the most accurate vorticity distribution in terms of circulation and peak vorticity results at a chord length from VG trailing edge.
2. (a) To test the hypothesis that with a 2D vortex profile imposed at a certain streamwise position it is possible to accurately mimic the development of the vortex shed by the VG, by applying it to a case that lies in the range of experiments conducted by [Wendt \(2001\)](#).
(b) To test the limitations of the Wendt model and assess if this can be applied to an unknown flow condition, by applying it to a case that lies within the limits of the experiments conducted by [Wendt \(2001\)](#) and another that does not lie in the range of experiments conducted.

3. (a) To understand the relation between the imposed circulation and peak vorticity and the vortex development and shape factor, by comparing simulations with calibrated circulation and peak vorticity with the results obtained with the Wendt model. The calibration of parameters is done with the results obtained in the gridded vortex generators simulations.
 - (b) To understand the relation between the imposed vortex position and the vortex development and shape factor, by comparing simulations with calibrated circulation and peak vorticity with calibrated circulation, peak vorticity and vortex position. The calibration of parameters is done with the results obtained in the gridded vortex generators simulations.
4. To understand how well the vortex peak vorticity is modelled by the Wendt model and to understand if the boundary layer shape factor is highly affected by changes in the vortex peak vorticity, by comparing the results obtained with solely circulation calibrated with the results obtained with circulation and peak vorticity calibrated.

1.6 Layout

This thesis is divided in five parts. In part II, the existing semi-empirical models (chapter 2) as well as the possible implementations of these in finite volume full Navier-Stokes codes (chapter 3) will be described.

Next, the implementation of a semi-empirical model is explained in part II. In chapter 4, the Bray and the Wendt models are compared. The one that produces best circulation and peak vorticity results is then implemented in OpenFOAM and verified as described in chapter 5.

In part IV, in chapter 6, the analysis of the implemented model is done and, in chapter 7, it is assessed which parameters are most relevant for the correct computation of the flow behaviour.

Lastly the conclusions and recommendations of the project are discussed in chapter 8.

Part II

Existing Semi-Empirical Models

Chapter 2

Semi-Empirical Models

In this chapter the existing semi-empirical models will be described. These models aim to predict the vortex vorticity field by estimate the vortex circulation and peak vorticity. The section 2.1 refers to the Wendt model, section 2.2 refers to the Bray model and section 2.3 refers to the May model.

During this chapter and throughout the thesis, the reference frame used is as indicated in figure 2.1.

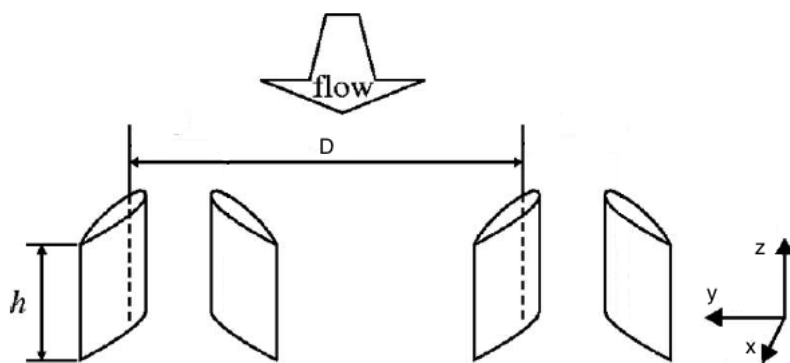


Figure 2.1: Definition of the coordinate system. Modified image from [Törnblom and Johansson \(2007\)](#).

2.1 Wendt Model

To derive empirically peak vorticity and circulation, a parametric study needed to be conducted in first place, this study is presented in the section 2.1.1. Based on that, [Wendt \(2001\)](#) formulated circulation and peak vorticity as described in the sections 2.1.2 and 2.1.3.

2.1.1 Parametric Study

[Wendt \(2001\)](#) performed the parametric study on a straight pipe with rectangular VG vanes placed at the wall.

During the experiments the incoming flow velocity was changed from 85m/s to 187m/s , the VG chord was changed from 0.85cm to 4.06cm , the VG height from 0.21cm to 3.56cm and angle of attack from 8° to 16° . Furthermore a NACA0012 profile was used for the VGs.

	min	max
$U_\infty[\text{m/s}]$	85	187
$\alpha[^\circ]$	8	16
$c[\text{cm}]$	0.85	4.06
$h[\text{cm}]$	0.21	3.56
$\mathcal{R}(\frac{8h}{\pi c})$	0.51	6.11
$\frac{h}{\delta}$	0.19	2.57

Table 2.1: Parameter range used during [Wendt \(2001\)](#) experiments.

The azimuthal velocity was measured, with pressure probes placed at 7 different radial positions, from the wall to the pipe core. Furthermore these measurements were taken at one chord length downstream the VG trailing edge; were, according to [Wendt \(2001\)](#), the vortex is fully developed and diffusion can be neglected.

With the recorded azimuthal velocity, the x -vorticity field at each position was then calculated using

$$\omega_x = \frac{\partial v_\theta}{\partial r} + \frac{v_\theta}{r} - \frac{1}{r} \frac{\partial v_r}{\partial \theta}, \quad (2.1)$$

where ω_x is vorticity in streamwise direction, v_θ is azimuthal velocity, v_r is the radial velocity, r is the radial position and θ is the azimuth angle.

From the vorticity field, the peak vorticity and its location are directly taken. However to obtain the circulation, first, one has to isolate the area were the vortex is located. The area chosen by [Wendt \(2001\)](#) contains streamwise vorticity values higher than $0.01\omega_{max}$. Afterwards circulation is calculated with the area integral

$$\Gamma = \int_A \omega_x dA. \quad (2.2)$$

The parametric study results are included in the appendix A.

2.1.2 Circulation

Under the assumption that the circulation distribution along the VG height equals the one of the shed vortex, then the shed vortex circulation can be expressed with Prandtl equation, that is derived for elliptical wings with symmetric profiles subjected to inviscid flow as

$$\Gamma = \frac{\pi U_\infty \alpha c}{1 + 2/\mathcal{R}}, \quad (2.3)$$

where U_∞ is freestream velocity, α is the angle of attack, c is chord and \mathcal{R} is the VG aspect ratio defined as $AR = 8h/\pi c$, with h being the VG height.

Wendt (2001) reformulates equation 2.3 as

$$\Gamma = \frac{k_1 \alpha U_\infty c}{1 + k_2/\mathcal{R}} \tanh \left[k_3 \left(\frac{h}{\delta} \right)^{k_4} \right], \quad (2.4)$$

where δ is the boundary layer thickness and the constants k_1, k_2 (substituting respectively π and 2 in equation 2.4) and k_3 and k_4 are empirical constants adjusted according to the parametric study data, table 2.2. Furthermore the hyperbolic tangent is introduced in Prandtl equation to account for boundary layer interactions.

	Coefficient value
k_1	1.61
k_2	0.48
k_3	1.41
k_4	1.00

Table 2.2: Wendt model coefficients.

2.1.3 Peak Vorticity

To obtain the peak vorticity Wendt (2001) used the Lamb-Oseen model. This model accounts with time vortex decay and is derived from the potential free-vortex formulation ($v_\theta = \Gamma/2\pi r$)

$$v_\theta = \frac{\Gamma}{2\pi r} \left[1 - e^{-r^2/4\nu t} \right], \quad (2.5)$$

where ν is the kinetic viscosity.

Squire developed this model further by substituting the time variable, t , with streamwise convective displacement $t \approx xU_\infty$. By differentiating the azimuthal velocity as shown in equation 2.1, the vorticity as function of radial position and streamwise position can be obtained as follow

$$\omega_x = \frac{U_\infty \Gamma}{4\pi \nu x} \exp \left(\frac{-U_\infty r^2}{4\nu x} \right). \quad (2.6)$$

As one can see, peak vorticity will equal $\omega_{max} = U_\infty \Gamma / 4\pi\nu x$. Using this result the azimuthal velocity can be re-written in the following form

$$v_\theta = \frac{\Gamma}{2\pi r} \left[1 - \exp\left(\frac{-\pi\omega_{max}r^2}{\Gamma}\right) \right]. \quad (2.7)$$

Using equation 2.7 derived by Squire, Wendt (2001) calculates the peak vorticity as a function of circulation, $\omega_{max} = f(\Gamma, \alpha, c, h, U_\infty)$. To do this, Wendt (2001) first calculates the vortex angular momentum, G , with two different approaches.

Approach 1: In the first approach, the angular momentum with streamwise position of a constrained Lamb-Oseen vortex is calculated.

The angular momentum of a Lamb-Oseen vortex can be written as follows

$$\frac{G}{\rho dz} = \int_0^{2\pi} \int_0^R (r \times v_\theta) 2\pi r dr d\theta = \Gamma \left[\frac{R^2}{2} - \left(\frac{\Gamma}{2\pi\omega_{max}} \right) \left(1 - \exp\left(\frac{-\pi\omega R^2}{\Gamma}\right) \right) \right]. \quad (2.8)$$

As one can see, as $r \rightarrow \infty$ so does the angular momentum. Consequently, the radius must be limited to $r = r_2$, see figure 2.2. The vortex outer boundary, r_2 , includes the entire viscous core but also a “good portion of the inviscid region of the Lamb vortex”, [Wendt (2001)]. When defining the velocity ratio as

$$\zeta = \frac{v_\theta}{v_{\theta_{max}}}, \quad (2.9)$$

the outer boundary equal, [Wendt (2001)]:

$$r_2 \approx \left[\frac{1}{\zeta(1 - e^{-1/2})^2} \right] \sqrt{\frac{\Gamma}{2\pi\omega_{max}}}. \quad (2.10)$$

If one applies this expression for r_2 to equation 2.8, then the angular momentum becomes

$$\frac{G}{\rho dz} = \left(\frac{\Gamma^2}{2\pi\omega_{max}} \right) [\beta - 1 + e^{-\beta}] \approx \frac{\Gamma^2(\beta - 1)}{2\pi\omega_{max}}, \quad (2.11)$$

where $\beta = \frac{1}{2\zeta^2(1 - e^{-1/2})}$.

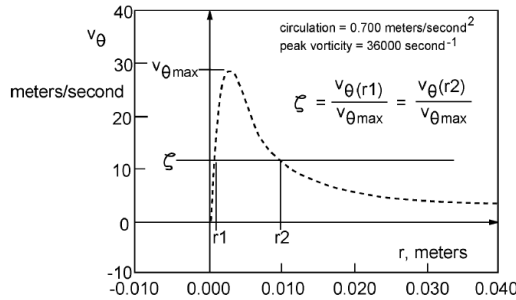


Figure 2.2: Velocity ratio definition, [Wendt (2001)].

Approach 2: In the second approach the angular momentum production at the tip of the VG will be calculated with

$$\sum(\text{moments at the tip}) = CF \times CMA = \frac{\partial G}{\partial t} \approx U_\infty \frac{G}{dz}. \quad (2.12)$$

The characteristic force CF , will be the lift created by the VG and is calculated by integration of the 2D inviscid pressure distribution $\Delta C_P = 4 \sin \alpha \sqrt{c/x - 1}$ over the wing, as

$$CF = 2\rho U_\infty^2 \alpha c \int_0^h \int_0^c \sqrt{\frac{c}{x} - 1} \frac{dx}{c} dz. \quad (2.13)$$

On the other hand, the characteristic moment arm CMA is the radius of the formed vortex, before diffusion takes place. By Rankine viscous core definition,

$$CMA = \sqrt{\frac{\Gamma}{2\pi\omega_{max}}}. \quad (2.14)$$

Substituting CF and CMA definitions in equation 2.12, one obtains:

$$\frac{G}{\rho dz} \approx \pi \alpha c h U_\infty \sqrt{\frac{\Gamma}{2\pi\omega_{max}}}. \quad (2.15)$$

By equating equation 2.11 to equation 2.15, the peak vorticity is found to be

$$\omega_{max} = \frac{\Gamma^3(\beta - 1)^2}{2\pi^3 \alpha^2 c^2 h^2 U_\infty^2}, \quad (2.16)$$

where the velocity ratio was determined to be $\zeta = \frac{v_\theta}{v_{\theta_{max}}} = 0.29$.

2.2 Bray Model

In [Bray \(1998\)](#) is presented another semi-empirical VG model. This model was made in order to improve a parabolized Navier-Stokes solver (PNS) and was inspired by [Wendt](#) early work developed in [Wendt et al. \(1995\)](#).

In the model proposed by [Bray \(1998\)](#), the vortex circulation and peak vorticity not only depend on the freestream velocity, angle of attack, chord and height but also on the streamwise vortex decay and dissipation. In section 2.2.1 the parametric study made by [Bray \(1998\)](#) is presented. Subsequently the derivations for circulation and peak vorticity are shown in section 2.2.2 and section 2.2.3.

2.2.1 Parametric Study

The parametric study was elaborated on a flat plate with thin rectangular VG vanes at different angles of attack. Two studies were conducted, in the low-speed study the Mach

number was kept constant and equal to $Ma = 0.0588$ (corresponding to $U_\infty = 20m/s$), while in the high speed study the Mach number range equal to $0.45 < Ma < 0.75$.

During the low speed experimental campaign the boundary layer thickness was kept constant and equal to $\delta = 4.15cm$, the VG chord was kept the double of the VG height, $\mathcal{R} = 1.27$, the angle of attack varied from $10^\circ < \alpha < 20^\circ$, height-to-boundary-layer-thickness varied from $0.554 < h/\delta < 1.639$ and the azimuthal velocity was recorded at $x/\delta = 3.855, 12.048, 26.506$, see table 2.3.

	min	max
$U_\infty [m/s]$	20	20
$\alpha [^\circ]$	10	20
$c [cm]$	4.6	13.6
$h [cm]$	2.3	6.8
$\frac{h}{\delta} [cm]$	0.554	1.639
$\mathcal{R}(\frac{8h}{\pi c})$	1.27	1.27
x/δ	3.855	26.506

Table 2.3: Parameter range used during Bray (1998) low speed experimental campaign.

During the high speed campaign smaller vanes with the aspect ratio $\mathcal{R} = 1.27$ were used, the boundary layer was kept at $\delta = 2cm$ and height-to-boundary-layer-ratio was kept at $h/\delta = 0.75$. Furthermore the angle of attack was varied from $15^\circ < \alpha < 20^\circ$, see table 2.4.

	min	max
Ma	0.45	0.75
U_∞	135	226
$c [cm]$	3	3
$h [cm]$	1.5	1.5
$\frac{h}{\delta}$	0.75	0.75
$\mathcal{R}(\frac{8h}{\pi c})$	1.27	1.27
$\alpha [^\circ]$	15	20
x/δ	8.75	23.75

Table 2.4: Parameters range used during Bray (1998) high speed experimental campaign.

To determine the vorticity, a 5-Holes Probe multi-directional system was used. In the low speed experimental campaign, the static pressure was obtained with a spacing of $5mm$ at a certain streamwise position. In the high speed campaign, the static pressure was obtained in every $3mm$. Furthermore, an interpolation of the $5mm$ and $3mm$ grids was done over a $0.5mm$ grid, [Bray (1998)].

After the probe calibration, y -velocity and z -velocity are known. The vorticity was calculated using equation 2.17.

$$\omega_x = -\frac{\partial v}{\partial z} + \frac{\partial w}{\partial y} \quad (2.17)$$

From this, the peak vorticity and circulation are obtained as explained in section 2.1.1.

The results obtained during the parametric study are included in the appendix B.

2.2.2 Circulation

In the Lamb-Oseen vortex model the term " $2\nu t$ " is the vortex viscous core. As so, the equation 2.6 can be written in a more generic way using the vortex radius, R , as

$$\omega(r) = \omega_{max} e^{-k(r/R)^2} \quad (2.18)$$

Since the vorticity vanish at the outer limits of the vortex, the vortex radius is a variable difficult to quantify. Consequently the vortex radius is substituted by the *half-life* radius, $R_{0.5}$, defined as the radius at which the vorticity is half of the peak vorticity, [Bray (1998)],

$$\omega(r) = \omega_{max} e^{\ln(1/2)(r/R_{0.5})^2} \quad (2.19)$$

Substituting equation 2.19 in the circulation definition, one obtains

$$\Gamma = \int_{dA} \omega dA = \omega_{max} \int_0^{2\pi} \int_0^\infty e^{\ln(1/2)(r/R_{0.5})^2} r dr d\theta, \quad (2.20)$$

which reduces to

$$\Gamma = \frac{\omega_{max} \pi R_{0.5}^2}{0.693}. \quad (2.21)$$

2.2.3 Peak Vorticity

The lift coefficient, C_L of an elliptical finite wing in inviscid flow is given by

$$C_L = a\alpha = \frac{2\pi}{1 + (8/R\pi)(1 + \tau)} \alpha, \quad (2.22)$$

where τ is the Prandtl constant. Combining this result with the Kutta-Joukowski theorem and assuming that the circulation of the shed vortex is the same of the wing, then the vortex circulation is given by

$$\Gamma = 1/2 U_\infty c C_L = \frac{U_\infty c \pi \alpha}{1 + (8/R\pi)(1 + \tau)}. \quad (2.23)$$

Substituting the circulation expression found in equation 2.21 into equation 2.23, the peak vorticity is derived

$$\omega_{max} = \frac{0.693 U_\infty c \alpha}{\left[1 + (8/R\pi)(1 + \tau)\right] R_{0.5}^2}. \quad (2.24)$$

To account for the vortex diffusion, [Bray \(1998\)](#) introduces the term $e^{-k\left(\frac{x}{\delta}\frac{\delta}{h}\right)}$ in equation 2.24. In addition, the velocity is substituted by a power law function. Furthermore, to account with vane stall at large angles of attack, the equation 2.24 is rewritten as a polar function of α . The peak vorticity derived in [Bray \(1998\)](#) thus becomes

$$\omega_{max} = k_{\alpha} \left[\frac{(Ma^{k_M})(a^{k_a})ce^{-k_e\left(\frac{x}{\delta}\frac{\delta}{h}\right)}}{[1 + (8/\mathcal{R}\pi)(1 + \tau)]R_{0.5}^2} \right] \alpha^2 + l_{\alpha} \left[\frac{(Ma^{l_M})(a^{l_a})ce^{-l_e\left(\frac{x}{\delta}\frac{\delta}{h}\right)}}{[1 + (8/\mathcal{R}\pi)(1 + \tau)]R_{0.5}^2} \right] \alpha, \quad (2.25)$$

where the *half-life* radius is a purely empirical equation equal to

$$\frac{R_{0.5}}{\delta} = \left[0.285\alpha^{0.6\frac{h}{\delta}} + 0.0001 \right] \left[1.1\left(\frac{h}{\delta}\right)^2 - 0.34\frac{h}{\delta} + 0.9 \right] \left[-0.275e^{-0.026\frac{x}{\delta}\frac{\delta}{h}} \right] \left[1.24Ma^{0.16} + 3.28 \right]. \quad (2.26)$$

The coefficients, shown in table 2.5, of equation 2.25 are found by fitting the equation to the data obtained during the experiments.

	k	l
suffix- α	1.7	0.38
suffix-M	1	1
suffix-a	1	1
suffix-e	0.015	0.015
τ	0.05	0.05

Table 2.5: Constants for equation 2.25, from [Bray \(1998\)](#).

2.3 May Model

[May \(2001\)](#) implements a simplification of the Bray model in a full Navier-Stokes (FNS) solver. This model uses the Bray circulation formulation, equation 2.21, but at only one streamwise position, one chord length downstream the VG location $\frac{\Delta x}{c} = 1$. Concerning the peak vorticity, as the model is intended to work on coarse grids, this value is underestimated by default. As so, [May \(2001\)](#) suggests to use a large peak vorticity value, and the value

$$\omega_{max} = 50 \frac{U_{\infty}}{\delta_0} \quad (2.27)$$

was used.

Chapter 3

Possible Implementations of Semi-Empirical Models in FNS Solvers

The equation 2.7 establish the relation between the azimuthal velocity and the vortex circulation and peak vorticity. By using one of the vortex models described in chapter 2, it is possible to estimate the vortex circulation and peak vorticity at a certain streamwise position and by that to calculate the azimuthal vortex velocity at that position. This azimuthal velocity can then be added to the FNS solver either as a velocity-jump-boundary-condition as [Dudek \(2006\)](#) did, or as a source-term in the momentum equations as [May \(2001\)](#) did. Both implementations are described in the present chapter. Section 3.1 explains Dudek implementation and section 3.2 explains May implementation.

In [Wendt et al. \(1995\)](#) the vortex velocity field in Cartesian coordinates is mathematically described. In first place the azimuthal velocity, equation 2.7, of an isolated vortex n with center at (y_n, z_n) is decomposed in the Cartesian coordinates $(x, y, z) = (x, r \cos(\theta), r \sin(\theta))$ as

$$v_n(y, z) = -\frac{\Gamma_n(z - z_n)}{2\pi R_n^2} F_n, \quad (3.1a)$$

$$w_n(y, z) = \frac{\Gamma_n(y - y_n)}{2\pi R_n^2} F_n, \quad (3.1b)$$

where:

$$F_n = 1 - \exp\left(\frac{-\pi\omega_{max_n}}{\Gamma_n} R_n^2\right), \quad R_n^2 = (y - y_n)^2 + (z - z_n)^2.$$

In addition, to ensure the impermeability condition, the imaged vortices are added, and to

account with the effect of the neighbour vortices, this are also added as

$$v(y, z) = \sum_{n=1}^N (v_n + v_{n_{im}}), \quad (3.2a)$$

$$w(y, z) = \sum_{n=1}^N (w_n + w_{n_{im}}), \quad (3.2b)$$

where N corresponds to the total amount of VGs.

It must be noticed however that with this formulation the non-slip condition is not met.

3.1 Dudek Implementation

Dudek (2006) implemented the Wendt vortex model in the *Wind-US CFD* code by making use of the assumption that if the induced velocities are applied in a plane downstream the VG, then because of the interaction between the unperturbed flow and induced velocities, a vortex similar to the one shed by the VG will be formed and convected downstream correctly. In the *Wind-US CFD* code, the vortex velocity field, as described in equation 3.2, was added in the form of a step boundary condition specified in the yz -plane located at one chord length from the VG trailing edge, [**Dudek (2006)**]. In each cell i , at this location, the resultant flow field is thus a composition of the unperturbed flow and the vortex secondary velocity equal to $U_i = U_{unperturbed_i} + u_i$. Furthermore, to avoid a singularity at the vortex core, **Dudek (2006)** used a lower bound of $R_n^2 = 0.001h_n^2$ if $R_n < 0.001h_n^2$.

3.2 May Implementation

Instead of adding the velocities as a boundary condition, in **May (2001)** is reported that the velocity field equation 3.2 is added as a source term in the FNS. However, no exact formulation is given.

It is believed that this is in the form of

$$W_i = \bar{U}_j \left(\frac{\partial \bar{u}_i}{\partial x_j} \right) + \bar{u}_i \left(\frac{\partial \bar{U}_j}{\partial x_j} + \frac{\partial \bar{u}_j}{\partial x_j} \right) + u_j \left(\frac{\partial \bar{U}_i}{\partial x_j} + \frac{\partial \bar{u}_i}{\partial x_j} \right) - \nu \left(\frac{\partial^2 \bar{u}_i}{\partial x^2} \right) \quad (3.3)$$

Where upper and lower case letters refer to undisturbed flow and vortex velocities, respectively.

To obtain equation 3.3 in first place the velocity field vectors were written as a sum of mean velocity, velocity fluctuations and vortex velocity ($U_i = \bar{U}_i + U'_i + u_i$); and the pressure as a sum of mean pressure, pressure fluctuations and vortex pressure ($P_i = \bar{P}_i + P'_i + p_i$). By re-writing the Navier-Stokes equations and isolate the terms that express the vortex velocity contribution, the equation 3.3 was derived. The full derivation of the force W_i can be read in appendix C.

Part III

Semi-Empirical Model Implementation

Chapter 4

Comparison Between Wendt and Bray Models

In order to assess which empirical model will be implemented in our study, a comparison between the semi-empirical models will be performed in this chapter. In this study the circulation and peak vorticity values found with the Wendt and Bray models are set side by side with the ones found by experimental means.

Let us first analyse the formulation differences found in each model. While [Wendt \(2001\)](#) uses circulation as an input for peak vorticity, [Bray \(1998\)](#) uses peak vorticity to calculate circulation. Due to this difference, circulation in the Wendt model and peak vorticity in the Bray model are the variables that were fitted to the experimental data. On the other hand, peak vorticity in the Wendt model and circulation in the Bray model are derived solely from theory.

As explained in section 2.1.1, because pressure probes are used in the experimental campaign to acquire the discrete velocity field - later transformed on the discrete vorticity field - the peak vorticity obtained will depend on the location where the local velocity is recorded. As so seems more natural to use circulation values to obtain peak vorticity as [Wendt \(2001\)](#) did. Furthermore both empirical models use the Lamb-Oseen vortex model and the finite wing theory to derive circulation and peak vorticity formulas. They account with circulation decrease in the boundary layer - [Wendt \(2001\)](#) with an hyperbolic tangent function and [Bray \(1998\)](#) with an exponential function -. However only [Bray \(1998\)](#) accounts with stall at large angles of attack, as well as for vortex streamwise decay, described with an exponential function. The Wendt model uses a *calibration constant* to calibrate changes in circulation with angle of attack, freestream velocity and chord and another two to calibrate aspect ratio and height-to-boundary-layer-thickness respectively. On the other hand the Bray model has a *calibration constant* associated to each variables but chord and aspect ratio. Consequently, although the peak vorticity formula in the Bray model has a high degree of freedom with Mach number, sound velocity, angle of attack and vortex radius - and so, in theory, it can provide better

fitting with experimental results -, the Bray model is more complex than the Wendt model. This statement is even more obvious when comparing the vortex radius definitions that each model uses.

As described in chapter 3, the implementation of a semi-empirical model in a FNS solver is made with the addition of the vortex velocity profile (either with a velocity boundary condition or as a source term) to the unperturbed flow at a streamwise distance of one VG chord length c downstream of the VG trailing edge, $\frac{\Delta x}{c} = 1$. As a result, it is important to study both semi-empirical models at this streamwise position.

The most complete parametric study done at $\frac{\Delta x}{c} = 1$ found in literature is from [Wendt \(2001\)](#), consequently this was the one chosen to perform this comparison study. In table 4.1 the cases in which the Bray model and Wendt model are compared with the experimental results are shown.

	case 1: α variation	case 2: U_∞ variation	case 3: c variation $\frac{h}{\delta} = 0.29$	case 4: c variation $\frac{h}{\delta} = 0.57$	case 5: c variation $\frac{h}{\delta} = 0.86$	case 6: c variation $\frac{h}{\delta} = 1.14$
$\alpha [^\circ]$	0 - 23	16	16	16	16	16
$c [cm]$	4.06	4.06	0.5 - 4.5	0.5 - 4.5	0.5 - 4.5	0.5 - 4.5
$h [cm]$	1.02	1.02	0.51	1.02	1.52	2.03
$\mathcal{R} = \frac{8h}{\pi c} [-]$	0.64	0.64	2.60-0.29	5.19-0.58	7.74-0.86	10.34-1.15
$\frac{h}{\delta} [-]$	0.57	0.57-0.65	0.29	0.57	0.86	1.14
$U_\infty [m/s]$	85	80-200	85	85	85	85

	case 7: $\frac{h}{\delta}$ variation $\mathcal{R} = 0.64$	case 8: $\frac{h}{\delta}$ variation $\mathcal{R} = 1.53$	case 9: $\frac{h}{\delta}$ variation $\mathcal{R} = 3.06$
$\alpha [^\circ]$	16	16	16
$c [cm]$	1.11 - 4.06	0.85-4.05	0.85-3.55
$h [cm]$	0.28 - 1.02	0.51-2.43	1.02-4.27
$\mathcal{R} = \frac{8h}{\pi c} [-]$	0.64	1.53	3.06
$\frac{h}{\delta} [-]$	0.19-0.57	0.29-1.37	0.57-2.4
$U_\infty [m/s]$	85	85	85

Table 4.1: Input parameters to compare with Wendt experiment.

In the figures 4.1 and 4.2, the variation of circulation and peak vorticity with angle of attack is shown. As one can see in the experimental results at higher angles, despite the decrease of peak vorticity, there is no loss of circulation.

In figure 4.1 the Bray model presents a good agreement with the experimental circulation results for changes in angle of attack. This is consequence of the *half-life radius* definition given by the Bray model where the *half-life radius* is exponential function of angle of attack. In contrast, due to the linear relation with angle of attack, the Wendt model is unable to follow the angle of attack curve, and so, it underpredicts circulation values for larger angles of attack. Furthermore, in figure 4.2, it can be seen that both models fail in the prediction of peak vorticity with angle of attack. Even with the polar relation, the Bray model is unable of model the reduction of peak vorticity with angle of attack. While the Wendt model overpredicts the slope of the curve, the Bray model underpredicts it.

The circulation and peak vorticity changes with increase of velocity are shown in figure 4.3 and in figure 4.4, respectively. It can be seen that, as expected, to an increase of velocity there is an increase of the vortex strength and peak vorticity.

Both models describe that circulation and peak vorticity evolves linearly with changes in freestream velocity, this assumption agrees reasonably well with the trends presented by the experimental results. For circulation the agreement with experimental results is good in both models although slightly underpredicted by both. For peak vorticity both models fail in the prediction of it with changes of freestream velocity. Similarly with angle of attack variation, the Wendt model overpredicts the slope of the curve and the Bray model underpredicts it.

With respect to the aspect ratio changes, it is seen in the experimental results that for lower values of the \mathcal{R} (large chord) the peak vorticity decreases, figures 4.6, 4.8, 4.10 and 4.12. It is known that for wings with much larger span than chord, the tip vortex created is less concentrated and that, in this conditions, the induced drag is reduced. The same applies in VGs with much larger chord than height. This explains the decrease of peak vorticity with lower values of \mathcal{R} . Nevertheless, since the VG area is increased with the decrease of \mathcal{R} , the circulation on the VG increases and so does in the vortex shed, see figure 4.5, 4.7, 4.9 and 4.11. Furthermore it can be noticed in figures 4.5 and 4.6 that changes in aspect ratio for low height-to-boundary-layer-thickness-ratio do not have a strong impact on circulation or peak vorticity.

Both models are able to predict the decrease of peak vorticity at lower \mathcal{R} . However, since peak vorticity is a required parameters to calculate circulation in the Bray model, at lower values of \mathcal{R} the circulation predicted by the Bray model will suffer from a sudden decrease that does not agree with the results found by experimental means. The Wendt model on the other hand depends directly on the aspect ratio and so it is able to predict reasonably well the circulation trend.

For all the height-to-boundary-layer-thickness-ratios but the smallest ($h/\delta = 0.29$), the Wendt model is able to predict better circulation than the Bray model, see figures 4.5, 4.7, 4.9 and 4.11. Furthermore it is seen that the Bray model underpredicts largely peak vorticity and that the Wendt model presents a reasonable agreement with the experiments for all height-to-boundary-layer-thickness-ratios, figures 4.6, 4.8, 4.10 and 4.12.

Similarly with aspect ratio, with an increase of height-to-boundary-layer-ratio it is expected an increase of vortex circulation. Besides the increase of area, there will be an increase of velocity at the tip of the VG that results in an increase of the pressure difference between each side of the vane and so a stronger vortex is created.

For smaller aspect ratio, circulation values with changes in height-to-boundary-layer-thickness-ratio are better predicted by the Bray model, figure 4.13. For larger aspect ratios, however, these are better predicted by the Wendt model, figure 4.15 and figure 4.17. It can be seen that, even with different formulations to describe vortex circulation in the boundary layer, both models predict evolution of circulation with height-to-boundary-layer-thickness-ratio with similar slopes. With respect to peak vorticity it can be seen, in figures 4.14, 4.16 and 4.18, that peak vorticity is underestimated by the Bray model but the agreement between the Wendt model and the experimental results is good for the higher aspect ratios.

In general, when analysing circulation values, it can be said that both models predict it reasonably well and that the Wendt model tends to underpredict it. In addition, the peak

vorticity comparisons show a bigger discrepancy between experimental results and empirical models. It can be said that the Bray model tends to underpredicts peak vorticity and the Wendt model tends to overpredicts it.

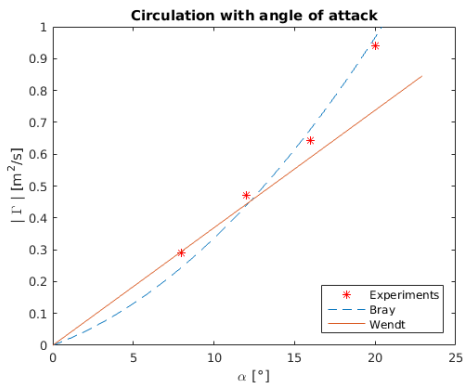


Figure 4.1: Circulation with varying VG angle of attack

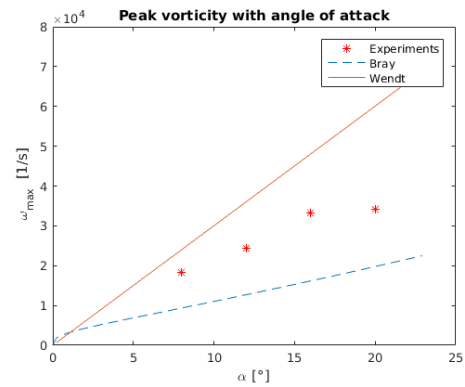


Figure 4.2: Peak vorticity with varying VG angle of attack.

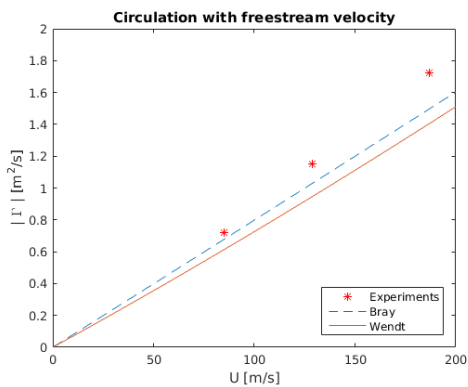


Figure 4.3: Circulation with varying freestream velocity.

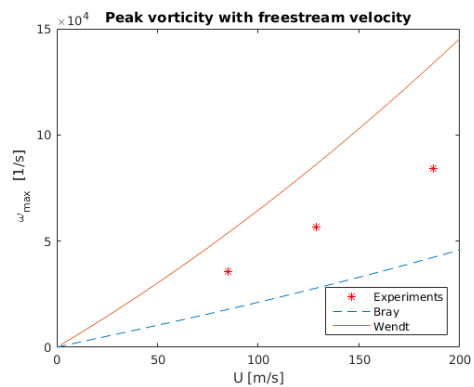


Figure 4.4: Peak vorticity with varying freestream velocity.

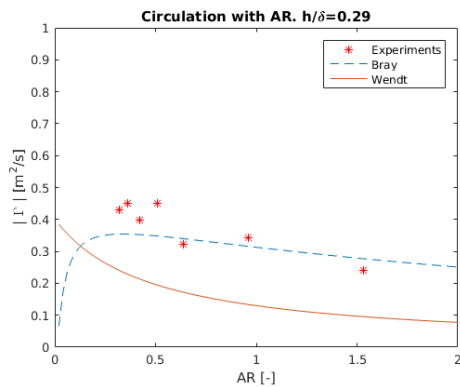


Figure 4.5: Circulation with varying VG aspect ratio. $\frac{h}{\delta} = 0.29$

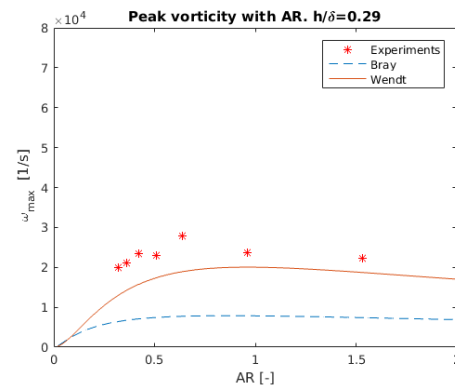


Figure 4.6: Peak vorticity with varying VG aspect ratio. $\frac{h}{\delta} = 0.29$

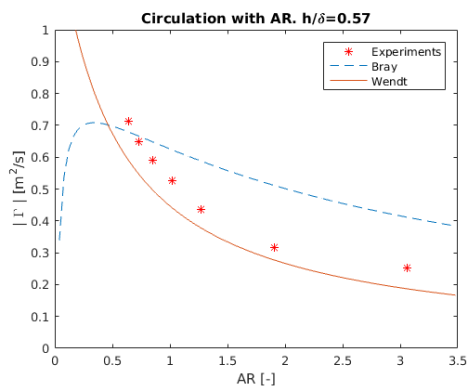


Figure 4.7: Circulation with varying VG aspect ratio. $\frac{h}{\delta} = 0.57$

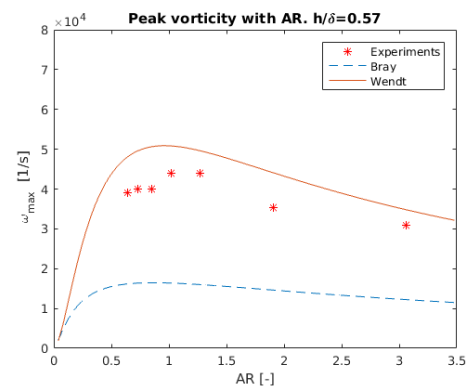


Figure 4.8: Peak vorticity with varying VG aspect ratio. $\frac{h}{\delta} = 0.57$

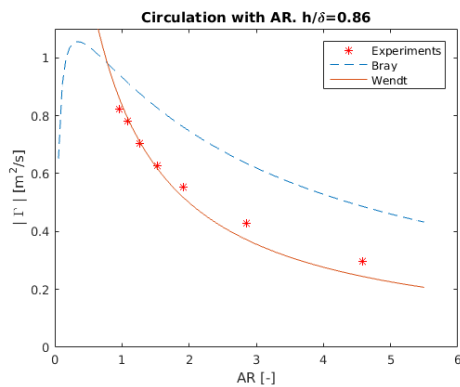


Figure 4.9: Circulation with varying VG aspect ratio. $\frac{h}{\delta} = 0.86$

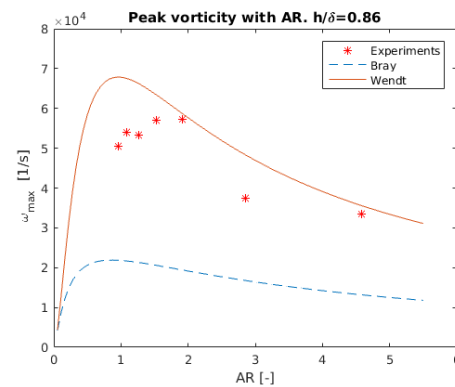


Figure 4.10: Peak vorticity with varying VG aspect ratio. $\frac{h}{\delta} = 0.86$

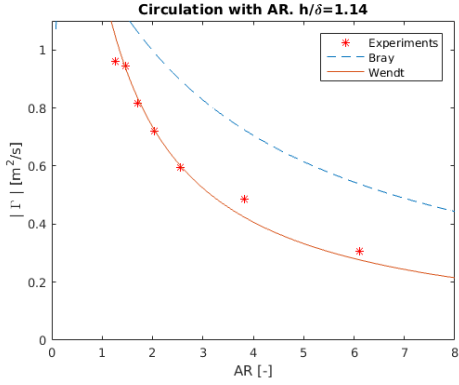


Figure 4.11: Circulation with varying VG aspect ratio. $\frac{h}{\delta} = 1.14$

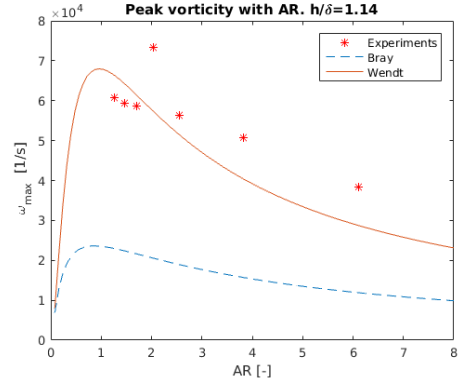


Figure 4.12: Peak vorticity with varying VG aspect ratio. $\frac{h}{\delta} = 1.14$

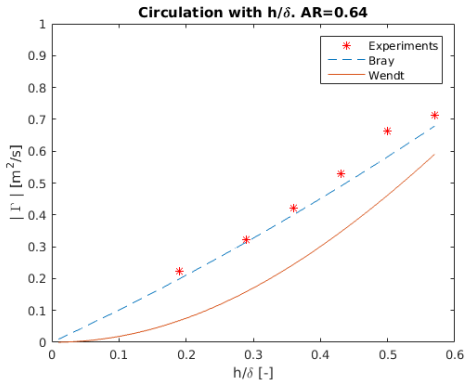


Figure 4.13: Circulation with varying h/δ . $\mathcal{R} = 0.64$.

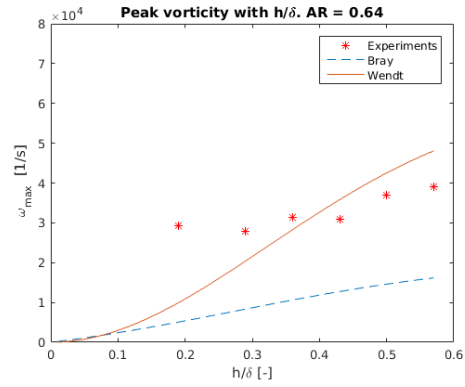


Figure 4.14: Peak vorticity with varying h/δ . $\mathcal{R} = 0.64$.

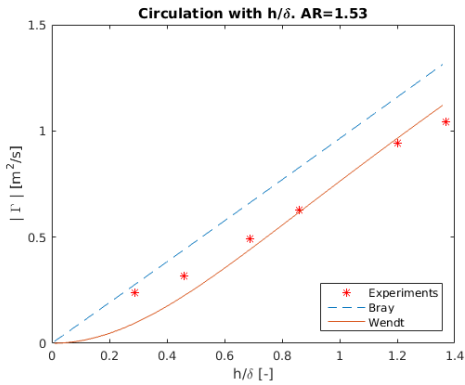


Figure 4.15: Circulation with varying h/δ . $\mathcal{R} = 1.53$

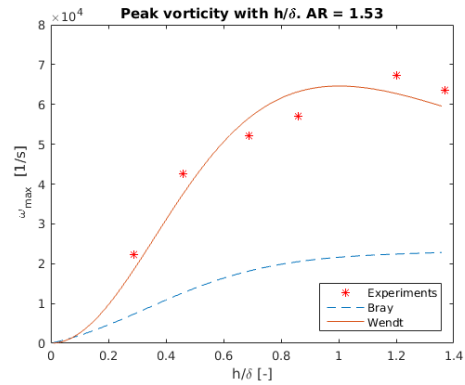


Figure 4.16: Peak vorticity with varying h/δ . $\mathcal{R} = 1.53$

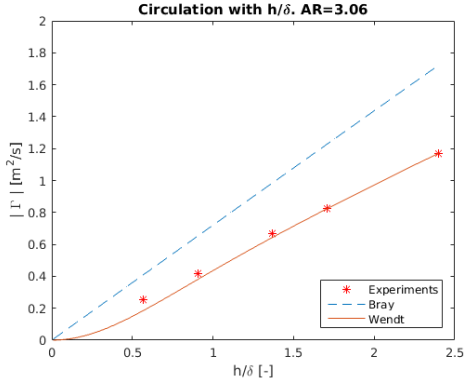


Figure 4.17: Circulation with varying h/δ . $\mathcal{R} = 3.06$

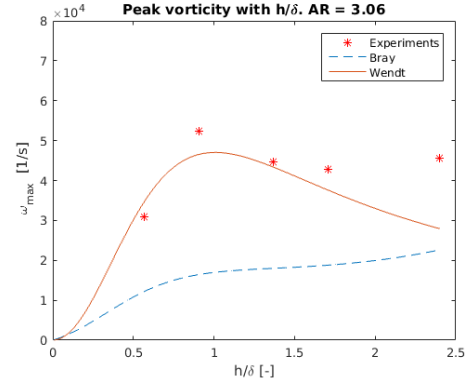


Figure 4.18: Peak vorticity with varying h/δ . $\mathcal{R} = 3.06$

Although the Wendt model predicted best the vortex circulation and peak vorticity in the tested range. The analysis was conducted at relatively high freestream velocity, $U_\infty = 85\text{m/s}$. Consequently, it is important to test the predictive capabilities of the Wendt model at lower free-stream velocities. For that it was decided to compare both empirical models with the ones found in Bray (1998) for the lower streamwise positions $\frac{x}{\delta} = [1.18, 1.51]$. In the table 4.2 the input parameters for each case are shown.

In the comparison between empirical models and Bray parametric study, the peak vorticity is not analysed because Wendt model does not account with streamwise vorticity decay and the parametric study is done for streamwise positions where this cannot be neglected.

	Case 1: α variation	Case 2: α variation
h/δ	1.639	1.277
α [°]	0 - 20	0-20
c [cm]	13.6	13.6
$\mathcal{R} = \frac{8h}{\pi c}$ [-]	1.27	1.27
U_∞ [m/s]	20	20
$\frac{\Delta x}{c}$ [-]	1.176	1.509

Table 4.2: Input parameters to the comparison between models using the low speed experimental campaign done by Bray (1998).

The circulation variation with angle of attack of case 1 and case 2 are shown in figure 4.20 and figure 4.19, respectively. As one can see that, similarly with the results found with $U_\infty = 85\text{m/s}$, the circulation in the Wendt model increases linearly with angle of attack and with the Bray model it increases asymptotically. Despite this, with $U_\infty = 20\text{m/s}$, the Wendt model predicts now better circulation for higher angles of attack than the Bray model and worse circulation for lower angles of attack than the Bray model. Furthermore it can be seen than in the case 2, where $\frac{\Delta x}{c} = 1.51$, Wendt model overpredicts more the circulation than in case 1, where $\frac{\Delta x}{c} = 1.18$. This might indicate that the vortex decayed and if so, that the Bray models fails slightly in the decay prediction.

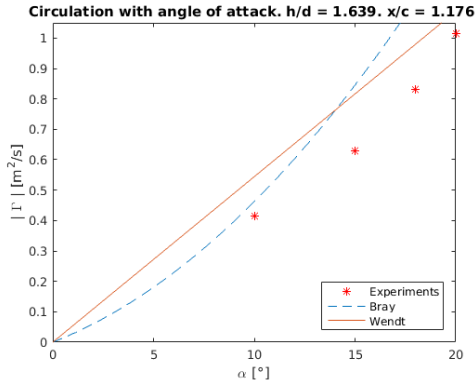


Figure 4.19: Circulation with VG angle of attack. $\frac{h}{\delta} = 1.639$, $\frac{\Delta x}{c} = 1.176$.

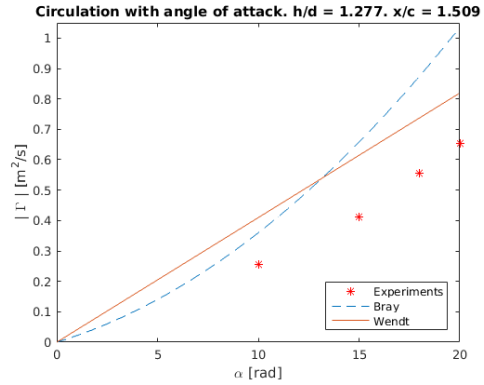


Figure 4.20: Circulation with VG angle of attack. $\frac{h}{\delta} = 1.277$, $\frac{\Delta x}{c} = 1.509$.

As one can see the results found with lower free-stream velocity, $U_\infty = 20m/s$, are not far from the ones found with higher velocities. The Wendt model did not predicted unreasonable circulation results. Consequently, it can be concluded that the Wendt model is able to predict slightly better circulation at $\frac{\Delta x}{c} = 1$ than the Bray model but for higher freestream velocities and lower values of aspect ratio and height-to-boundary-layer-ratio. Furthermore, in all the cases it predicted best the vortex peak vorticity. Consequently this model was the one implemented during this thesis.

Chapter 5

Wendt Model Implementation

Based on the findings in chapter 4, the Wendt model was implemented in OpenFOAM. In this chapter the implementation procedure as well as the verification process will be discussed in section 5.1 and section 5.2, respectively.

5.1 Implementation Procedure

In order to implement Wendt Model, in first place, a code that calculates the induced velocities in the yz -plane at $\frac{\Delta x}{c} = 1$ must be created. A simplified flow chart of this code is shown in figure 5.1.

In the code, the first step is to read each vane's geometry and cell centre positions. Afterwards the circulation and peak vorticity of each vortex n are calculated with Wendt model (equation 2.4 and equation 2.16). With this, it is then possible to calculate the velocity induced by each vortex n - with core located at (y_n, z_n) - in each cell centre i with coordinate (y_i, z_i) (see figure 5.2) using

$$v_{n,i} = -\frac{\Gamma_n(z_i - z_n)}{2\pi R_{n,i}^2} F_{n,i} + \frac{\Gamma_n(z_i - z_{im_n})}{2\pi R_{im_n,i}^2} F_{im_n,i}, \quad (5.1a)$$

$$w_{n,i} = \frac{\Gamma_i(y_i - y_n)}{2\pi R_{n,i}^2} F_{n,i} - \frac{\Gamma_i(y_i - y_{im_n})}{2\pi R_{im_n,i}^2} F_{im_n,i}, \quad (5.1b)$$

where

$$R_{n,i}^2 = (y_i - y_n)^2 + (z_i - z_n)^2, \quad R_{im_n,i}^2 = (y_i - y_n)^2 + (z_i + z_n)^2, \quad (5.2a)$$

$$F_{n,i} = 1 - \exp\left(\frac{-\pi\omega_{max_n} R_{n,i}^2}{\Gamma_n}\right), \quad F_{im_n,i} = 1 - \exp\left(\frac{-\pi\omega_{max_n} R_{im_n,i}^2}{\Gamma_n}\right). \quad (5.2b)$$

At last in each cell the influence of each vortex is added such that the total induced velocities become

$$v_i = \sum_{n=1}^N (v_{n,i}), \quad (5.3a)$$

$$w_i = \sum_{n=1}^N (w_{n,i}). \quad (5.3b)$$

The code is included in appendix D.

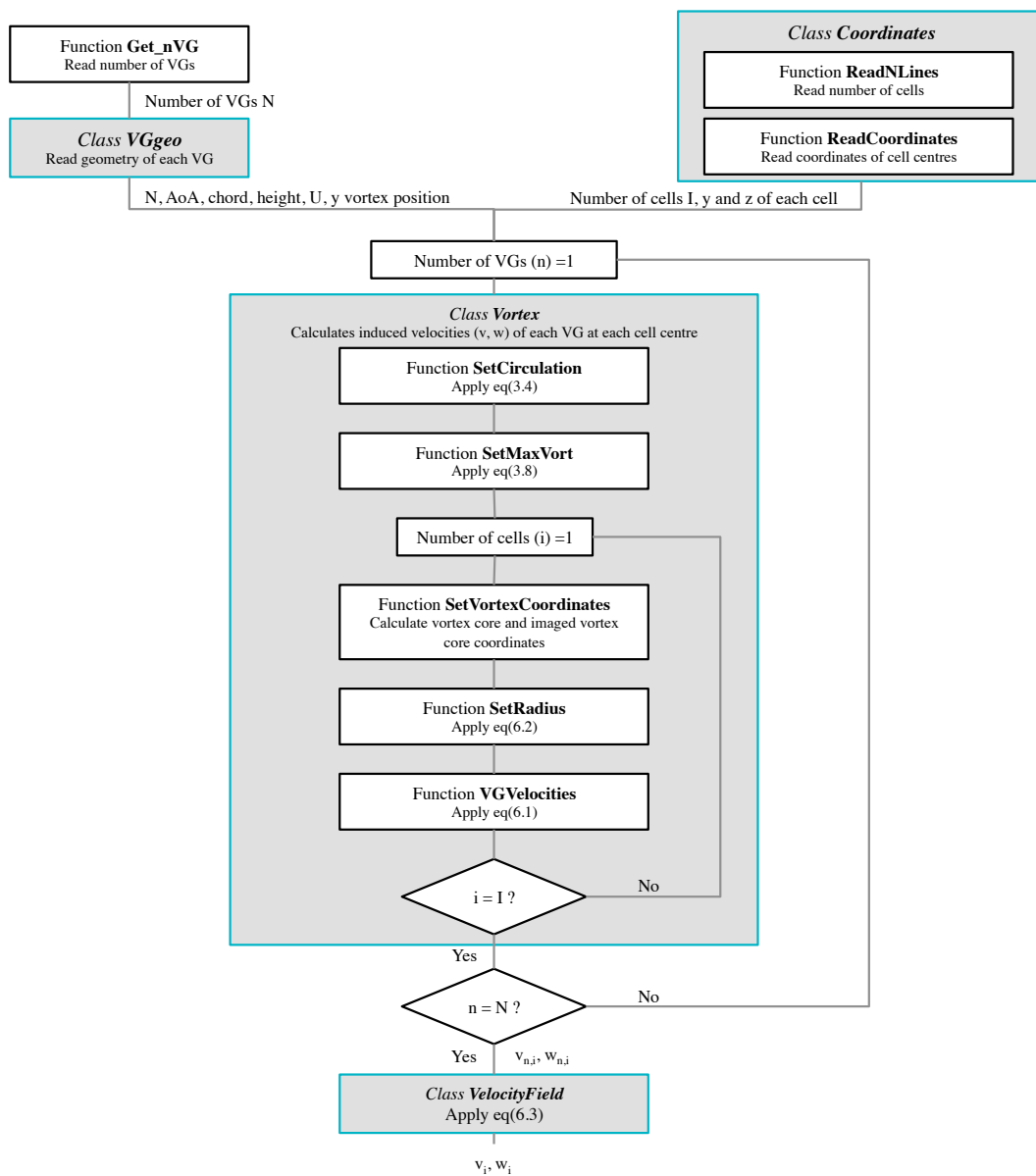


Figure 5.1: Flow chart of induced velocities code

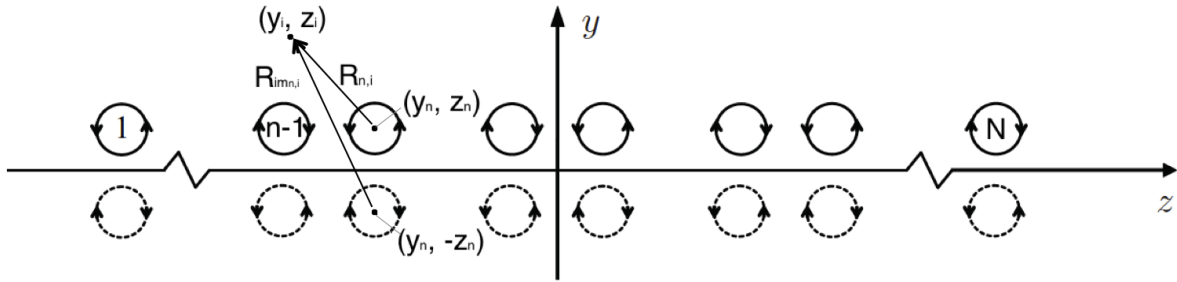


Figure 5.2: Vortex array with N real and mirror images and with cell i . Modified image from von Stillfried (2012).

With the 2D vortex velocity field calculated the only thing left is to introduce it in the open source CFD solver, OpenFOAM. This was done in a form of a velocity step boundary condition as described in section 3.1.

The already presented step boundary condition in OpenFOAM (*fixedJump*) only accounts for jumps of scalar properties like pressure. With a slight modification of the files from *fixedJump* and *jumpCyclic*, a boundary condition that also allows vector variable jumps was created. In appendix E the files of the new boundary condition, *myFixedJump* and *myJumpCyclic*, are shown.

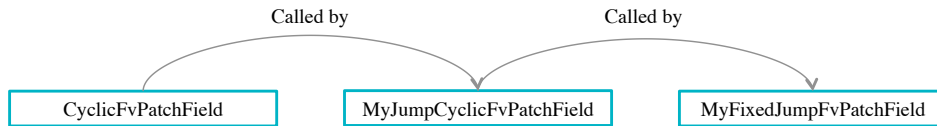


Figure 5.3: Simplified OpenFOAM class diagram

Additionally, during the mesh generation, it is necessary to create two boundary cyclic patches at $\Delta x/c = 1$. Both cyclic patches are addressed with the boundary condition *myfixedJump* and to one of those, the induced velocity at each cell is imposed. An example of the velocity boundary conditions file is shown in figure 5.4.

```

FoamFile
{
    version      2.0;
    format       ascii;
    class        volVectorField;
    location     "0";
    object       U;
}

dimensions      [0 1 -1 0 0 0 0];

internalField   uniform (15 0 0);

boundaryField
{
    inlet
    {
        type          fixedValue;
        value         uniform (15 0 0);
    }
    outlet
    {
        type          zeroGradient;
    }
    sides
    {
        type          symmetry;
    }
    wall_plate
    {
        type          fixedValue;
        value         uniform (0 0 0);
    }
    vortex_left
    {
        type          myFixedJump;
        patchType     cyclic;
        value         $internalField;
        jump          nonuniform List<vector>
                    5984
                    (
                    (0 -0.379749 0.001492)
                    ...
                    (0 -0.001445 -0.002192)
                    );
    }
    vortex_right
    {
        type          myFixedJump;
        patchType     cyclic;
        value         $internalField;
    }
    top
    {
        type          zeroGradient;
    }
}

```

Figure 5.4: Example of velocity boundary condition file with vortex imposed on the patch “*vortex_left*”

5.2 Verification Procedure

In Dudek (2006), the Wendt model and gridded VG are compared with experimental results for straight pipe and two S-Ducts. In order to verify that the Wendt Model implementation was done correctly, a simulation with the same characteristics of the straight pipe flow VG model simulation presented in Dudek (2006) was conducted.

In Dudek (2006) only a section of 30° of the pipe was simulated. This pipe has 237.5cm length and 20.4cm of diameter. As one can see in figure 5.5, a single VG was mounted with its the leading edge in the middle of the section, at 15° . The simulated VG, with the same characteristics of the one used in the experimental study presented in Dudek (2006), was approximated to a thin flat plate and has height of $h = 1.02\text{cm}$, chord of $c = 4.06\text{cm}$ and an angle of attack equal to $\alpha = 16^\circ$. In Dudek (2006) simulation, the VG was mounted at $x = 114\text{cm}$ where the boundary layer thickness, equal to $\delta = 8.16\text{mm}$, and the pipe core velocity, equal to 85m/s , matched the experimental one. Furthermore, a coarse grid was used to initialize a fine grid. Both Mentor SST and SA turbulence models were used and compared with each other in Dudek (2006).

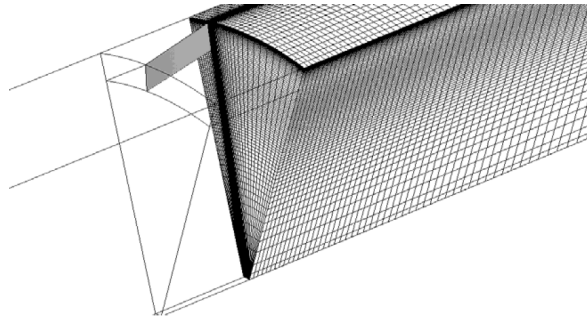


Figure 5.5: Fine computational grid behind the VG used in the gridded VG and Wendt model simulations performed by Dudek (2006).

In order to infer if the Wendt model was implemented correctly, the same straight pipe with the VG was simulated using SA turbulence model and compared with the correspondent results obtained in Dudek (2006).

To obtain a pipe core velocity of $U_\infty = 85\text{m/s}$ at the streamwise position where the boundary layer thickness equals the experimental value, a combination of eddy viscosity ratio of $\chi = 0.04$ and an inlet velocity of $U_{inlet} = 82.5\text{m/s}$ were used. The VG vortex was placed at 46.41cm from the inlet.

Furthermore, similarly with Dudek (2006) simulation, a coarse grid was used to initialize the fine grid. As one can see in figure 5.6, the mesh is non-uniform in streamwise and radial directions. In addition, the grid has 1.12 million cells and average $y^+ = 3.65$.

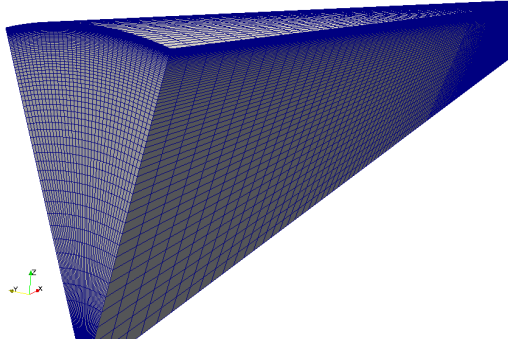


Figure 5.6: Fine computational grid used in the pipe flow simulation.

Figure 5.7 shows the vortex peak vorticity at different streamwise positions found by experimental means by Dudek (2006), Wendt model simulation performed by Dudek (2006) and the implemented Wendt model simulation. As one can see, the difference between the peak vorticity found in Dudek (2006) and the implemented one is very small. The largest difference is found at the first point, where the grid size influences more.

Besides the peak vorticity, the velocity contours at different streamwise positions were compared, see figure 5.8. Despite some small differences, it can be seen that the obtained flow fields are very similar.

Due to a good match between peak vorticity and velocity contours, the model is considered to be implemented correctly.

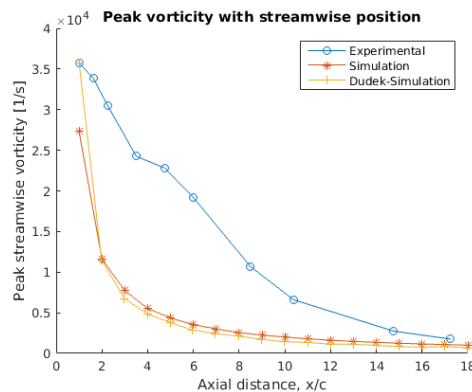


Figure 5.7: Peak vorticity comparison between Dudek implementation, author implementation and experimental results

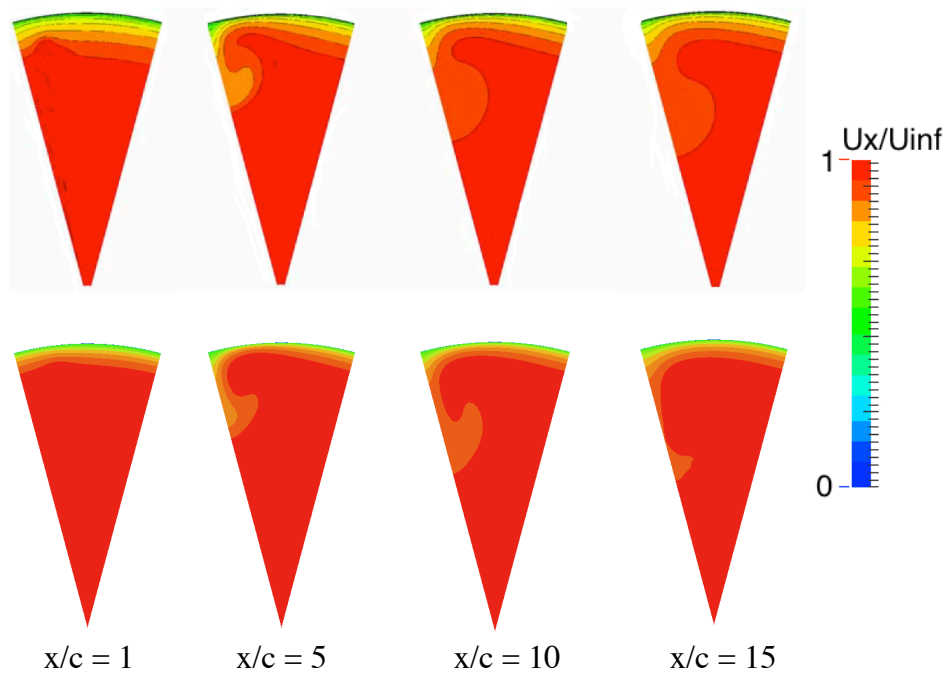


Figure 5.8: Dudek velocity contours (top) compared with writer velocity contours (bottom) at different streamwise stations.

Part IV

Analysis of the Wendt Model

Chapter 6

Analysis of the Wendt Model

In order to understand how does the Wendt model perform when compared with the gridded VG simulations, it was elaborated three different case studies of a flat plate flow with no pressure gradient and with a pair of counter-rotating VG. These three cases will serve to test the model when applied to a flow condition that lies in the middle of the parameters range tested by [Wendt et al. \(1995\)](#) (*case 2*), another that lies in the limit (*case 1*) and one that lies outside the parameter range (*case 3*).

In section 6.1, the description of each test case is presented. The comparison between the Wendt model and gridded VG simulation is done in section 6.2. Furthermore, in order to assess if the Wendt model can be implemented without mirror vortices, a comparison between the model implemented with and without mirror vortices is done in section 6.3.

6.1 Test Cases

In the *case 1*, *case 2* and *case 3*, two simulations of a flat plate with a pair of counter rotating VG were setted-up and compared. In one, the VG is gridded, and in the other, the Wendt model is used.

The test cases are inspired on the one described in [Florentie et al. \(2014\)](#). In the *case 1* and in the *case 2* the freestream velocity equals $U_\infty = 85m/s$. This velocity corresponds to the one used in most experimental tests made by [Wendt \(2001\)](#). In order to obtain a height-to-boundary-layer-thickness-ratio that lies in the limit of the parametric study range and another that lies in the middle, the location of the VG as well as the vanes height varied from *case 1* to *case 2*. In the *case 1*, the vanes leading edges are placed at $L = 1219.15m$ and are their height is $h = 5mm$. With these conditions the height-to-boundary-layer-thickness-ratio is $\frac{h}{\delta} = 0.3$. In the *case 2* the vanes leading edges are placed at $L = 0.973m$ from inlet, the VG height is $h = 8mm$ and the height-to-boundary-layer-thickness-ratio equals $\frac{h}{\delta} = 0.67$. In addition to the two previous cases, in order to understand how the Wendt model performs when applied to an unknown condition, a case with lower freestream velocity condition was

created. The *case 3* is a replica of the one described in Florentie et al. (2014), where the freestream velocity equals $U_\infty = 15m/s$, the VG height equals $h = 5mm$, the VG is placed at $L = 0.973m$ and the height-to-boundary-layer-thickness-ratio is $\frac{h}{\delta} = 0.34$.

In all the three cases, the VGs are placed at an incidence angle of $\alpha = 18^\circ$, the vanes trailing edges are $D = 12.5mm$ apart from each other and the vanes chord is $c = 12.5mm$. The VG geometry and flow conditions used in each test case are described in the table 6.1.

While in the *gridded VG simulation* the vanes are thin plates, in the *Wendt model* the vortices velocity profile is imposed at a chord length from the VG trailing edge. Besides the VG characteristics presented before, in order to calculate the velocity profile, the vortices location is also required. As suggested by Dudek (2006), the vortices were placed a chord length downstream the VG, and at the same trailing edge lateral and vertical positions. In the table 6.1, the vortices positions of each case are indicated.

	$U_\infty[m/s]$	$\alpha[^\circ]$	$c[mm]$	$h[mm]$	$\frac{h}{\delta}[-]$	distance between vanes ($D[mm]$)	VG x-location $L[m]$
Case 1	85	18	12.5	5	0.3	12.5	1.22
Case 2	85	18	12.5	8	0.67	12.5	0.973
Case 3	15	18	12.5	5	0.34	12.5	0.973
	Vortex x -position [mm]		Vortex y -position [mm]		Vortex z -position [mm]		
Case 1	1243.69		± 6.25		5		
Case 2	997.58		± 6.25		8		
Case 3	997.58		± 6.25		5		

Table 6.1: Flow characteristics and VG geometry details.

6.1.1 Computational Strategy

In order to determine the VG x -position that corresponds to the desired boundary layer thickness, a *flat plate without VGs simulation* was prepared for each case and the boundary layer along the plate was determined for each. The *flat plate without VGs simulations* were setted-up with uniform freestream velocity, no pressure gradient and lateral symmetry boundary conditions.

To reduce the number of iterations to steady state and enhance computational stability, the results from the *flat plate without VGs simulations* were used to initialize the *gridded VG* and the *Wendt model* simulations.

Furthermore, according to Florentie et al. (2014), the $k - \omega$ SST turbulence model is capable of accurately representing the vortex dissipation and decay. As so, this turbulence model was chosen to perform the simulations and a turbulence intensity of 0.01% has been used.

With respect to the discretization schemes, in the *gridded VG simulations* first order schemes were used in the convective terms, fully orthogonal schemes were used for diffusive terms and the Gauss method was used for the gradient terms. In the *Wendt model simulations*, in the *case 1* and *case 2*, the same discretization schemes used in the *gridded simulations* were used; in the *case 3*, the convective terms were discretized with second order schemes.

6.1.2 Mesh Details

To ensure that the results obtained in the *gridded VG* and *Wendt model* have a negligible discretization error, a mesh independence study was performed for each simulation of the *case 1* and the *case 3*. The discretization error of each was calculated with Richardson extrapolation method.

As one can see in figure 6.1, in the *gridded VG simulations* there is a mesh refinement in the space that enclosure the VG. Downstream the VG location the meshes used in the *gridded VG simulations* are identical to the ones of the *Wendt model simulations* and present a refinement in y in the VG trailing edge location and a refinement in z near the wall, see figure 6.2.

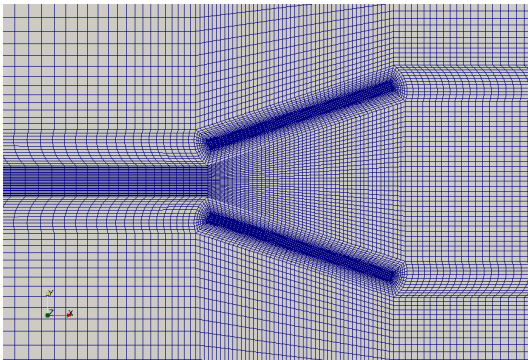


Figure 6.1: Bottom view of a coarse mesh with gridded VG.

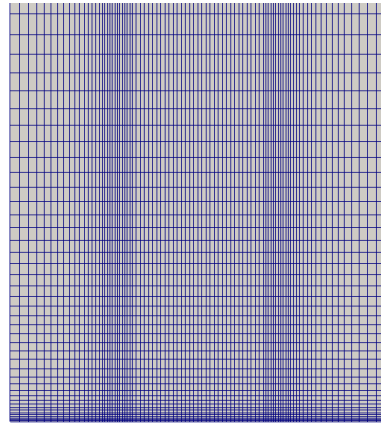


Figure 6.2: Front view of a coarse mesh downstream the VG position.

Case 1

In the *gridded VG simulation*, the *mesh 1* was created with a level of refinement of 2 in all the directions with respect to the *mesh 3*. The *mesh 2* lies in the middle of the two.

In the *Wendt model simulation*, three grids were created with a factor of refinement of 2 in all directions. The mesh size together with the average y^+ of each simulation are presented in the table 6.2.

<i>Gridded VG</i>	Mesh 1	Mesh 2	Mesh 3
Mesh Size [million cells]	32.7	13.8	4.1
Average y^+	0.69	0.92	1.37
Relative error ϵ_{Γ} [%]	3.93	7.3	16.55
Absolute error ϵ_{Γ} [m^2/s]	0.00998	0.01916	0.04374
<i>Wendt Model</i>	Mesh 1	Mesh 2	Mesh 3
Mesh Size[million cells]	12.4	1.5	0.2
Average y^+	0.66	1.31	2.59
Relative error ϵ_{Γ} [%]	0.51	0.56	0.98
Absolute error ϵ_{Γ} [m^2/s]	0.00064	0.00071	0.00125

Table 6.2: Case 1: Mesh details of the gridded VG simulations and VG model simulations.

The circulation, peak vorticity and shape factor obtained with each *gridded VG* mesh is shown in figure 6.3, figure 6.4 and figure 6.5 respectively. It can be seen that the meshes present a slightly higher difference between each other on the circulation and shape factor than on the peak vorticity. Still, it can be said that the results found are converging towards the most refined grid, mesh 1.

In table 6.2 the absolute and relative circulation errors of each mesh are presented. Once the average circulation discretization error of *mesh 1* along the domain is below 5% - corresponding a variation of $\Gamma_{computational} = \Gamma \pm 0.01m^2/s$ - this mesh was chosen to perform the comparison between the *Wendt model* and the *gridded VG* simulations. It should be noticed however that the discretization error is still high.

It would be also important to compute the discretization error for the shape factor. However it was found that the three meshes are not in the asymptotic part. A more refined mesh should have been done, although due to computational constrains this was not possible.

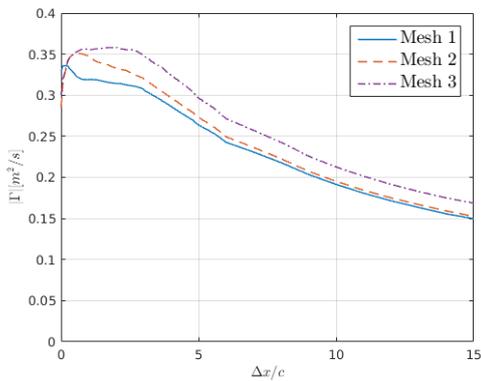


Figure 6.3: Mesh study case 1, gridded VG: Circulation with streamwise position.

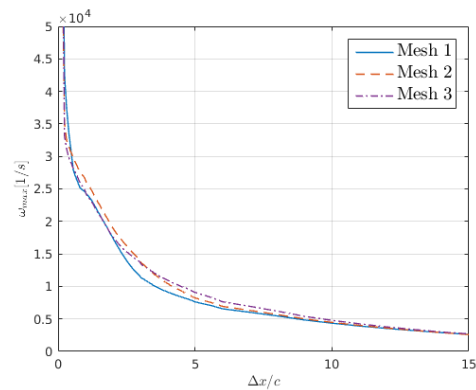


Figure 6.4: Mesh study case 1, gridded VG: Peak vorticity with streamwise position.

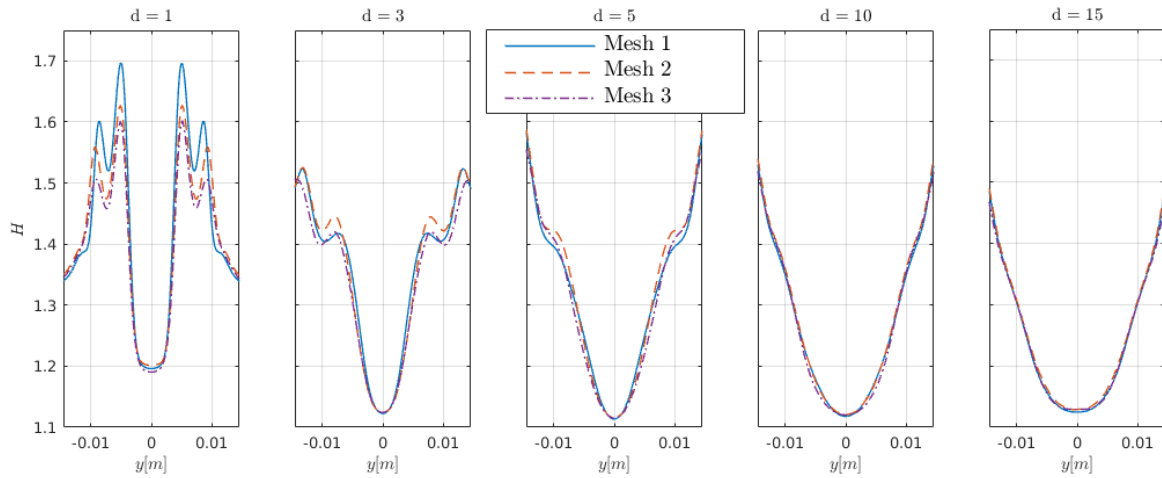


Figure 6.5: Mesh study case 1, gridded VG: Shape factor at $d = \Delta x/c = 1, 3, 5, 10, 15$.

With respect to the *Wendt model simulation*, as one can see in figure 6.6, figure 6.7 and figure 6.8, very little difference is found between meshes. The solutions found with *mesh 1* and *mesh 2* present a discretization error that is below 1%, therefore both meshes could had been used and *mesh 1* was chosen to perform the comparison between the *Wendt model* and the *gridded VG* simulations. This mesh presents a circulation discretization error of 0.5%, to which it corresponds a variation of $\Gamma_{\text{computational}} = \Gamma \pm 0.0006 \text{ m}^2/\text{s}$, much smaller than the variation found in the *gridded VG simulation*, $\Gamma_{\text{computational}} = \Gamma \pm 0.0010 \text{ m}^2/\text{s}$.

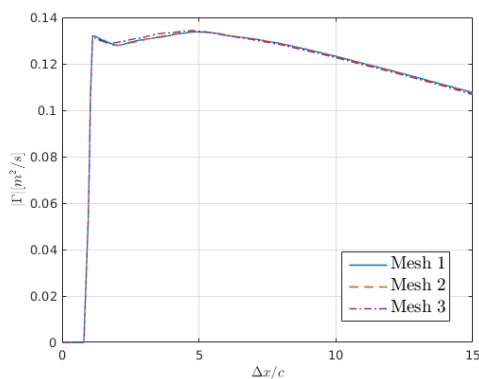


Figure 6.6: Mesh study case 1, Wendt model: Circulation with streamwise position.

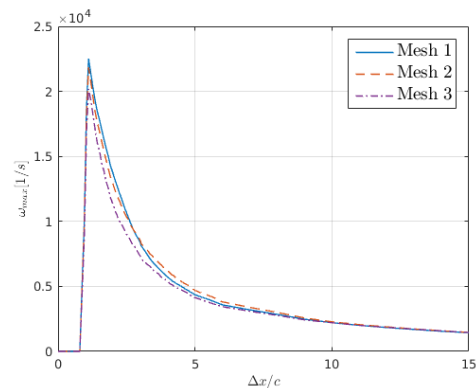


Figure 6.7: Mesh study case 1, Wendt model: Peak vorticity with streamwise position.

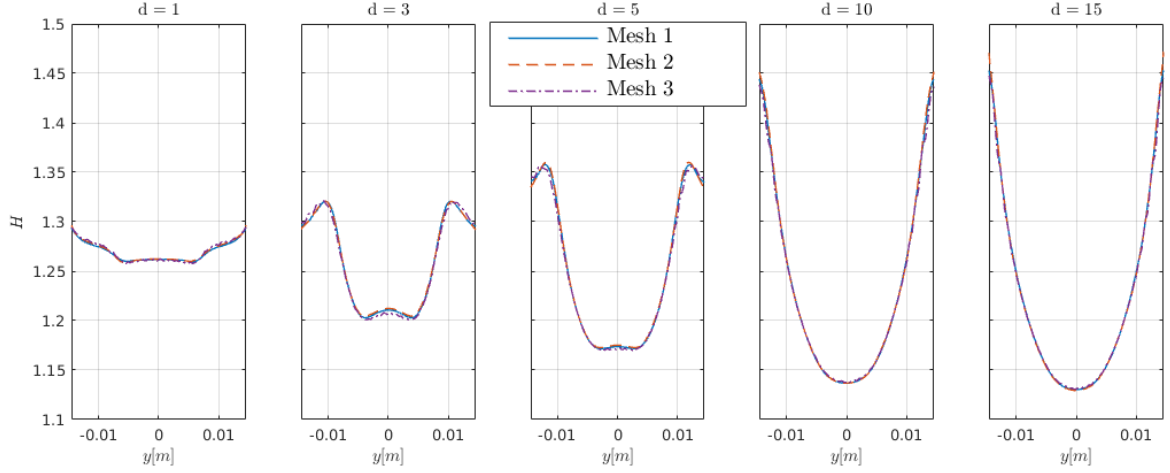


Figure 6.8: Mesh study case 1, Wendt VG: Shape factor at $d = \Delta x/c = 1, 3, 5, 10, 15$.

Case 2

Because the same freestream velocity is used in the *case 1* and in the *case 2*, it was chosen to use the same *meshes 1* presented before. With those, in the *gridded VG simulation* a $y^+ = 1.10$ was found and in the *Wendt model simulation* a $y^+ = 1.11$ was found.

Case 3

The mesh used in the *gridded VG simulation* corresponds to the named “*body fitted - medium mesh*” from Florentie et al. (2016). The circulation and shape factor errors of this mesh can be seen in the table 6.3.

For the *Wendt model simulation* three grids with a factor of 2 refinement in x , y and z directions were created. In figure 6.9, figure 6.10 and figure 6.11, the circulation, peak vorticity and shape factor obtained with each mesh are presented. One can see that the difference between *mesh 1* and *mesh 2* is negligible for all the parameters, and that the shape factor does no longer oscillate as in the *mesh 3* solution.

The circulation and shape factor discretization errors in both *mesh 1* and *mesh 2* are below 1%, and so the *mesh 2* was chosen to perform the comparison between the *gridded VG simulation* and the *Wendt model simulation*, table 6.3. This mesh presents an absolute circulation error of $\Gamma_{computational} = \Gamma \pm 0.00008 m^2/s$, that is slightly smaller than the one found in the *gridded VG simulation*; and an absolute shape factor error of $H_{computational, \frac{\Delta x}{c}=15} = H_{\frac{\Delta x}{c}=15} \pm 0.0072$, slightly bigger than the one found in the *gridded VG simulation*.

	Gridded VG	Wendt Model		
		Mesh 1	Mesh 2	Mesh 3
Mesh size[millions cells]	1.622	1.388	0.173	0.021
Average y^+	1.83	0.89	1.72	3.30
Relative error ϵ_{Γ} [%]	1.7	0.18	0.29	1.12
Absolute error ϵ_{Γ} [m^2/s]	0.00067	0.00005	0.00008	0.00031
Relative error $\epsilon_{H_{\frac{\Delta x}{c}=15}}$ [%]	0.20	0.45	0.55	0.74
Absolute error $\epsilon_{H_{\frac{\Delta x}{c}=15}}$ [-]	0.003	0.0069	0.0072	0.0098

Table 6.3: Case 3: Mesh details of the gridded VG simulations and Wendt model simulations.

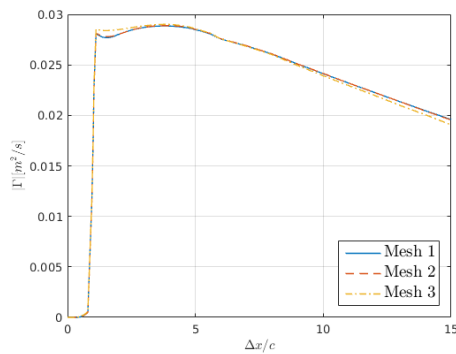


Figure 6.9: Mesh study case 3, Wendt model: Circulation with streamwise position.

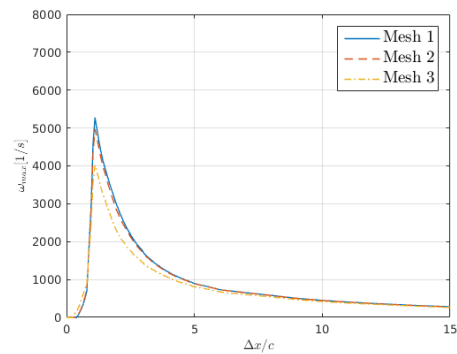


Figure 6.10: Mesh study case 3, Wendt model: Peak vorticity with streamwise position.

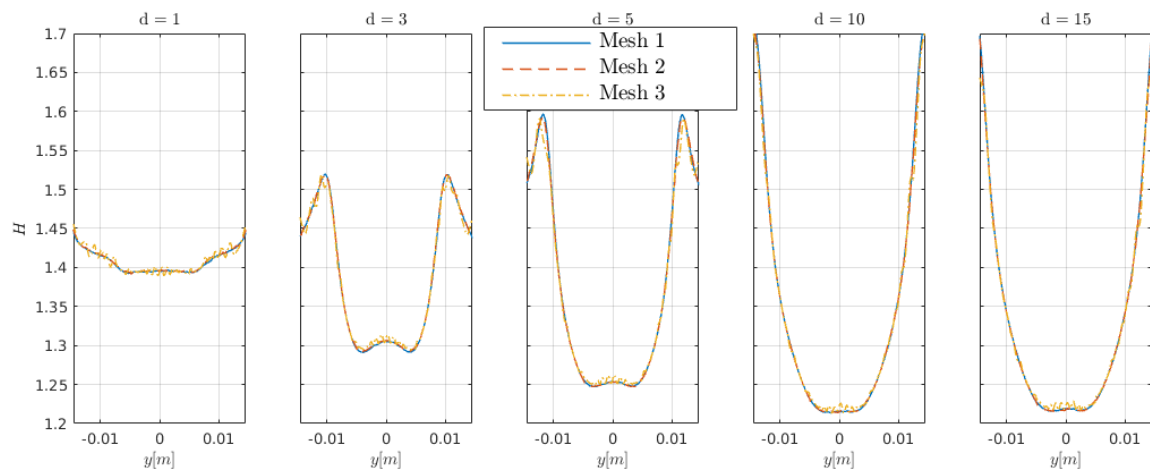


Figure 6.11: Mesh study case 3, Wendt model: Shape factor at $d = \Delta x/c = 1, 3, 5, 10, 15$.

6.2 Comparison between the Wendt Model and the Gridded VG Simulations

In this section the results found with the *Wendt model simulation* and the *gridded VG simulation* will be compared analysed for each case. The relative Wendt model error presented during the analysis were calculated with

$$\epsilon_x = \frac{|(x_{gridded} - x_{wendt})|}{x_{gridded}} * 100, \quad (6.1)$$

where x stands for any variable.

6.2.1 Case 1

The vortex circulation of both simulations (*gridded VG simulation* and *Wendt model simulation*) is show in figure 6.12. As one can see, the circulation is highly underpredicted by the model, specially near the vane. Because the height-to-boundary-layer-thickness-ratio is very low $\frac{h}{\delta} < 0.3$, an underpredicted circulation at $\frac{\Delta x}{c} = 1$ was not a surprise, see figure 4.5.

In the region between $1 < \frac{\Delta x}{c} < 5$, the difference between the *gridded VG simulation* and the *Wendt model simulation* lies between 50% and 59% - much higher than the discretization error $\pm 4\%$ -, see table 6.4. This error however decreases with streamwise position since the vortex decay is smaller in the *Wendt model simulation*.

The peak vorticity in the *Wendt model simulation* shows a reasonable agreement with the one found in the *gridded VG simulation*, see figure 6.13. At $\frac{\Delta x}{c} = 1$ the peak vorticity is only slightly underpredicted, $\epsilon_{\omega_{max}} = 1\%$. Despite the initial agreement, it can be seen that the peak vorticity in the *Wendt model simulation* decreases much faster than in the *gridded VG simulation*. The vortex dissipation is much higher in the *Wendt model simulation*.

Figure 6.14 shows the vortex radius with streamwise position. As one can see, due to the circulation underprediction, at $\frac{\Delta x}{c} = 1$ the vortex in the *Wendt model vortex* is smaller than in the *gridded VG simulation*. Due to vortex dissipation, the vortex grows with streamwise position. And far from the VG, the vortex in the *Wendt model simulation* will be bigger than the vortex in the *gridded VG simulation*.

	$\frac{\Delta x}{c} = 1$	$\frac{\Delta x}{c} = 3$	$\frac{\Delta x}{c} = 5$	$\frac{\Delta x}{c} = 10$	$\frac{\Delta x}{c} = 15$	Average
Circulation $\epsilon_{\Gamma} [\%]$	58.55	57.54	49.69	35.09	28.06	52.76
Peak Vorticity $\epsilon_{\omega_{max}} [\%]$	1.14	27.87	43.32	49.09	45.02	31.07
Radius $\epsilon_R [\%]$	33.44	22.59	3.61	9.48	7.56	18.62

Table 6.4: Case 1: Error Analysis.

6.2 Comparison between the Wendt Model and the Gridded VG Simulations 49

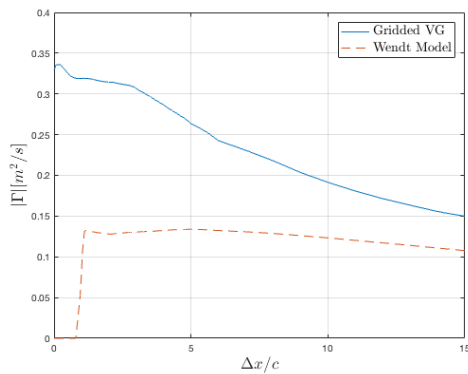


Figure 6.12: Case 1: Vortex circulation with streamwise position.

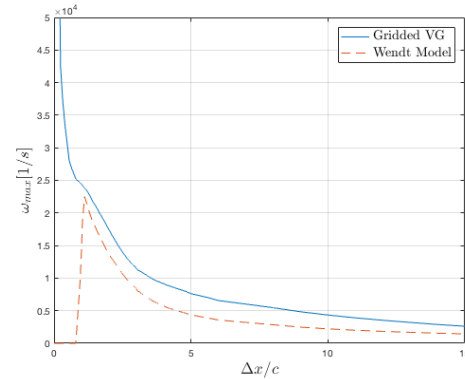


Figure 6.13: Case 1: Peak vorticity with streamwise position.

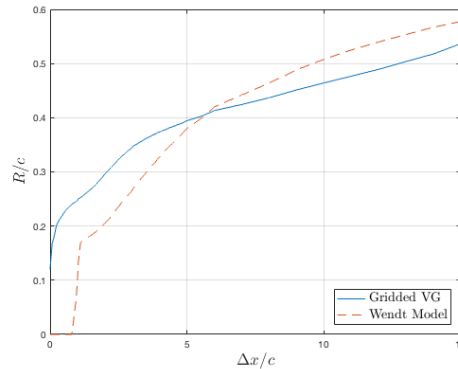


Figure 6.14: Case 1: Vortex radius with streamwise position.

When looking at the vorticity field, it is possible to understand why the vortex of the *Wendt model simulation* presents a lower circulation decay and a higher vortex dissipation than the vortex from the *gridded VG simulation*.

Let us first study why the vortex dissipation is higher in the *Wendt model simulation*. As pointed by [Bray \(1998\)](#), a vortex in free space (outside the boundary layer) tends to grow faster than an embedded vortex (inside the boundary layer). The sudden growth or vortex breakdown of a free vortex seems to be caused by a “large deceleration of the core in the streamwise direction” and does not usually occur in embedded vortices, [[Bray \(1998\)](#)]. Figure 6.15 shows the streamwise vorticity field at different streamwise positions. As one can see, in the *gridded VG simulation* the vortices cores are below the vortices cores of the *Wendt model simulation*. Furthermore it can be seen that in the *gridded VG simulation* the vortices are flattened until $\frac{\Delta x}{c} = 5$. As consequence, in contrast with the *Wendt model vortices*, the *gridded VG vortices* are very near the wall, and so these will grow at a slower pace - the vortex dissipation will be lower - than in the *Wendt model simulation*.

As reported in Westphal et al. (1987), the vortex flattening happens when a vortex shed by a VG measures about 50% of the VG height. This phenomena is even more pronounced in a VG pair, where, due to the action of the neighbour vortex, the core is pushed downwards, [Lögberg et al. (2009)]. In the *Wendt model simulation*, the flattening is non-existent because the model is derived from Prandtl equation, and so, at $\frac{\Delta x}{c} = 1$ the *Wendt model* predicts a circular and more concentrated vortex than in reality. As consequence the vortex takes more time to meet the condition $R_{vortex} > 0.5h_{VG}$. Furthermore because the vortices cores in the *Wendt model simulation* are more apart from each other, the downward influence of the neighbour vortex will be smaller than in the *gridded VG simulation*.

Let us now look at the circulation decay. As explained in chapter 1, one of the main decay mechanism is the wall friction. Due to the non-slip condition, a rather high azimuthal velocity gradient and consequently a zone with high vorticity and opposite sign to the vortex vorticity appears at the wall. Due to the negative effect of the wall vorticity in the vortex, the angular momentum and circulation are reduced, [Lögberg et al. (2009)].

As indicated before, the *Wendt model vortex* is farther from the wall than the *gridded VG vortex*. Furthermore, because the strength of the vortex is smaller in the *Wendt model simulation*, the vortex velocity near the wall is also smaller. Together these facts will result on a smaller azimuthal velocity gradient at the wall, and so, a smaller wall vorticity. This is specially true near the vane (where the vortex radius is still very small). Thereafter is understandable that the *gridded VG simulation* has a much higher circulation decay than the one presented in the *Wendt model simulation*.

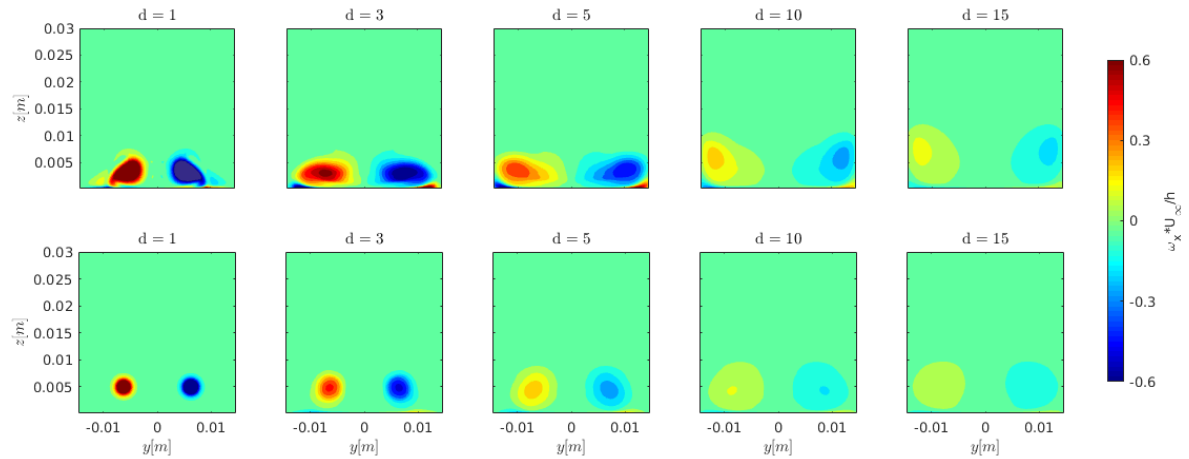


Figure 6.15: Case 1: Vorticity field, $\omega_x U_\infty / h$, at $d = \Delta x / c = 1, 3, 5, 10, 15$. On the top the gridded VG vorticity, on the bottom the Wendt model vorticity.

Because the goal of the VGs is to mix the low momentum fluid particles at the lower part of the boundary layer with the higher momentum fluid particles, besides parameters that characterize the vortex, it is important to look as well to the effect of the vortex in the boundary layer.

For counter-rotating VG arrays, the boundary layer becomes thicker on the outer part of the vortices, where the flow is pushed upwards, and thinner in the inner part of the vortices, where the flow is pushed downwards. This change should go along with an increase of streamwise velocity in the inner part of the vortices.

It can be seen in figure 6.16 that the *gridded VG vortex* is strong enough to produce the desired effect. However, near the vane the effect of the *Wendt model vortex* in the boundary layer is very small. Nevertheless the difference between the simulations decreases with streamwise position.

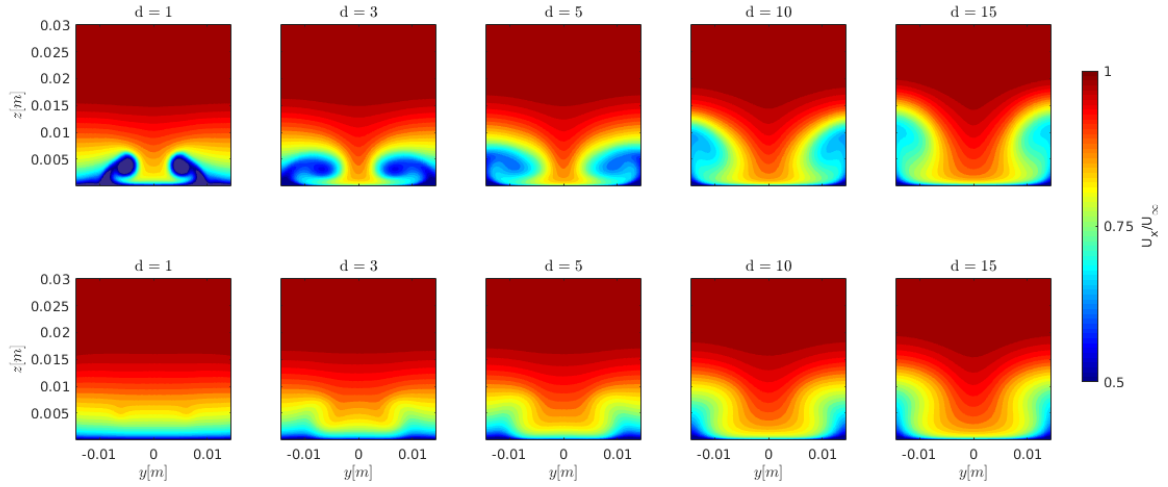


Figure 6.16: Case 1: U_x/U_∞ contour at $d = \Delta x/c = 1, 3, 5, 10, 15$. On the top the gridded VG velocity field, on the bottom the Wendt model velocity field.

Together with the streamwise velocity, the shape factor is a quantity that allows to understand how stable is the boundary layer and how far it is from separation. According to [Schubauer and Spangenberg \(1959\)](#), the presence of a vortex is equivalent to a decrease of adverse pressure gradient. In both situations the shape factor is decreased, the velocity profiles become fuller and the separation point is likely to be delayed.

In the outer part of the vortices, because the flow is pushed upwards, the streamwise velocity is reduced and both the displacement thickness and momentum thickness increase and so does shape factor. In the inner part of the vanes, where the flow is compressed against the wall, the displacement thickness, momentum thickness and shape factor decrease.

In figure 6.17, the shape factor at $\Delta x/c = 1, 3, 5, 10, 15$ is shown. One can see that the variations in shape factor are much smaller near the vane for the *Wendt model simulation*. However, the difference between both simulations decreases with streamwise position, and at $\frac{\Delta x}{c} = 15$ the agreement between shape factors is very good, $\frac{\overline{\epsilon H}}{\Delta x} = 1.75\%$. Since the vorticity field in the *Wendt model simulation* agrees well with the *gridded VG simulation*, a good agreement in the shape factor was also expected. Nevertheless it should be noticed that this fact is consequence of a conjugation of three major model flaws: underprediction of the vortex circulation at $\frac{\Delta x}{c} = 1$, underprediction of the vortex decay and overprediction of vortex dissipation.

It can be concluded that, when applied to a condition with low $\frac{h}{\delta}$ or low \mathcal{R} ratios, due to a circulation underestimation, the Wendt model will only provide an accurate shape factor at *one* certain point far from the vane.

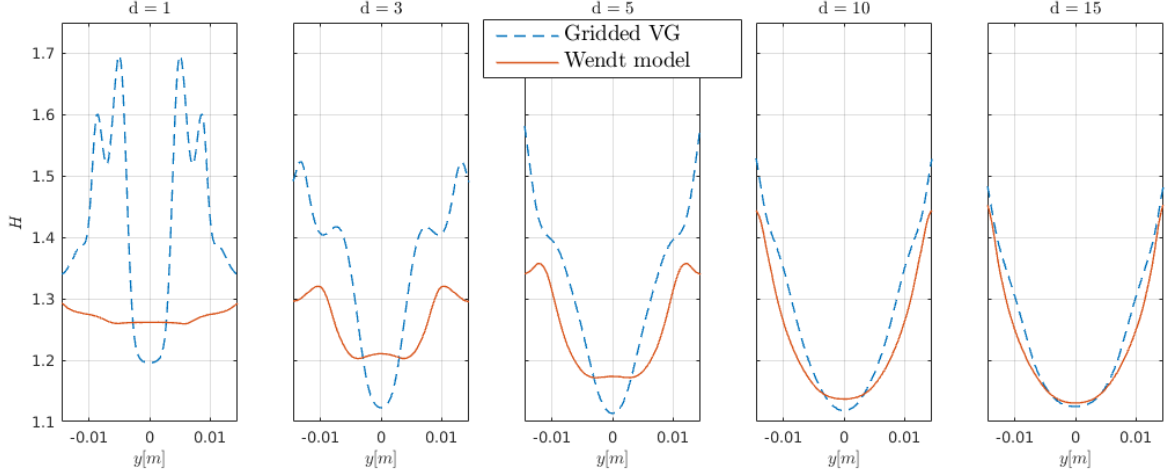


Figure 6.17: Case 1: Shape factor at $d = \Delta x/c = 1, 3, 5, 10, 15$.

6.2.2 Case 2

As one can see in the figure 6.18, the vortex in the *gridded VG simulation* is not entirely developed until $\frac{\Delta x}{c} = 5$. Even though, in contrast with the *case 1*, it can be said that the Wendt model is predicting reasonably well the vortex circulation. At $\frac{\Delta x}{c} = 1$ the difference between the *gridded VG simulation* and the *Wendt model simulation* is only $\epsilon_{\Gamma} = 3.44\%$, table 6.5. Again, the vortex decay in the *Wendt model simulation* is lower than in the *gridded VG simulation*, as so the circulation error will increase with streamwise position and an average circulation error of $\overline{\epsilon_{\Gamma}} = 9\%$ is found.

Furthermore, the peak vorticity is highly overpredicted, see figure 6.19. At $\frac{\Delta x}{c} = 1$, the difference between the simulations is $\epsilon_{\omega_{max}} = 253\%$, table 6.5. Consequently, it is not a surprise when at this position a much more concentrated vortex in the *Wendt model simulation* is found, figure 6.20. Also, because the vortex dissipation is much higher in the *Wendt model simulation*, a reasonable peak vorticity and radius agreement is found further downstream, see table 6.5.

In the figure 6.21 the vorticity field at different streamwise positions is shown. It can be seen that initially the *Wendt model vortex* is more concentrated and that it is placed above the location of the *gridded VG vortex*. As discussed in the previous case, the conjugation of these two factors will imply a lower vortex decay but an higher vortex dissipation.

Let us now analyse the shape factor and streamwise velocity field. As one can see in the streamwise velocity field figure 6.22, in the vicinity of the vanes, due to their physical presence, a much higher velocity deficit is found in the *gridded VG simulation*. As in the *Wendt*

6.2 Comparison between the Wendt Model and the Gridded VG Simulations 53

model simulation, the streamwise velocity deficit is consequence solely of the vortex presence, the streamwise velocity deficit near the vanes will be more concentrated and smaller. Because of this, near the vanes, a very different shape factor between simulations is found, see figure 6.23.

Far from the vanes however, since the vorticity field agrees reasonably well between simulations, a better shape factor agreement than $\overline{\epsilon H \frac{\Delta x}{c}} = 4\%$ was expected. It can be seen that the *Wendt model simulation* exhibits a wider shape factor profile than the *gridded VG simulation*. This may be consequence of an initial higher peak vorticity prediction in conjugation with an wider lateral vortex placement - the vortices in the *Wendt model simulation* are more apart than in the *gridded VG simulation* -.

Taking into consideration the shape factor profile found, it can be said that the Wendt model cannot be used to obtain an accurate shape factor near the vane. And that even when applied to a condition that lies in the middle of the parametric study made by [Wendt \(2001\)](#), the Wendt model produces inconsistent shape factor results far from the vanes.

	$\frac{\Delta x}{c} = 1$	$\frac{\Delta x}{c} = 3$	$\frac{\Delta x}{c} = 5$	$\frac{\Delta x}{c} = 10$	$\frac{\Delta x}{c} = 15$	Average
Circulation $\epsilon_{\Gamma} [\%]$	3.44	8.39	16.37	1.07	7.61	9.41
Peak Vorticity $\epsilon_{\omega_{max}} [\%]$	253.2	278.9	52.832	2.85	9.84	109
Radius $\epsilon_R [\%]$	49.98	34.48	24.24	7.73	6.6	30.51

Table 6.5: Case 2: Error Analysis.

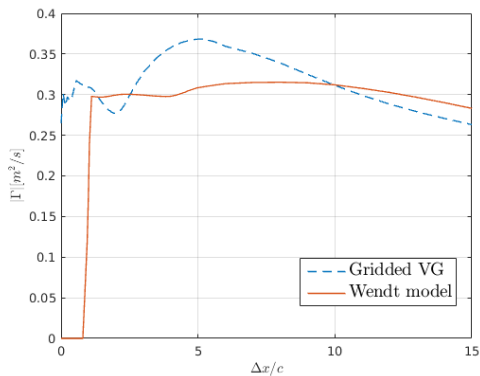


Figure 6.18: Case 2: Vortex circulation with streamwise position.

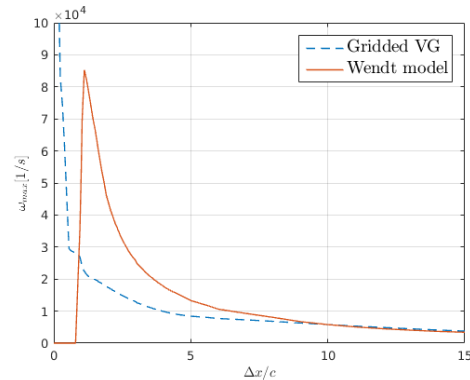


Figure 6.19: Case 2: Peak vorticity with streamwise position.

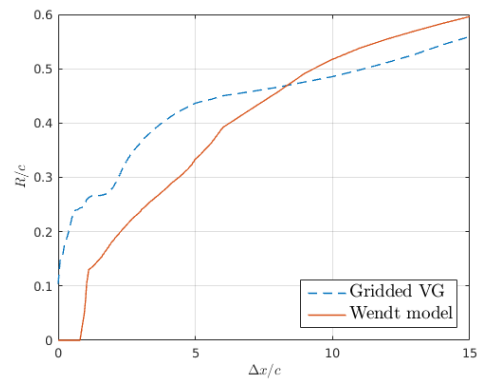


Figure 6.20: Case 2: Vortex radius with streamwise position.

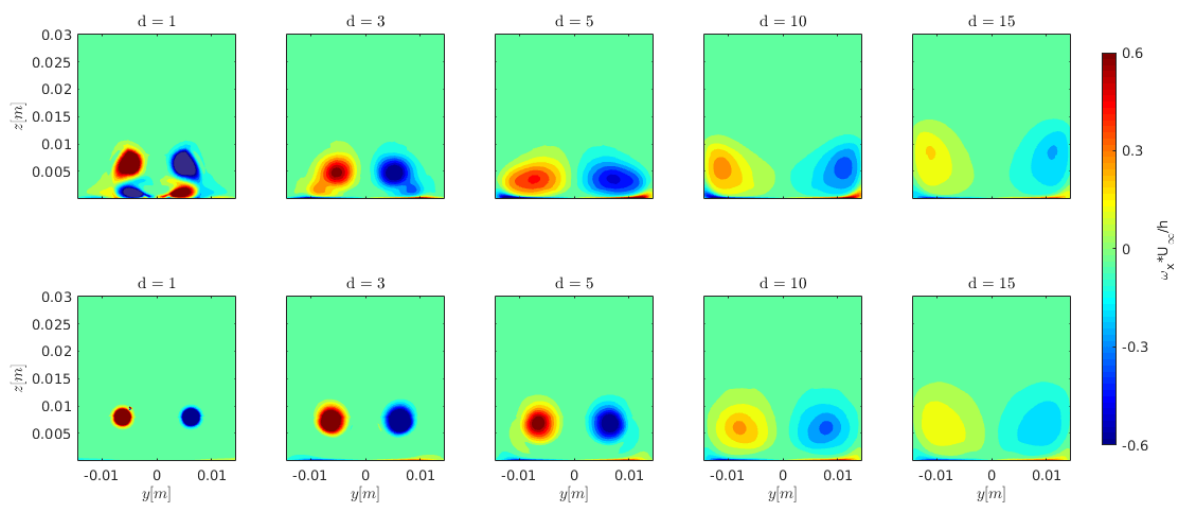


Figure 6.21: Case 2: Vorticity field, $\omega_x U_\infty / h$, at $d = \Delta x / c = 1, 3, 5, 10, 15$. On the top the gridded VG vorticity, on the bottom the Wendt model vorticity.

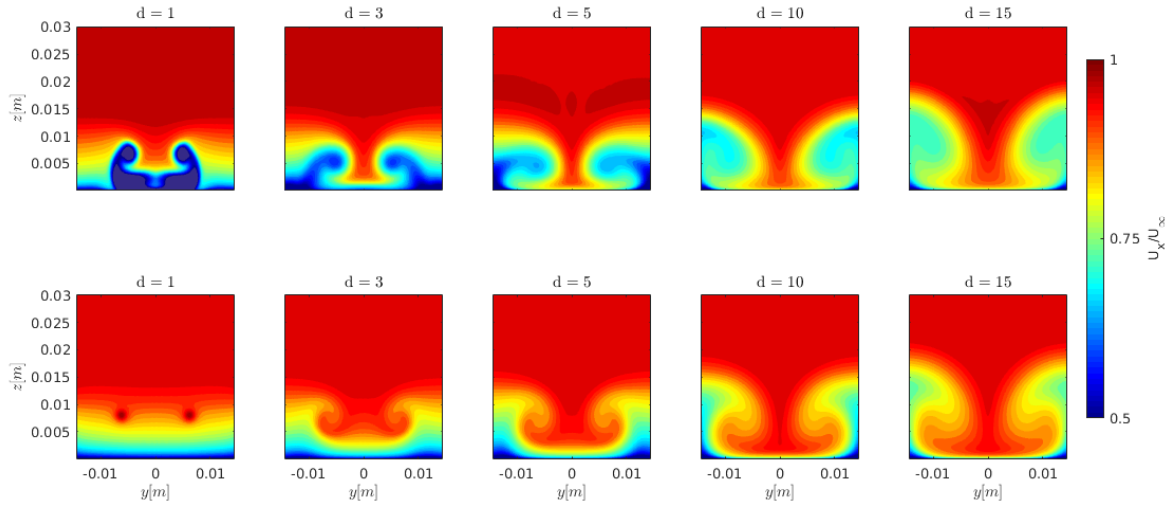


Figure 6.22: Case 2: Streamwise velocity field, $\frac{U_x}{U_\infty}$, at $d = \Delta x/c = 1, 3, 5, 10, 15$. On the top the gridded VG vorticity, on the bottom the Wendt model vorticity.

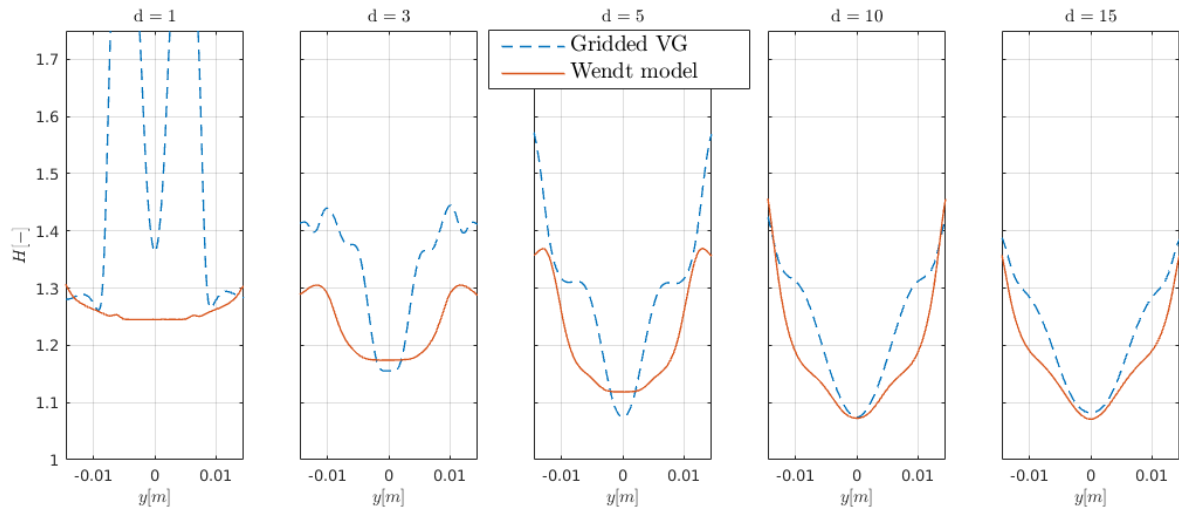


Figure 6.23: Case 2: Shape factor at $\Delta x/c = 1, 3, 5, 10, 15$.

6.2.3 Case 3

In the figure 6.24 and figure 6.25, the circulation and peak vorticity along the streamwise position is shown for both simulations. As one can see, at $\frac{\Delta x}{c} = 1$ the circulation is underestimated and the peak vorticity is overestimated by the Wendt model. Consequently, at this position, the vortex radius in the *Wendt model simulation* is much lower than in the *gridded VG simulation*. The quantitative error analysis can be seen in the table 6.6. Because in the *case 1*, the circulation was as well underpredicted and the peak vorticity was overpredicted,

the analysis of the *case 3* will not vary much from the one made in section 6.2.1.

	$\frac{\Delta x}{c} = 1$	$\frac{\Delta x}{c} = 3$	$\frac{\Delta x}{c} = 5$	$\frac{\Delta x}{c} = 10$	$\frac{\Delta x}{c} = 15$	Average
Circulation ϵ_{Γ} [%]	48.43	43.74	31.63	16.54	9.52	38.70
Peak Vorticity $\epsilon_{\omega_{max}}$ [%]	72.97	3.61	23.90	21.34	17.28	21.59
Radius ϵ_R [%]	46.08	26.73	10.07	0.61	1.76	24.12

Table 6.6: Case 3: Error Analysis.

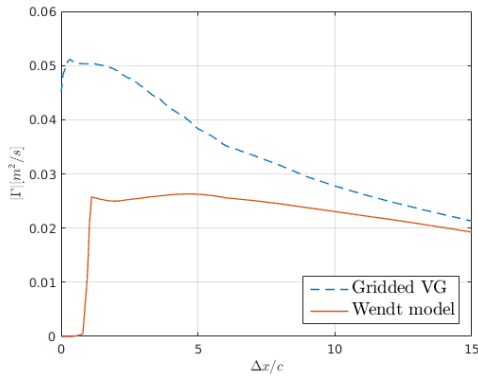


Figure 6.24: Case 3: Circulation with streamwise position.

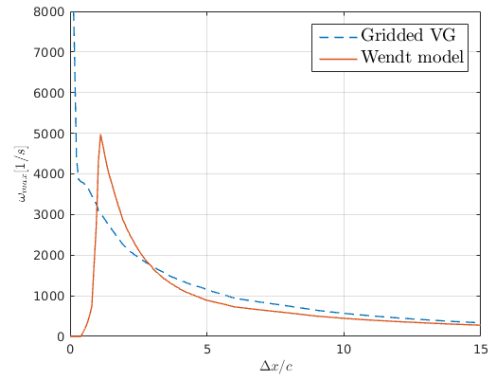


Figure 6.25: Case 3: Peak vorticity with streamwise position.

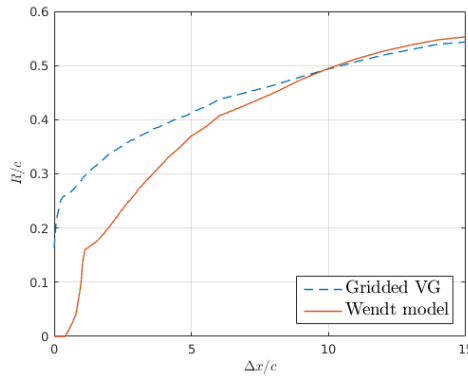


Figure 6.26: Case 3: Vortex radius with streamwise position.

Figure 6.27 shows the vorticity field at different streamwise positions. Again, the vortex from the *Wendt model simulation* is circular, much more concentrated and located above the one found in the *gridded VG simulation*. As result, the wall vorticity will be smaller in the *Wendt model simulation* as well as the circulation decay. Furthermore, the vortex dissipation will be higher and so will be the peak vorticity reduction with streamwise position, as explained in the section 6.2.1.

6.2 Comparison between the Wendt Model and the Gridded VG Simulations 57

When looking at the shape factor, figure 6.28, it can be seen that near the vane, where the circulation is underpredicted and the effect of the vane in the streamwise vorticity is still very large, the agreement between simulations is poor. After $\frac{\Delta x}{c} = 10$ however a reasonable agreement is found and at $\frac{\Delta x}{c} = 15$ the averaged shape factor error is $\overline{\epsilon H_{\frac{\Delta x}{c}=15}} = 2.4\% \pm 0.65\%$.

As a conclusion, it can be said that when one applies the model to a situation that does not lie in the range tested in the parametric study made by [Wendt \(2001\)](#), the circulation will most likely be underestimated, and so will be the shape factor near the vane. Consequently, it is not suggested to apply this model to an unknown condition if the separation point (without VGs) is near the VG location.

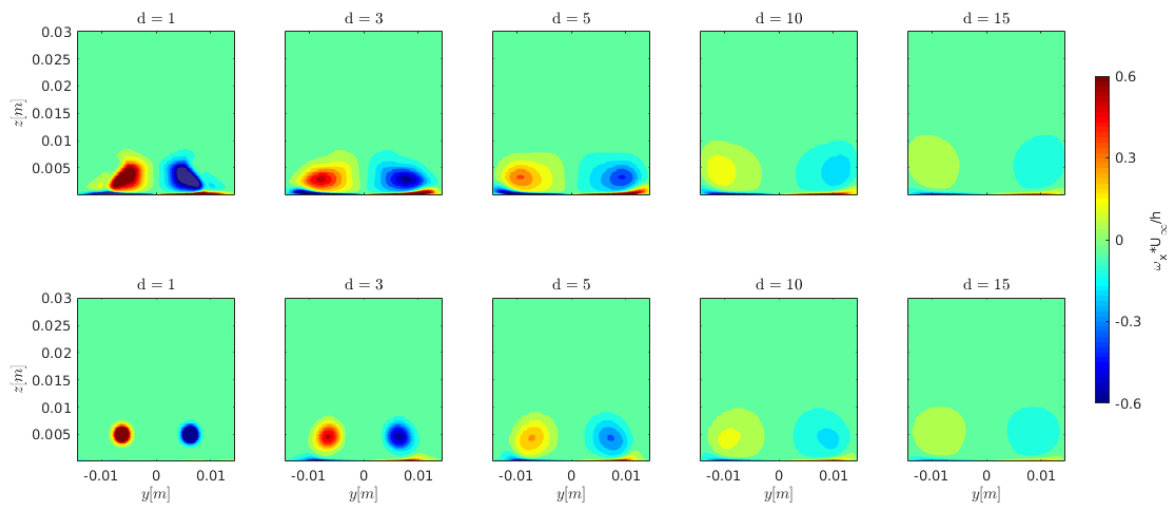


Figure 6.27: Case 3: Vorticity field, $\omega_x U_\infty / h$, at $d = \Delta x / c = 1, 3, 5, 10, 15$. On the top the gridded VG vorticity, on the bottom the Wendt model vorticity.

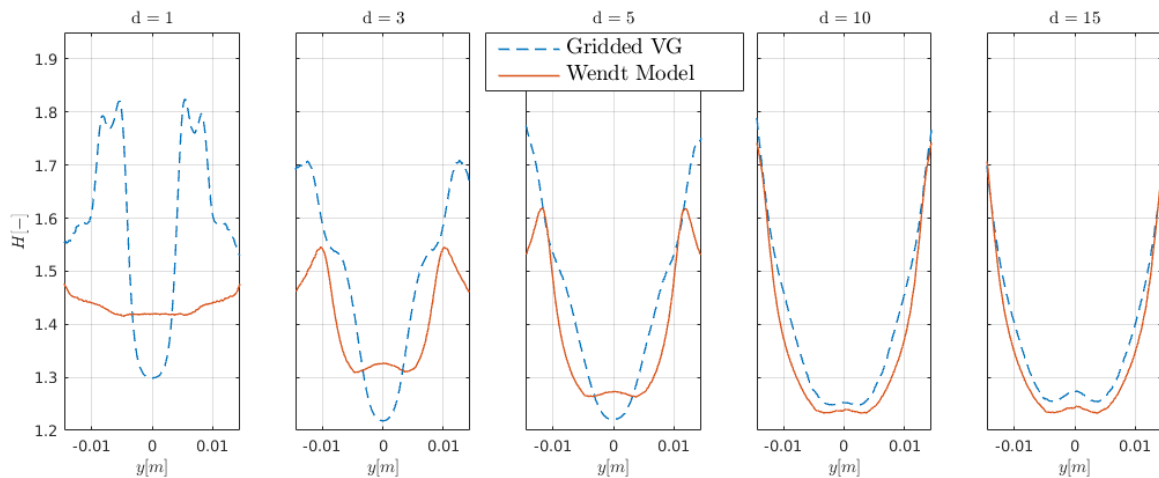


Figure 6.28: Case 3: Shape factor at $d = \Delta x / c = 1, 3, 5, 10, 15$.

6.3 Effect of the Mirror Vortices

During the implementation of the semi-empirical model, one can choose to equate the vortex velocity taking into account, or not, the mirror vortices as one can see in equation 3.2. Therefore it is important to understand the difference between each vortex formulation and to assess which will reproduce the vortex that is most similar to the one found in the *gridded VG simulation*.

Besides the *gridded VG* and the *Wendt model* simulations, another was set up, where the Wendt model was used without mirror vortices, the *without mirror vortices simulation*.

The mirror vortices are introduced to ensure that at the wall the impermeability condition is met. They will although alter the vortex velocity. At the same time that the mirror vortex induces an increase of velocity at the wall, it induces a decrease of velocity at the upper part of the real vortex. Furthermore it causes the U_z velocity to decrease. As one can see in figure 6.29, to each vertical vector velocity represented there is a imaged counter-part with opposite sign.

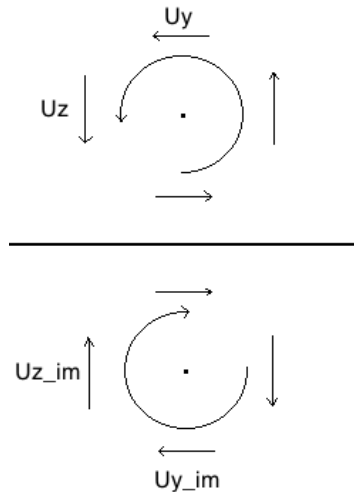


Figure 6.29: Schematic representation of the real and mirror vortices.

Figures 6.30 and 6.31 present the U_y velocity profile at different streamwise positions for the *case 1* and *case 3* respectively. For both cases, it can be seen that the velocity U_y is stronger at the wall in the simulations *with mirror vortices*. And that at the upper part of the vortex, the difference in the velocity profiles between the simulations *with* or *without mirror vortices* is negligible. It should also be noticed that the non-slip condition is met in all the simulations. In addition, the figures 6.32 and 6.33 show the U_z velocity profiles of both *case 1* and *case 3*. It can be seen that in both cases, the velocity U_z is stronger in the simulations *without mirror vortices*. Also, the impermeability condition is nicely met in both *with mirror vortices* and *without mirror vortices* simulations. As a consequence, since the impermeability condition overrules the velocity profile imposed, the addition of mirror vortices is not imperial in OpenFOAM.

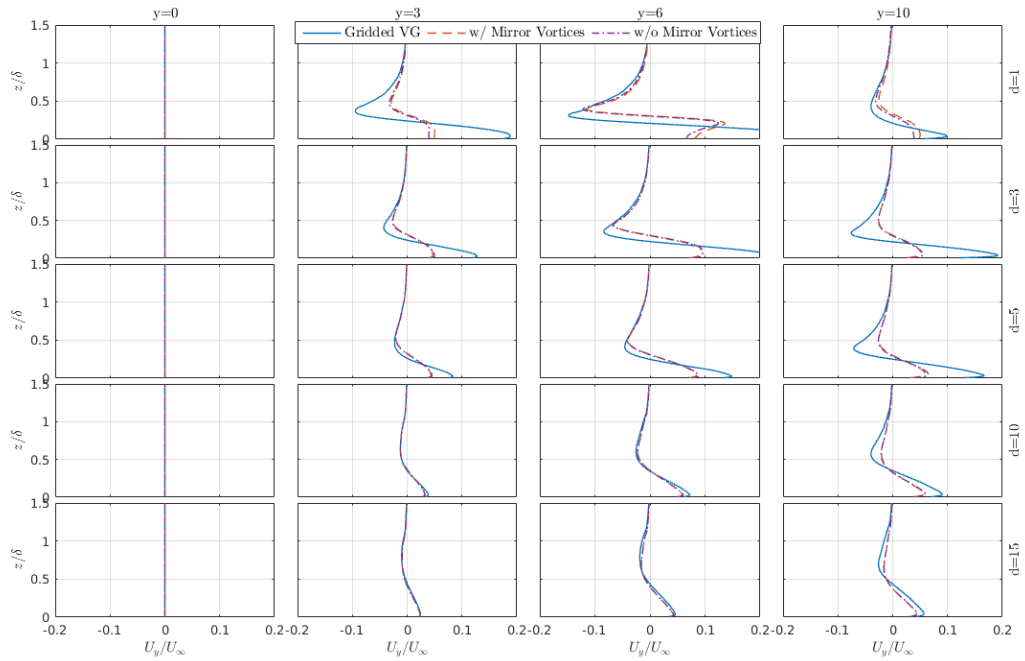


Figure 6.30: Case 1: $\frac{U_z}{U_\infty}$ profiles with(out) mirror at $d = \Delta x/c = 1, 3, 5, 10, 15$, starting at the top, and $y = 0\text{mm}, 3\text{mm}, 5\text{mm}, 10\text{mm}$.

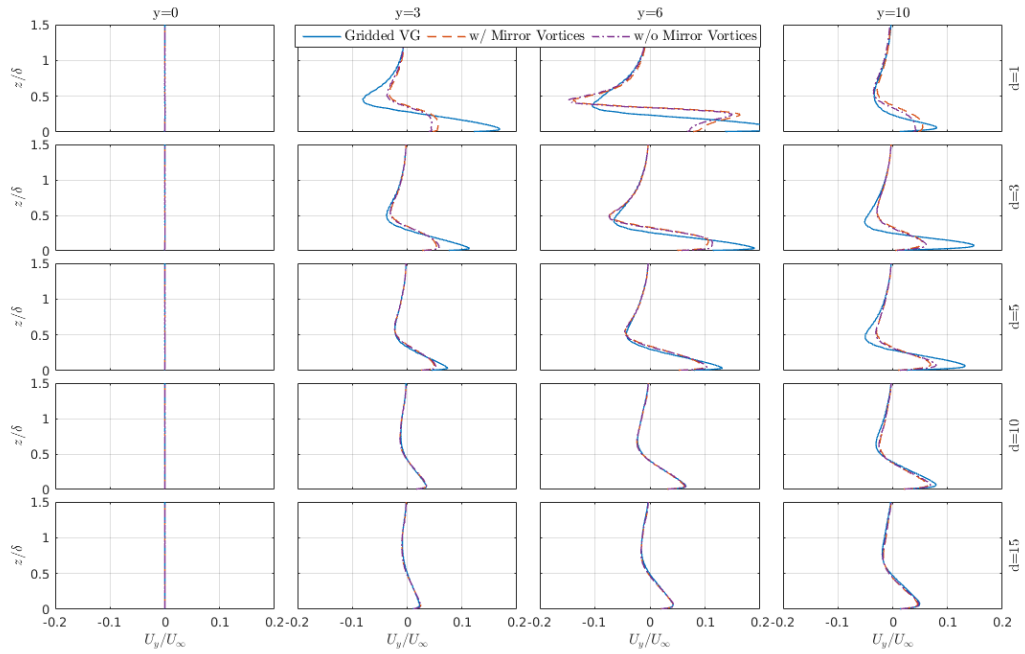


Figure 6.31: Case 3: $\frac{U_y}{U_\infty}$ profiles with(out) mirror at $d = \Delta x/c = 1, 3, 5, 10, 15$, starting at the top, and $y = 0\text{mm}, 3\text{mm}, 5\text{mm}, 10\text{mm}$.

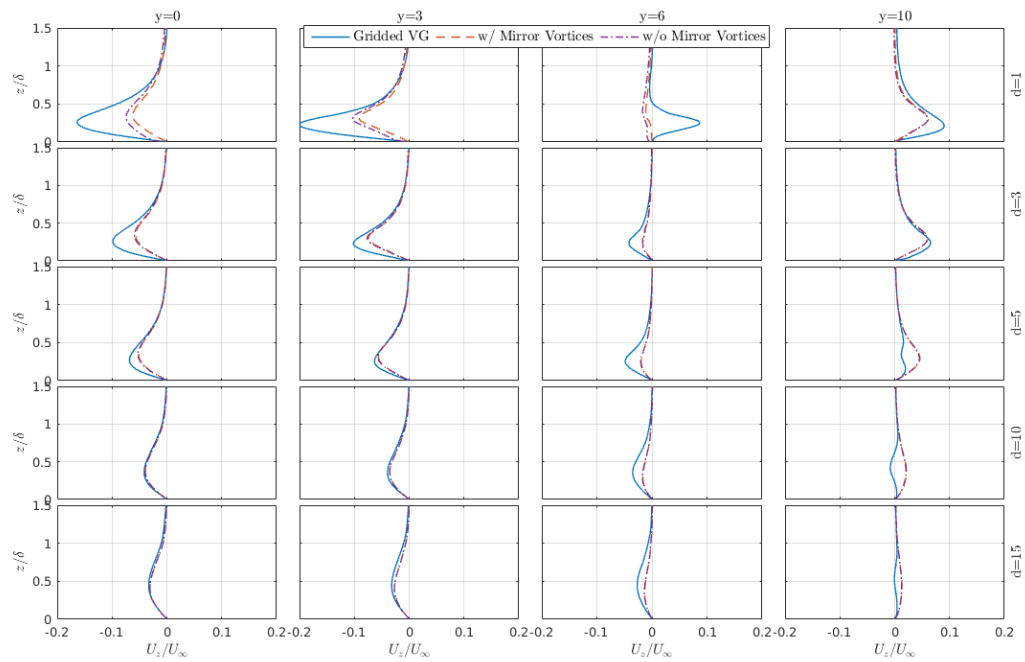


Figure 6.32: Case 1: $\frac{U_z}{U_\infty}$ profiles with(out) mirror at $d = \Delta x/c = 1, 3, 5, 10, 15$ and $y = 0\text{mm}, 3\text{mm}, 5\text{mm}, 10\text{mm}$.

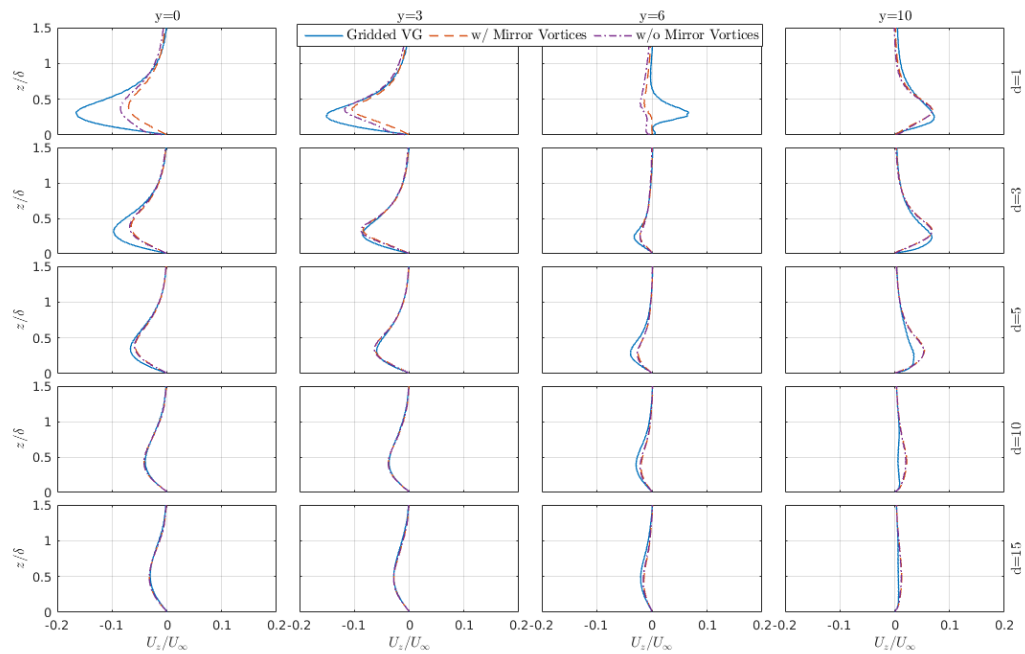


Figure 6.33: Case 3: $\frac{U_z}{U_\infty}$ profiles with(out) mirror at $d = \Delta x/c = 1, 3, 5, 10, 15$ and $y = 0\text{mm}, 3\text{mm}, 5\text{mm}, 10\text{mm}$.

As expected the peak vorticity in both simulations is kept the same, see figure 6.36 and figure 6.37. With respect to the circulation, since the overall vortex velocity is smaller in the simulations *with mirror vortices*, the vortex circulation is also smaller, figure 6.34 and figure 6.35. Furthermore, due to the increase of velocity at the wall, a higher wall vorticity is created, and so the circulation decay is stronger. However, the difference in circulation between both simulations is very small.

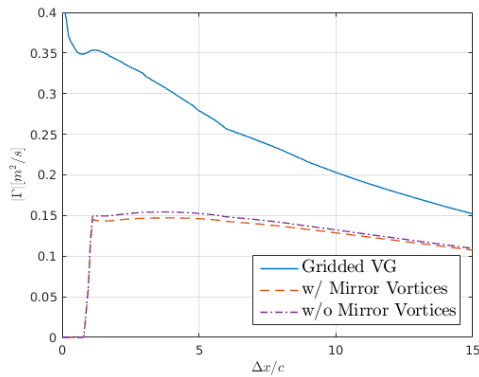


Figure 6.34: Case 1: Circulation with(out) mirror vortices.

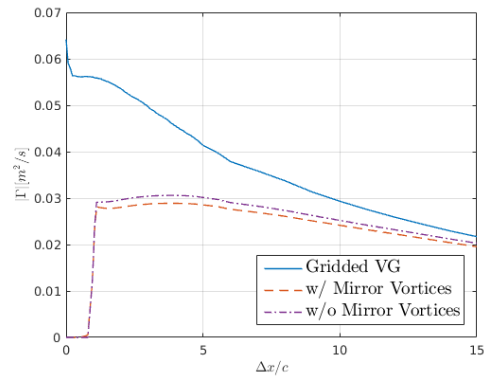


Figure 6.35: Case 3: Circulation with(out) mirror vortices.

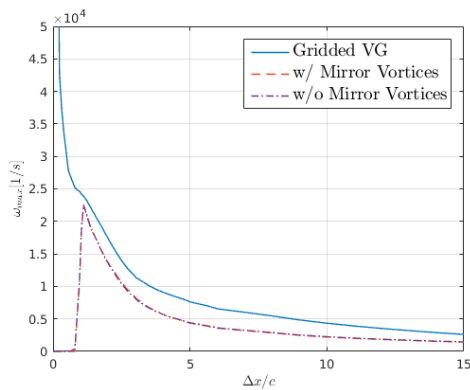


Figure 6.36: Case 1: Peak vorticity with(out) mirror vortices.

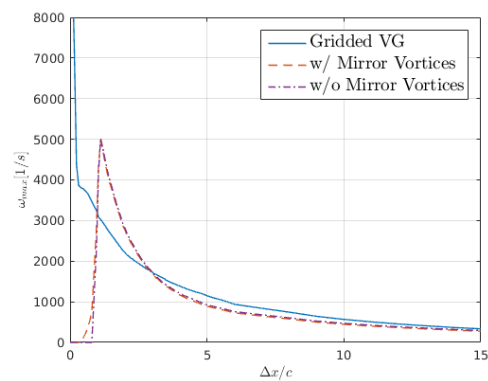


Figure 6.37: Case 3: Peak vorticity with(out) mirror vortices.

Regarding the shape factor, it can be seen, in figure 6.38 and figure 6.39, that the simulation *without mirror vortices* performs slightly better in all streamwise positions but the first. Because the vortex in the simulations *without mirror vortex* is slightly stronger, the two vortices (left and right) apart more quickly - it can be seen that at $\frac{\Delta x}{c} = 3$ and $\frac{\Delta x}{c} = 5$ the center of the vortices is slightly more apart in the simulations *without mirror vortices*-. This agrees better with the *gridded VG* simulations, where the effect of the neighbour vortex is higher.

Nevertheless, similarly with circulation results, the differences between simulations in the shape factor are very small and the flow behaviour is the same in both simulations. Thereafter, it can be stated that the Wendt model can be implemented either with or without mirror vortices in OpenFOAM.

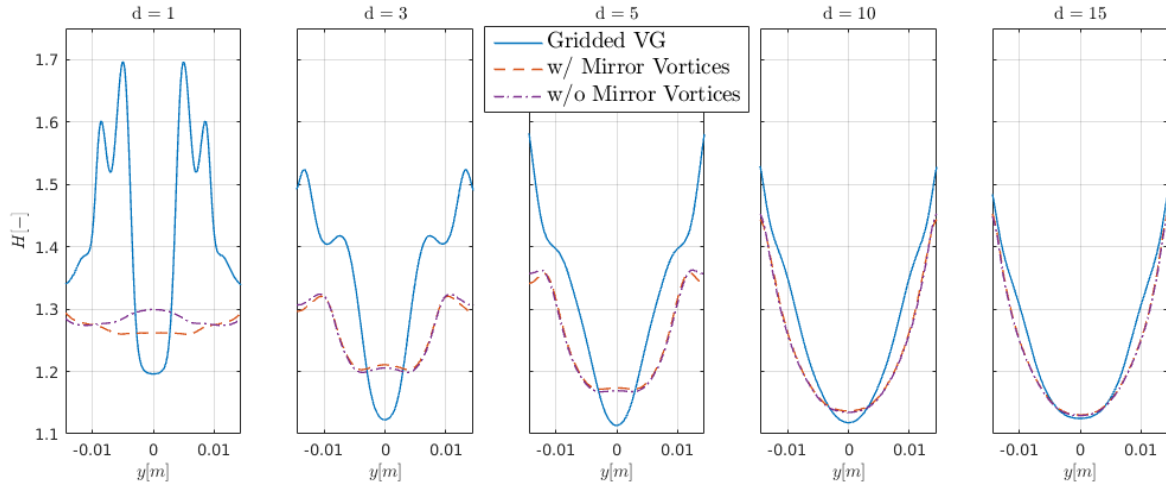


Figure 6.38: Case 1: Shape factor with(out) mirror vortices. $d = \Delta x/c = 1, 3, 5, 10, 15$.

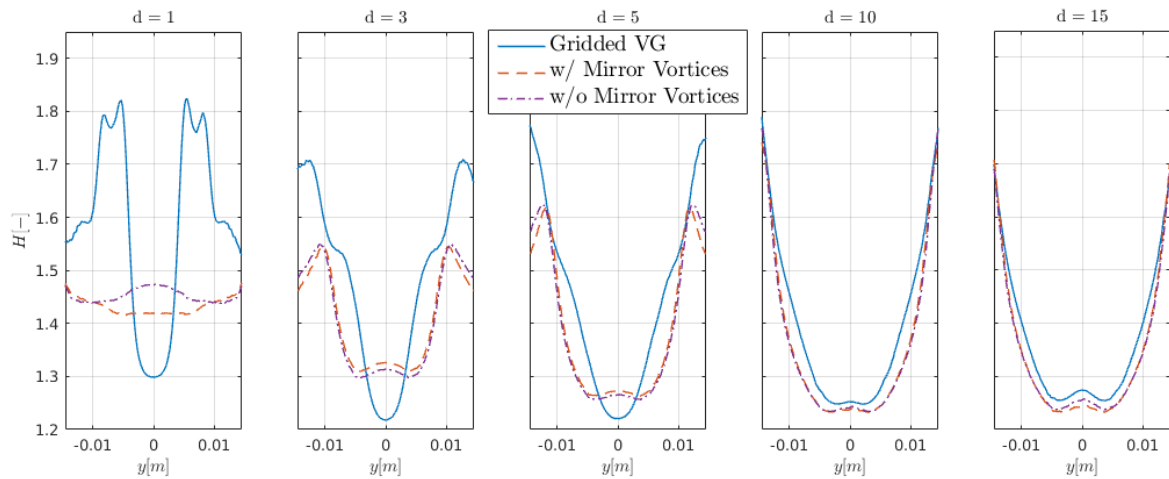


Figure 6.39: Case 3: Shape factor with(out) mirror vortices. $d = \Delta x/c = 1, 3, 5, 10, 15$.

Chapter 7

Model Behaviour with Calibrated Inputs

As described in the section 2.1, with the flow characteristics and the VG geometry inputs, the Wendt model is able to calculate the circulation - with equation 2.4 -, and peak vorticity - with equation 2.16 - of the vortex shed by the VG. With those, the vortex velocity profile at $\frac{\Delta x}{c} = 1$ is obtained with equation 5.1. If the vortex circulation, peak vorticity or position are known a priori, by experimental or computational means, then instead of using the Wendt model one can use those values to obtain the velocity profile.

To understand how the model can be improved and which are the most relevant parameters to obtain the correct flow behaviour, for the *case 1* and for the *case 3*, besides the *Wendt model simulation* and *gridded VG simulation*, three others simulations were made - with Γ *calibrated*, with Γ and ω_{max} *calibrated* and with Γ , ω_{max} and *position calibrated*. In the three simulations, the vortex circulation, peak vorticity and position inputs were calibrated with the results found in the *gridded VG simulation* at $\frac{\Delta x}{c} = 1$.

In section 7.1, the results found with Γ and ω_{max} *calibrated* will be compared to the ones obtained with the *Wendt model*. By that, it is aimed to understand how important is the correct computation of Γ and ω_{max} at $\frac{\Delta x}{c} = 1$. Furthermore, in order to study the relevance of a good vortex location estimation, in section 7.2, the simulation with Γ , ω_{max} and *position calibrated* will be compared with the simulation with Γ and ω_{max} *calibrated*. Lastly, to assess how accurate is the peak vorticity estimation by the Wendt model (equation 2.16), a simulation with Γ *calibrated* was compared with the simulation with Γ and ω_{max} *calibrated*, section 7.3.

7.1 Vortex Circulation and Peak Vorticity Calibration

In this section the importance of the circulation and peak vorticity estimation at $\frac{\Delta x}{c} = 1$ will be analysed in both, *case 1* and *case 3*. For that the simulation with Γ and ω_{max} *calibrated* will be compared with the *Wendt model simulation*. In first place, the images of *case 1* and

case 3 are shown. It follows the analysis of those.

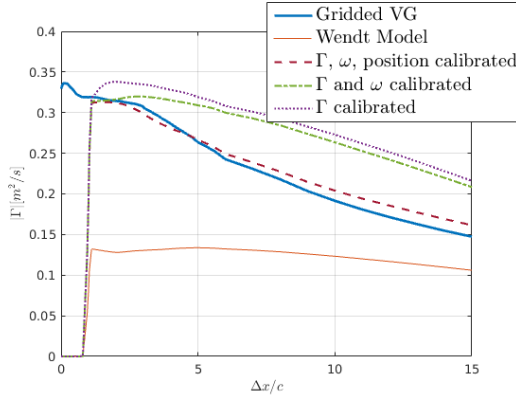


Figure 7.1: Case 1 calibrated: Vortex circulation with streamwise position.

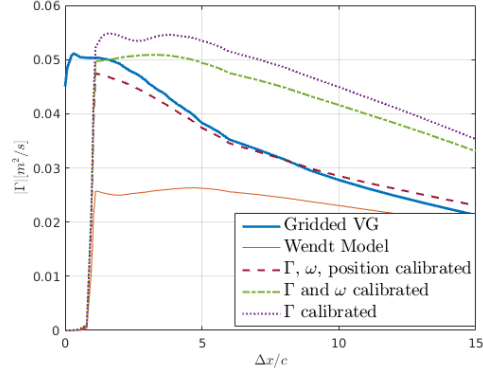


Figure 7.2: Case 3 calibrated: Vortex circulation with streamwise position.

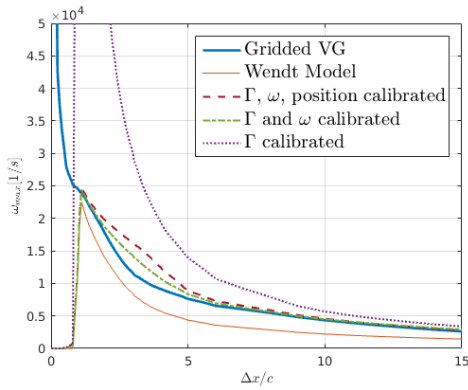


Figure 7.3: Case 1 calibrated: Vortex peak vorticity with streamwise position zoomed in.

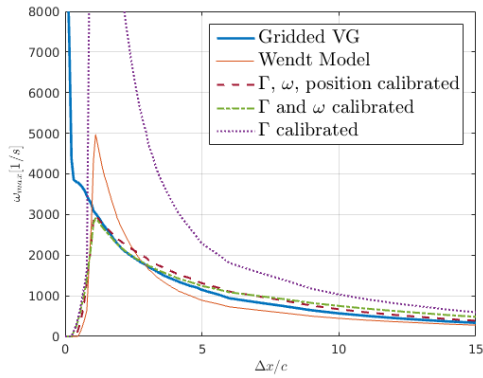


Figure 7.4: Case 3 calibrated: Vortex peak vorticity with streamwise position zoomed in.

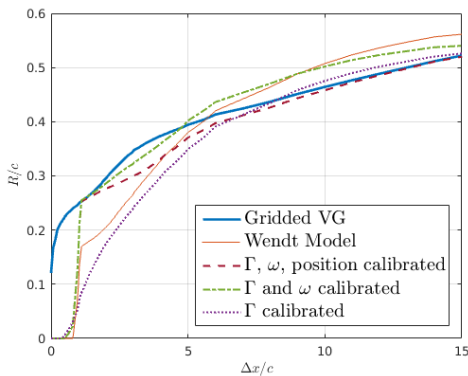


Figure 7.5: Case 1 calibrated: Radius with streamwise position.

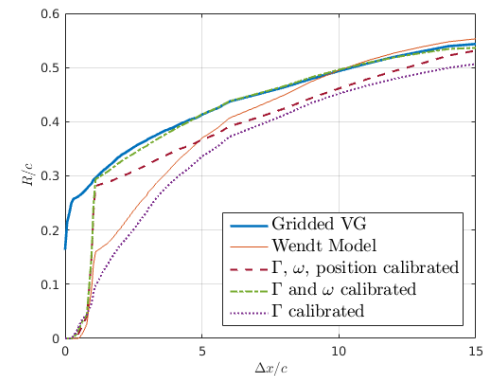


Figure 7.6: Case 3 calibrated: Radius with streamwise position.

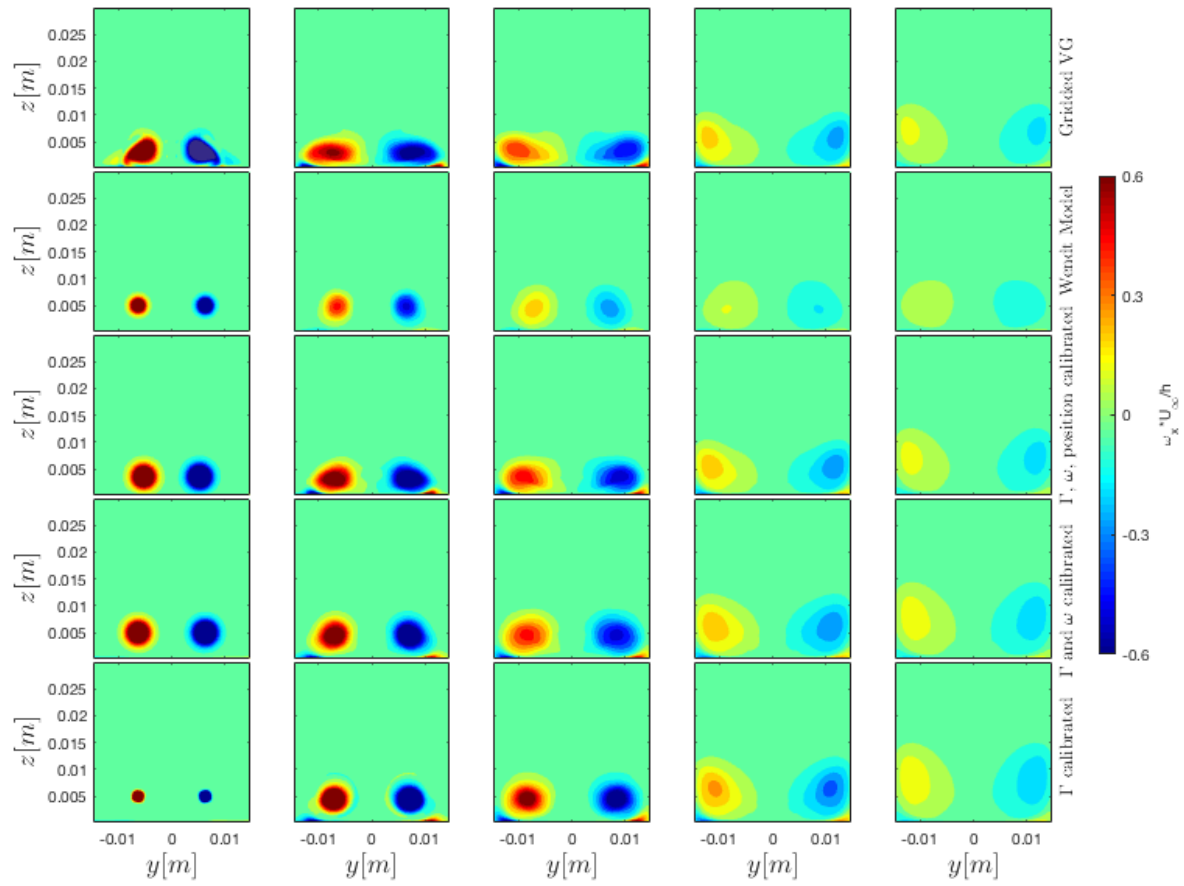


Figure 7.7: Case 1 calibrated: Vorticity field, $\omega_x U_\infty / h$, at $d = \Delta x / c = 1, 3, 5, 10, 15$.

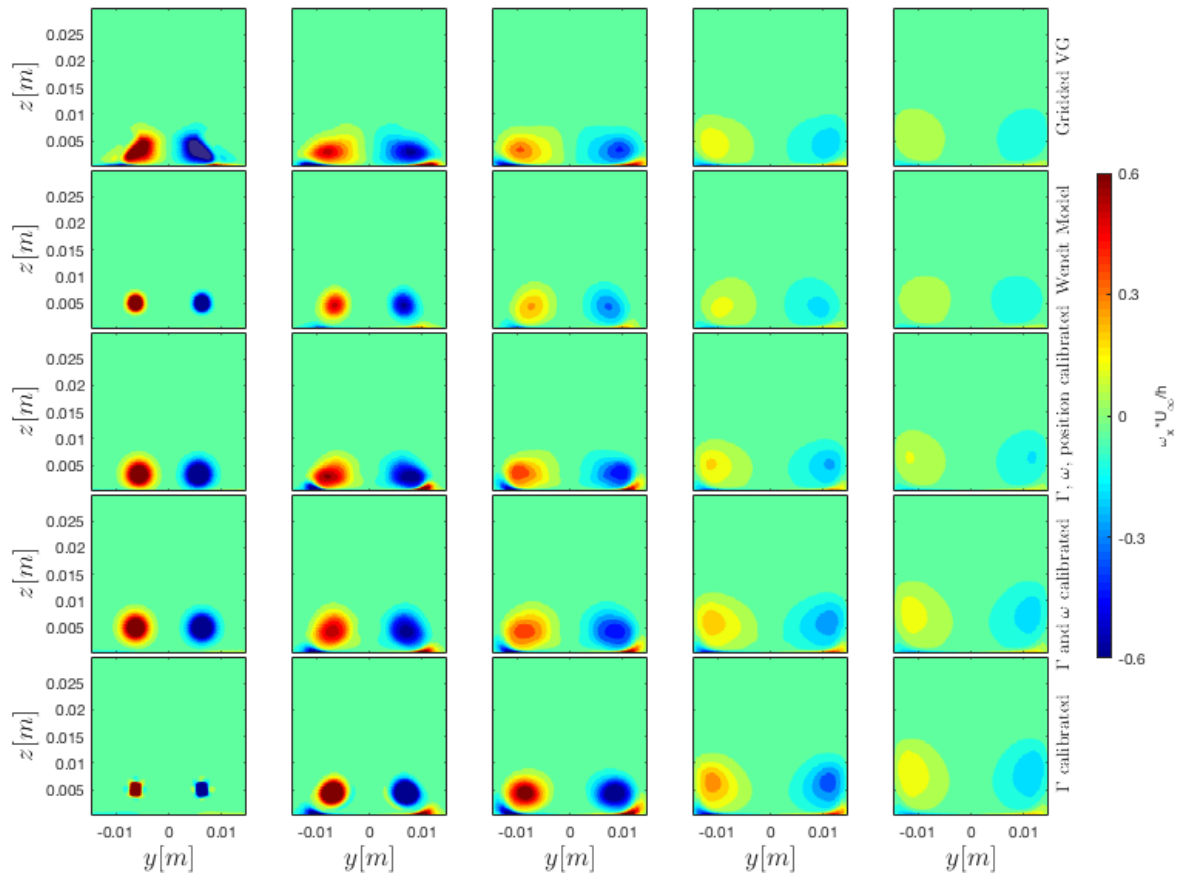


Figure 7.8: Case 3 calibrated: Vorticity field, $\omega_x U_\infty / h$, at $d = \Delta x / c = 1, 3, 5, 10, 15$.

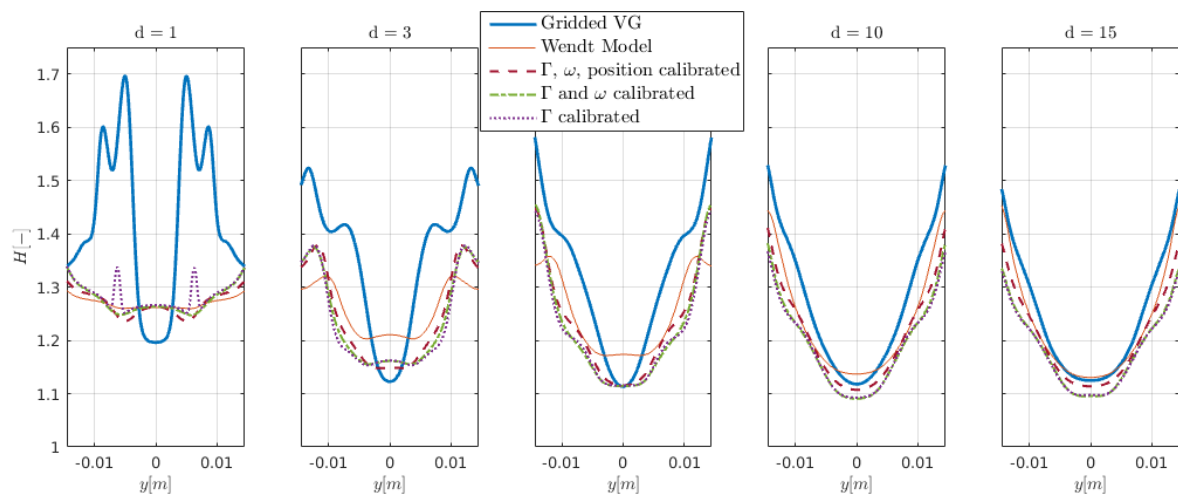


Figure 7.9: Case 1 calibrated: Shape factor at $d = \Delta x / c = 1, 3, 5, 10, 15$.

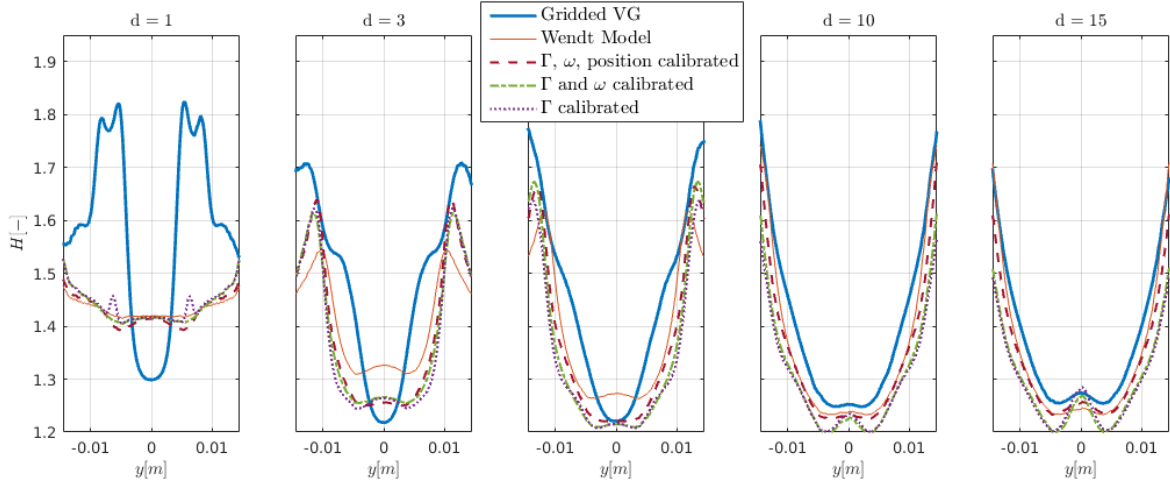


Figure 7.10: Case 3 calibrated: Shape factor at $d = \Delta x/c = 1, 3, 5, 10, 15$.

Relative Error [%]	Wendt Model	Γ , ω_{max} and position calibrated
Averaged H in y , $\overline{\epsilon_H \frac{\Delta x}{c} = 15}$	1.75	3.09
Averaged Γ in x , $\overline{\epsilon_\Gamma}$	52.76	2.41
Averaged ω_{max} in x , $\overline{\epsilon_{\omega_{max}}}$	31.07	21.82
Averaged R in x , $\overline{\epsilon_R}$	18.62	7.38

Relative Error [%]	Γ and ω_{max} calibrated	Γ calibrated
Averaged H in y , $\overline{\epsilon_H \frac{\Delta x}{c} = 15}$	4.8	4.91
Averaged Γ in x , $\overline{\epsilon_\Gamma}$	11.01	15.46
Averaged ω_{max} in x , $\overline{\epsilon_{\omega_{max}}}$	11.83	211.36
Averaged R in x , $\overline{\epsilon_R}$	3.97	27.77

Table 7.1: Case 1 calibrated: Error Analysis.

Relative Error [%]	Wendt Model	Γ , ω_{max} and position calibrated
Averaged H in y , $\overline{\epsilon_H \frac{\Delta x}{c} = 15}$	2.38	3.14
Averaged Γ in x , $\overline{\epsilon_\Gamma}$	38.70	4.55
Averaged ω_{max} in x , $\overline{\epsilon_{\omega_{max}}}$	21.59	10.72
Averaged R in x , $\overline{\epsilon_R}$	24.12	10.22

Relative Error [%]	Γ and ω_{max} calibrated	Γ calibrated
Averaged H in y , $\overline{\epsilon_H \frac{\Delta x}{c} = 15}$	5.58	5.71
Averaged Γ in x , $\overline{\epsilon_\Gamma}$	17.92	26.31
Averaged ω_{max} in x , $\overline{\epsilon_{\omega_{max}}}$	8.33	230
Averaged R in x , $\overline{\epsilon_R}$	1.76	33.55

Table 7.2: Case 3 calibrated: Error Analysis.

When imposing the correct values for the circulation and peak vorticity, the size of the vortex is accurately computed at $\frac{\Delta x}{c} = 1$, see figures 7.5 and 7.6. In the *case 1*, while in the *Wendt model simulation* the vortex radius relative error at $\frac{\Delta x}{c} = 1$ is $\epsilon_{R_{\frac{\Delta x}{c}=1}} = 33\%$, the simulation with Γ and ω_{max} calibrated presents an error of $\epsilon_{R_{\frac{\Delta x}{c}=1}} = 2\%$. In the *case 3*, the radius error at decreased from $\epsilon_{R_{\frac{\Delta x}{c}=1}} = 46\%$ to $\epsilon_{R_{\frac{\Delta x}{c}=1}} = 0.5\%$.

Due to a better vortex size estimation, the vortex edge will be closer to the wall, see figures 7.7 and figure 7.8. As so, near the vane the vortex dissipation in the simulation with Γ and ω_{max} calibrated agrees well with the *gridded VG simulation*. In the *case 1* the peak vorticity relative error averaged along the streamwise position decreased from $\overline{\epsilon_{\omega_{max}}} = 31\%$ in the *Wendt model simulation* to $\overline{\epsilon_{\omega_{max}}} = 12\%$ in the simulation with Γ and ω_{max} calibrated; in the *case 3* it decreased from $\overline{\epsilon_{\omega_{max}}} = 22\%$ to $\overline{\epsilon_{\omega_{max}}} = 8\%$, see figures 7.3 and 7.4.

Besides the improvement in the vortex dissipation there is an improvement in the vortex decay. Since at $\frac{\Delta x}{c} = 1$ the vortex circulation and radius do now correspond to the one found in the *gridded VG simulation*, in the simulation with Γ and ω_{max} calibrated is found an higher wall vorticity than in the *Wendt model simulation*. And so, the vortex decay will also be higher in this simulation. Although improved, the vortex decay is still underestimated. Nevertheless, in the *case 1* the averaged circulation error decreased from $\overline{\epsilon_{\Gamma}} = 53\%$ in the *Wendt model simulation* to $\overline{\epsilon_{\Gamma}} = 11\%$ in the simulation Γ and ω_{max} calibrated; and in the *case 3* the error decreased from $\overline{\epsilon_{\Gamma}} = 38\%$ to $\overline{\epsilon_{\Gamma}} = 18\%$, see figures 7.1 and 7.2.

With respect to the shape factor it can be seen in figures 7.9 and 7.10 that, near the vane, this parameter is greatly improved in the simulations with Γ and ω_{max} calibrated. However since the influence of the vane is still very large, a mismatch between the simulation with Γ and ω_{max} calibrated and *gridded VG simulation* is found in this region.

Far from the vane, the circulation in the *Wendt model simulation* agrees better with the one found in the *gridded VG simulation*. Consequently, this simulation will agree better with the *gridded VG simulation*. In the *case 1*, the averaged shape factor error at $\frac{\Delta x}{c} = 15$ of *Wendt model simulation* equals $\overline{\epsilon_{H_{\frac{\Delta x}{c}=15}}} = 2\%$ and in the simulation with Γ and ω_{max} calibrated equals $\overline{\epsilon_{H_{\frac{\Delta x}{c}=15}}} = 5\%$. In the *case 3* the averaged shape factor error at $\frac{\Delta x}{c} = 15$ of *Wendt model simulation* equals $\overline{\epsilon_{H_{\frac{\Delta x}{c}=15}}} = 2\%$ and in the simulation with Γ and ω_{max} calibrated equals $\overline{\epsilon_{H_{\frac{\Delta x}{c}=15}}} = 6\%$.

In summary it can be said that near the vanes, when circulation and peak vorticity are calibrated the vortex vorticity field is improved. As a consequence, in this region the shape factor is improved. Still due to the influence of the vanes in the streamwise velocity deficit, a mismatch in this region will always be found.

Far from the vanes, since the vortex decay is still underpredicted by the simulation with Γ and ω_{max} calibrated, the influence of the vortex in the boundary layer will be greater. Thereafter, the shape factor does not present a good match with the *gridded VG simulations* in this region.

7.2 Vortex Position Calibration

To study the importance of the vortex position, it was done a simulation with the vortex core positioned at the same place as in the *gridded VG simulation*. By analysing the differences between the simulation with Γ , ω_{max} and *position calibrated* and the simulation with Γ and ω_{max} *calibrated* in the *case 1* as well as in the *case 3*, the effect of the vortex position will be assessed.

Before the comparison between simulations, let us first analyse the vortex core position in the *gridded VG simulation*. With respect to the vortex height, one can see in the vorticity field, figures 7.7 and 7.8, that initially the vortex is below the VG height. This results from the downward influence of the neighbour vortex as studied in Lögdberg et al. (2009). Far from the vane, due to the vortex growth, the vortex core will apart from the wall. With respect to the vortex lateral position, in the *gridded VG simulation*, the vortices are initially more close to each other. Since in the inner part of the vanes there is a low pressure zone, the vortices are dragged initially to this position. With the increase of the streamwise position, the vortices apart from each other due to the influence of the neighbour vortex.

In the simulations with Γ and ω_{max} *calibrated*, the vortices are placed at $(y, z) = (\pm 6.25\text{mm}, 5\text{mm})$ as suggested by Dudek (2006). In the simulations with Γ , ω_{max} and *position calibrated*, in *case 1* the vortices are placed at $(y, z) = (\pm 5.2\text{mm}, 3.6\text{mm})$, and in the *case 3* the vortices are placed at $(y, z) = (\pm 5.6\text{mm}, 3.3\text{mm})$.

When one calibrates the vortex position, the circulation line is able to follow reasonably well the result found in the *gridded VG simulation*, see figures 7.1 and 7.2. With position calibrated, the vortex decay can be finally accurately computed. Consequently, in the *case 1*, the average error along the streamwise position dropped from $\overline{\epsilon}_\Gamma = 11\%$ in the simulation with Γ and ω_{max} *calibrated* to $\overline{\epsilon}_\Gamma = 2\%$ in the simulation with Γ , ω_{max} and *position calibrated*; in the *case 3*, the error dropped from $\overline{\epsilon}_\Gamma = 18\%$ to $\overline{\epsilon}_\Gamma = 5\%$.

The figures 7.3 and 7.4 show the peak vorticity along the streamwise position of *case 1* and *case 3* respectively. The figures 7.5 and 7.6 show the radius with streamwise position. As one can see, both simulations with calibrated inputs in both *case 1* and *case 3* present a reasonable agreement of peak vorticity and radius with the *gridded VG simulation*.

It can also be verified, in the vorticity field images 7.7 and 7.8, that the shape of the vortex in the simulations with Γ , ω_{max} and *position calibrated* is very similar to the one found in the *gridded VG simulations*. Near the vanes, the vortices are flattened, and far from the vanes, the vortices are at the same height and lateral position. This is a major improvement when compared with the simulations with Γ and ω_{max} *calibrated*.

Near the vane, it can be seen, in figures 7.9 and 7.10, that the difference found in the shape factor between the simulations with Γ , ω_{max} and *position calibrated* and the simulations with *gridded VG simulation* is very small. Far from the vane however, since the vortex already decayed and the vane influence can be neglected, the simulations with Γ , ω_{max} and *position calibrated* agree well with the *gridded VG simulations*. The relative error at $\frac{\Delta x}{c} = 15$ in *case 1* decreased from $\overline{\epsilon}_{H \frac{\Delta x}{c} = 15} = 5\%$ in the simulation with Γ and ω_{max} *calibrated* to $\overline{\epsilon}_{H \frac{\Delta x}{c} = 15} = 3\%$,

and decreased from $\overline{\epsilon_{H \frac{\Delta x}{c} = 15}} = 6\%$ to $\overline{\epsilon_{H \frac{\Delta x}{c} = 15}} = 3\%$ in the *case 3*.

The correct circulation and peak vorticity prediction at $\frac{\Delta x}{c} = 1$ is very important to obtain a good vortex development near the vane. Nevertheless, to obtain a good shape factor result far from the vane, then the vortex position at $\frac{\Delta x}{c} = 1$ should be calibrated.

7.3 Peak Vorticity Estimation

In order to study how good is the peak vorticity estimation by the Wendt model and how important is this parameter to obtain the correct shape factor, in this chapter the simulation with Γ *calibrated* will be compared to the simulation with Γ and ω_{max} *calibrated*.

In the *case 1* as well as in the *case 3*, in the simulation with Γ *calibrated* the peak vorticity is highly overestimated by the Wendt model at $\frac{\Delta x}{c} = 1$, see figure 7.3 and figure 7.4. In the *case 1*, the relative error at $\frac{\Delta x}{c} = 1$ is $\epsilon_{\omega_{max}} = 1219\%$ and in the *case 3* the relative error at this position is $\epsilon_{\omega_{max}} = 917\%$. As a consequence, initially the vortex will be much more concentrated.

Since the vortex is far from the wall, the simulation with Γ *calibrated* will as well present a much higher vortex dissipation near the vane. As so the difference observed in the radius but also in the vortex shape decreases rapidly with streamwise position, see vorticity field images 7.7 and 7.8. Furthermore after $\frac{\Delta x}{c} = 5$ the difference in vortex shape between simulations with Γ and ω_{max} *calibrated* and the simulations with Γ *calibrated* is very small.

Furthermore, it can be seen in the *case 1* and in the *case 3* that the difference in shape factor between the simulations with Γ and ω_{max} *calibrated* and the simulations with Γ *calibrated* is negligible, see figures 7.9 and 7.10. This means that, despite the size of the vortex, if its strength is the same, then the same amount of momentum will enter in the boundary layer.

Therefore, it can be concluded that, to obtain the correct flow behaviour downstream the VG location, the peak vorticity is not a parameter as relevant as the circulation or vortex position.

Part V

Conclusion

Chapter 8

Conclusion

8.1 Conclusions

The thesis intends to answer the research question: “*Can the Bray model or the Wendt model be applied in CFD simulations of incompressible airfoil flows to reproduce a similar boundary layer shape factor to the one found in simulations with gridded vortex generators?*”

By applying the implementation suggested in Dudek (2006) in OpenFOAM, it was concluded that, because this implementation does not take into account the influence of the vane in the flow, the vortex vorticity field near the vane will differ significantly from the one found in the *gridded VG simulations*. As a result, a good shape factor agreement cannot be obtained near the vanes where this influence is still very large. Moreover, it was found that to obtain a good shape factor result at a certain streamwise position far from the vane, then the vortex circulation at that position must agree with the one of the *gridded VG simulation*. For that, it is essential to impose the correct vortex circulation *and* the correct vortex position inputs. As the vortex strength and vortex proximity with wall will dictate the wall vorticity - responsible for the vortex decay -, both entities are crucial to obtain the correct vortex circulation throughout the domain.

Furthermore it was show that the peak vorticity is not a parameter as relevant for the shape factor as the vortex circulation and position. Also, since a concentrated vortex dissipates very quickly, to obtain the correct vortex radius far from the vanes, a high value of peak vorticity can be used as an input. This will not have a negative impact on the shape factor result agreement far from the vanes.

The findings stated before were established by comparing simulations with inputs - vortex circulation, peak vorticity and position - calibrated with the results from the *gridded VG simulations*. Nevertheless, in most of the cases, the vortex circulation, peak vorticity and position at $\frac{\Delta x}{c} = 1$ are not known. Consequently, it becomes important to study models that can predict these entities at this streamwise position.

Both Bray model and Wendt model are able to predict circulation and peak vorticity, but not vortex position. When compared, it was found that on the tested range the models were able to predict reasonably well circulation. Although the Wendt model tends to underpredict circulation, this model predicts circulation slightly better than the Bray model *but* for higher freestream velocities and lower height-to-boundary-layer-thickness-ratios and aspect-ratios. Concerning peak vorticity, it was found that there is a higher discrepancy between the models and the experimental results than in the circulation prediction. In addition, while the Wendt model tends to overpredict peak vorticity, the Bray model tends to underpredict it. Still the peak vorticity is better estimated by the Wendt model.

Because the Wendt model predicted better peak vorticity and slightly better circulation than the Bray model, this model was used to assess how accurate can a semi-empirical model be. While [Wendt \(2001\)](#) formulates the vortex velocity profile by including the real and the mirror vortices, it was shown that the formulation with solely real vortices produce similar shape factor results. And so, both model formulations can be implemented in OpenFOAM.

[Dudek \(2006\)](#) suggests that the vortices should be placed at a chord length downstream the VG location, at the same horizontal and vertical position of the vanes trailing edges. However, it was found, in the *gridded VG simulations*, that the vortices cores near the vane are closer to each other and below the trailing edge location. Since the vortices are located neared each other, the influence of the neighbour vortex will be bigger. Consequently, the vortices will apart quicker from each other and initially pushed down towards the wall. Furthermore, due the lower vortex position, the wall vorticity will be higher in the *gridded VG simulations* than in the *Wendt model simulations*, and so will be the vortex decay.

When applied to two cases with low height-to-boundary-layer-ratio, the Wendt model greatly underpredicted circulation. When applied to a case that lies in the middle of the parametric range tested by [Wendt \(2001\)](#), the circulation was well predicted by the model. Despite this, a rather different shape factor profile was found at all the streamwise positions. In order to verify that with the correct vortex position input, the shape factor agreement can be greatly improved, it would be relevant to test this case with vortex position calibrated and a more refined mesh. Nonetheless, this was not done due to computational and time constrains.

Lastly, the results show that with the correct circulation input, the Wendt model overpredicts greatly peak vorticity.

Taking into account the conclusions made, the answer to the main research question can be summarized in the following words:

While the Wendt model produces inconsistent shape factor results, the implementation proposed by [Dudek \(2006\)](#) can be used - with vortex circulation and position calibrated - to obtain good shape factor results far from the vane, where the physical influence of those is small.

8.2 Recommendations

- Even though the parametric studies provide an acceptable circulation estimation on the tested range, they are bounded to this. The theoretical approaches however can be applied in a much wider range. As so it would be important to assess how does the lifting line theory compares with the semi-empirical models.
- Since to impose the correct vortex position at $\frac{\Delta x}{c} = 1$ is very important for the correct computation of circulation along the domain, a model that predicts the vortex position at $\frac{\Delta x}{c} = 1$ should be created.
- When using the implementation proposed by [Dudek \(2006\)](#), because the cells that mesh the VG are no longer required, the computational time is reduced. Furthermore it was found that the peak vorticity is not a parameter as relevant as circulation for the shape factor.

It would be useful to test the hypothesis that a coarser grid can be used with this implementation without a major impact in the shape factor. As well as to access how much can the mesh size be reduced without loss of accuracy.

- To study the relation between the shape factor and the separation point, and by that to study how does the implementation made performs regarding the separation point.

Bibliography

- E. E. Bender, B. H. Anderson, and P. J. Yagle. Vortex Generator Modeling for Navier-Stokes Codes. *Aerodynamics and CFD Group Lockheed Martin Tactical Aircraft Systems*, 1999.
- T. P. Bray. *A Parametric Study of Vane and Air-jet Vortex Generators*. PhD thesis, Cranfield University, 1998.
- J. C. Dudek. An Empirical Model for Vane-Type Vortex Generators in a Navier Stokes Code. Technical report, National Aeronautics and Space Administration, Cleveland, Ohio, 2006.
- U. Fernandez. *Fluid Dynamic Characterization of Vortex Generators and Two-dimensional Turbulent Wakes*. PhD thesis, Polytechnic University of Catalonia, 2013.
- L. Florentie, A. H. Van Zuijlen, and H. Bijl. Towards a Multi-Fidelity Approach for CFD Simulations of Vortex Generator Arrays. *WCCM XI: 11th World Congress on Computational Mechanics*, 2014.
- L. Florentie, A. H. van Zuijlen, S. J. Hulshoff, and H. Bijl. Effectiveness of Side Force Models for Flow Simulations Downstream of Vortex Generators. *AIAA Journal*, 2016.
- A. (Swedish Defense Research Agency) Jirasek. Vortex-Generator Model and Its Application to Flow Control. *Journal of Aircraft*, 2005. ISSN 0021-8669. doi: 10.2514/1.12220.
- W. G. Kunik. Application of a computational model for vortex generators in subsonic internal flows. Technical report, National Aeronautics and Space Administration Lewis Research Center, Cleveland, Ohio, 1986.
- O. Lögdberg, J. H. M. Fransson, and P. H. Alfredsson. Streamwise evolution of longitudinal vortices in a turbulent boundary layer. *Journal of Fluid Mechanics*, 2009.
- N. May. A new vortex generator model for use in complex configuration CFD solvers. Technical report, Aircraft Research Association (ARA), Bedford, UK, 2001.
- G.B. Schubauer and W.G. Spangenberg. Forced Mixing in Boundary Layers. Technical Report September, National Bureau of Standards, Washington, D.C., 1959.
- H.B. Squire. The Growth of a Vortex in Turbulent Flow. *The Aeronautical Quarterly*, pages 302–306.

- F. (KTH) Stillfried, S. Wallin, and A. Johansson. An improved passive vortex generator model for flow separation control. *5th Flow Control Conference*, (July), 2010.
- O. (KTH) Törnblom and A. V. Johansson. A Reynolds stress closure description of separation control with vortex generators in a plane asymmetric diffuser. *Physics of Fluids*, 2007.
- F. von Stillfried. *Computational fluid-dynamics investigations of vortex generators for flow-separation control*. PhD thesis, Royal Institute of Technology, 2012.
- B. J. (Modern Technologies Corporation) Wendt, B. A. (Kansas State University) Reichert, and J. D. (Iowa State University) Foster. The Decay of Longitudinal Vortices Shed From Airfoil Vortex Generators. Technical report, Lewis Research Center NASA, 1995.
- Bruce J. Wendt. Initial Circulation and Peak Vorticity Behavior of Vortices Shed from Airfoil Vortex Generators. Technical Report August, Modern Technologies Corporation, Middleburg Heights, Ohio, 2001.
- R. V. (Ames Research Center) Westphal, W. R. Pauley, and J. K. (Stanford University) Eaton. Interaction Between a Vortex and 1 I a Turbulent Boundary Layer Part I: Mean Flow Evolution and Turbulence Properties. Technical report, Ames Research Center, 1987.

Appendix A

Wendt Parametric Study Results

α [°]	c [cm]	h [cm]	\mathcal{R} [-]	$\frac{h}{\delta}$ [-]	U_∞ [m/s]	Mach	Γ [m^2/s]	ω_{max} [1/s]
8	4.06	1.02	0.64	0.57	85	0.25	0.291	18193
12	4.06	1.02	0.64	0.57	85	0.25	0.471	24346
16	4.06	1.02	0.64	0.57	85	0.25	0.643	33189
20	4.06	1.02	0.64	0.57	85	0.25	0.940	34055
16*	4.06	1.02	0.64	0.57	85	0.25	0.722	34714
16*	4.06	1.02	0.64	0.62	129	0.4	1.149	56831
16*	4.06	1.02	0.64	0.65	187	0.6	1.724	84000
16	0.85	0.21	0.64	0.12	85	0.25	0.156	20297
16	0.85	0.51	1.53	0.29	85	0.25	0.24	22340
16	0.85	1.02	3.06	0.57	85	0.25	0.253	30881
16	0.85	1.52	4.58	0.86	85	0.25	0.297	33368
16	0.85	2.03	6.11	1.14	85	0.25	0.307	38301
16	1.36	0.28	0.64	0.19	85	0.25	0.223	29194
16	1.36	0.51	0.96	0.29	85	0.25	0.342	23734
16	1.36	0.81	1.53	0.46	85	0.25	0.315	42509
16	1.36	1.02	1.91	0.57	85	0.25	0.315	35415
16	1.36	1.52	2.86	0.86	85	0.25	0.429	37397
16	1.36	1.63	3.06	0.91	85	0.25	0.419	52295
16	1.36	2.03	3.82	1.14	85	0.25	0.485	50676
16	1.36	2.54	4.78	1.43	85	0.25	0.428	44093
16	1.36	3.05	5.73	1.71	85	0.25	0.476	60375
16	1.36	3.56	6.68	2.00	85	0.25	0.446	63832
16	2.03	0.51	0.64	0.29	85	0.25	0.322	27772
16	2.03	1.02	1.27	0.57	85	0.25	0.435	43956
16	2.03	1.22	1.53	0.69	85	0.25	0.493	52181
16	2.03	1.52	1.91	0.86	85	0.25	0.552	57278
16	2.03	2.03	2.55	1.14	85	0.25	0.596	56235
16	2.03	2.44	3.06	1.37	85	0.25	0.667	44619
16	2.54	0.51	0.51	0.29	85	0.25	0.451	22914
16	2.54	0.64	0.64	0.36	85	0.25	0.421	31387
16	2.54	1.02	1.02	0.57	85	0.25	0.525	43913

α [°]	c [cm]	h [cm]	\mathcal{R} [-]	$\frac{h}{\delta}$ [-]	U_∞ [m/s]	Mach	Γ [m^2/s]	ω_{max} [$1/s$]
16	2.54	1.52	1.53	0.86	85	0.25	0.626	57104
16	2.54	2.03	2.04	1.14	85	0.25	0.719	73333
16	2.54	2.54	2.55	1.43	85	0.25	0.781	58750
16	2.54	3.05	3.06	1.71	85	0.25	0.825	42748
16	2.54	3.56	3.56	2.00	85	0.25	0.862	46882
16	2.54	4.57	4.58	2.57	85	0.25	0.866	70289
16	3.05	0.51	0.42	0.29	85	0.25	0.399	23345
16	3.05	0.76	0.64	0.43	85	0.25	0.530	30924
16	3.05	1.02	0.85	0.57	85	0.25	0.591	40099
16	3.05	1.52	1.27	0.86	85	0.25	0.704	53251
16	3.05	1.83	1.53	1.03	85	0.25	0.776	59852
16	3.05	2.03	1.70	1.14	85	0.25	0.817	58695
16	3.05	3.66	3.06	2.06	85	0.25	0.9845	35505
							$\pm 5\%$	$\pm 7\%$
16	3.56	0.51	0.36	0.29	85	0.25	0.451	21114
16	3.56	0.89	0.64	0.50	85	0.25	0.662	36897
16	3.56	1.02	0.73	0.57	85	0.25	0.648	40085
16	3.56	1.52	1.09	0.86	85	0.25	0.78	54079
16	3.56	2.03	1.46	1.14	85	0.25	0.944	59439
16	3.56	2.13	1.53	1.20	85	0.25	0.941	67331
16	3.56	4.27	3.06	2.40	85	0.25	1.17	45710
16	4.06	0.51	0.32	0.29	85	0.25	0.429	19956
16	4.06	1.02	0.64	0.57	85	0.25	0.713	39161
16	4.06	1.52	0.96	0.86	85	0.25	0.824	50476
16	4.06	2.03	1.27	1.14	85	0.25	0.961	60834
16	4.06	2.44	1.53	1.37	85	0.25	1.044	63493
16	4.06	2.54	1.59	1.43	85	0.25	1.044	66113
16	4.06	3.05	1.91	1.71	85	0.25	1.21	66124
16	4.06	3.56	2.23	2.00	85	0.25	1.243	69638
							$\pm 5\%$	$\pm 7\%$

*Data from full counter-rotating airfoil arrays.

Table A.1: Results from [Wendt \(2001\)](#) parametric study for isolated VGs and VGs tested in full counter-rotating arrays. [[Wendt \(2001\)](#)]

Appendix B

Bray Parametric Study Results

α [°]	Mach	$\frac{h}{\delta}$	$\frac{x}{\delta}$	c [cm]	ω_{max} [1/s]	Γ [m^2/s]	$\frac{R_{0.5}}{\delta}$	y [mm]	ω_{model} [1/s]	Δ [%]	$\frac{R_{0.5}}{\delta}_{model}$	Δ [%]
10	0.058	0.554	3.855	4.6	791.2	0.1370	0.149	8.5	803.1	1.5	0.1511	1.4
15	0.058	0.554	3.855	4.6	1174.1	0.2352	0.157	14.0	1123.5	4.3	0.1728	7.9
20	0.058	0.554	3.855	4.6	1427.5	0.3578	0.183	20.5	1461.1	2.4	0.1900	6.0
10	0.058	0.916	3.855	7.6	1855.2	0.2541	0.116	5.0	1660.4	10.5	0.1379	4.1
15	0.058	0.916	3.855	7.6	2344.1	0.4119	0.137	10.0	1951.7	16.7	0.1720	14.6
18	0.058	0.916	3.855	7.6	2122.8	0.5559	0.165	14.0	2126.5	0.2	0.1900	3.7
20	0.058	0.916	3.855	7.6	2082.8	0.6547	0.192	16.5	2242.6	7.7	0.2012	0.3
10	0.058	1.277	3.855	10.6	2638.1	0.3883	0.123	2.0	2408.4	8.7	0.1364	0.7
15	0.058	1.277	3.855	10.6	2309.1	0.4711	0.132	5.5	2383.0	3.2	0.1855	14.7
18	0.058	1.277	3.855	10.6	2424.1	0.8212	0.189	9.0	2402.0	0.9	0.2130	2.2
20	0.058	1.277	3.855	10.6	2119.5	0.9730	0.229	12.0	2421.5	14.3	0.2308	4.8
10	0.058	1.639	3.855	13.6	2508.4	0.4150	0.117	-0.5	3235.7	29.0	0.1340	8
15	0.058	1.639	3.855	13.6	2457.9	0.6306	0.142	1.0	2699.6	9.8	0.1984	9.4
18	0.058	1.639	3.855	13.6	1651.7	0.8306	0.215	4.0	2518.2	52.5	0.2368	6.7
20	0.058	1.639	3.855	13.6	1484.6	1.0144	0.247	7.5	2427.1	63.5	0.2624	11.3
10	0.058	0.554	12.048	4.6	293.2	0.1268	0.285	19.5	359.5	22.6	0.2019	14.2
15	0.058	0.554	12.048	4.6	447.5	0.2053	0.272	32.5	507.1	13.3	0.2302	5.1
18	0.058	0.554	12.048	4.6	581.9	0.2740	0.266	42.0	597.6	2.7	0.2445	0.5
20	0.058	0.554	12.048	4.6	702.5	0.3197	0.261	49.5	659.5	6.1	0.2531	4.8
10	0.058	0.916	12.048	7.6	945.4	0.2380	0.156	15.0	927.3	1.9	0.1725	3.9
15	0.058	0.916	12.048	7.6	1140.8	0.4018	0.180	28.5	1090.0	4.5	0.2152	1.3
18	0.058	0.916	12.048	7.6	1203.3	0.5434	0.219	39.5	1187.5	1.3	0.2377	1.2
20	0.058	0.916	12.048	7.6	1201.0	0.6477	0.255	49.0	1252.4	4.3	0.2518	4.2
10	0.058	1.277	12.048	10.6	1762.2	0.3399	0.132	11.0	1520.2	13.7	0.1636	4.1
15	0.058	1.277	12.048	10.6	1924.8	0.5852	0.169	25.0	1504.2	21.9	0.2225	12.7
20	0.058	1.277	12.048	10.6	1479.0	0.7859	0.256	44.5	1547.9	4.7	0.2746	5.3
10	0.058	1.639	12.048	13.6	2374.8	0.4607	0.133	7.0	2212.6	6.8	0.1561	1.0
15	0.058	1.639	12.048	13.6	2316.3	0.7820	0.171	19.5	1846.0	20.3	0.2311	11.1
18	0.058	1.639	12.048	13.6	1684.9	1.0486	0.250	30.0	1722.0	2.2	0.2758	2.3
20	0.058	1.639	12.048	13.6	1568.8	1.2593	0.280	39.0	1659.7	5.8	0.3056	4.7
10	0.058	0.554	19.277	4.6	177.7	0.1127	0.376	31.0	222.0	25	0.2328	18.3
15	0.058	0.554	19.277	4.6	302.1	0.1854	0.314	47.5	313.6	3.8	0.2654	5.4
18	0.058	0.554	19.277	4.6	393.7	0.2388	0.280	58.5	369.6	6.1	0.2819	1.1
20	0.058	0.554	19.277	4.6	485.6	0.2744	0.272	67.0	407.9	16	0.2919	8.5
10	0.058	0.916	19.277	7.6	590.4	0.2310	0.196	25.0	631.3	6.9	0.1971	12
15	0.058	0.916	19.277	7.6	851.5	0.3978	0.211	46.0	742.0	12.9	0.2458	0.5
18	0.058	0.916	19.277	7.6	865.5	0.5323	0.263	62.0	808.5	6.6	0.2716	3.3
20	0.058	0.916	19.277	7.6	969.3	0.6290	0.273	75.0	852.7	12.0	0.2876	0.2
10	0.058	1.277	19.277	10.6	1346.3	0.3368	0.146	21.0	1102.5	18.1	0.1842	2.9
15	0.058	1.277	19.277	10.6	1485.3	0.5849	0.184	41.5	1090.9	26.6	0.2504	11.5
18	0.058	1.277	19.277	10.6	1247.1	0.7827	0.260	59.0	1099.6	11.8	0.2876	1.4
20	0.058	1.277	19.277	10.6	1222.1	0.9231	0.289	73.0	1108.6	9.3	0.3115	0.1

α [$^{\circ}$]	Mach	$\frac{h}{\delta}$	$\frac{x}{\delta}$	c [cm]	ω_{max} [1/s]	Γ [m^2/s]	$\frac{R_{0.5}}{\delta}$	y [mm]	ω_{model} [1/s]	Δ [%]	$\frac{R_{0.5}}{\delta}_{model}$	Δ [%]
10	0.058	1.639	19.277	13.6	1473.7	0.3396	0.129	17.0	1679.5	14.0	0.1733	0.9
15	0.058	1.639	19.277	13.6	1388.9	0.5493	0.168	36.0	1401.2	0.9	0.2566	14
18	0.058	1.639	19.277	13.6	984.0	0.7178	0.241	52.0	1307.1	32.8	0.3063	0.2
20	0.058	1.639	19.277	13.6	968.0	0.8648	0.269	65.0	1259.8	30.1	0.3394	0.3
10	0.058	0.550	26.506	4.6	118.5	0.0992	0.462	38.5	152.2	28.4	0.2547	22.2
15	0.058	0.554	26.506	4.6	203.3	0.1608	0.365	55.5	215.3	5.9	0.2905	8.8
18	0.058	0.554	26.506	4.6	270.9	0.2084	0.340	69.0	253.7	6.3	0.3085	1.7
20	0.058	0.554	26.506	4.6	306.0	0.2278	0.319	75.5	279.9	8.5	0.3194	3.4
10	0.058	0.916	26.506	7.6	353.3	0.2175	0.259	33.5	462.3	30.8	0.2171	22.7
15	0.058	0.916	26.506	7.6	621.7	0.3657	0.239	58.5	543.3	12.6	0.2708	1.4
18	0.058	0.916	26.506	7.6	728.8	0.4783	0.263	78.0	592.0	18.8	0.2991	3.2
20	0.058	0.916	26.506	7.6	803.0	0.5603	0.279	91.0	624.3	22.2	0.3168	6
10	0.058	1.277	26.506	10.6	1029.2	0.3229	0.162	28.5	842.9	18.1	0.2019	0.7
15	0.058	1.277	26.506	10.6	1215.1	0.5487	0.197	54.5	834.0	31.4	0.2745	14.1
18	0.058	1.277	26.506	10.6	1018.6	0.7412	0.281	75.5	840.6	17.5	0.3152	3.2
20	0.058	1.277	26.506	10.6	1045.2	0.8849	0.306	93.0	847.4	18.9	0.3415	3.7
10	0.058	1.639	26.506	13.6	1722.2	0.4147	0.139	25.5	1326.3	23.0	0.1887	7.4
15	0.058	1.639	26.506	13.6	1201.1	0.5306	0.175	51.5	1106.6	7.9	0.2793	17.4
18	0.058	1.639	26.506	13.6	1163.0	1.0046	0.302	73.0	1032.2	11.2	0.3335	0.2
20	0.058	1.639	26.506	13.6	1152.7	1.1985	0.349	89.0	994.9	13.7	0.3695	1.2

Table B.1: Low-mach number study results from Bray (1998) parametric study. [Bray (1998)]

α [$^{\circ}$]	Mach	$\frac{h}{\delta}$	$\frac{x}{\delta}$	c [cm]	ω_{max} [1/s]	Γ [m^2/s]	$\frac{R_{0.5}}{\delta}$	y [mm]	ω_{model} [1/s]	Δ [%]	$\frac{R_{0.5}}{\delta}_{model}$	Δ [%]
15	0.4481	0.75	8.75	0.03	11760	1.0918	0.203	5.7	14587.2	24.0	0.2141	4.0
15	0.5920	0.75	8.75	0.03	17530	1.4630	0.206	5.8	18840.7	7.5	0.2165	0.9
15	0.7434	0.75	8.75	0.03	24540	1.9307	0.180	6.0	23212.6	5.4	0.2186	4.9
20	0.4502	0.75	8.75	0.03	15830	1.9619	0.249	11.8	17816.3	12.5	0.2435	6.9
20	0.6015	0.75	8.75	0.03	21780	2.5416	0.249	12.2	23249.7	6.7	0.2464	2.9
20	0.7545	0.75	8.75	0.03	29130	3.1750	0.236	13.3	28614.9	1.8	0.2487	1.4
15	0.4490	0.75	16.25	0.03	7057	1.0350	0.281	12.7	8908.8	26.2	0.2544	10.6
15	0.5930	0.75	16.25	0.03	10580	1.4024	0.264	12.7	11503.1	8.7	0.2573	4.9
15	0.7486	0.75	16.25	0.03	15590	1.8087	0.234	13.5	14240.9	8.7	0.2598	2.7
20	0.4536	0.75	16.25	0.03	10970	1.8253	0.279	23.2	10936.2	0.3	0.2894	4.5
20	0.6050	0.75	16.25	0.03	15530	2.3362	0.264	23.7	14248.7	8.3	0.2928	1.7
20	0.7524	0.75	16.25	0.03	21970	2.9116	0.245	24.0	17399.2	20.8	0.2955	9.3
15	0.4559	0.75	23.75	0.03	5165	1.0396	0.351	18.8	6175.4	19.6	0.2856	14.3
15	0.5977	0.75	23.75	0.03	7611	1.3752	0.319	18.8	7919.8	4.1	0.2888	8.5
15	0.7521	0.75	23.75	0.03	11680	1.7163	0.289	19.0	9775.6	16.3	0.2916	2.4
20	0.4676	0.75	23.75	0.03	5661	1.0684	0.286	31.3	7687.1	35.8	0.3252	0.8
20	0.6027	0.75	23.75	0.03	7685	1.3991	0.263	31.0	9705.3	26.3	0.3285	3.7
20	0.7551	0.75	23.75	0.03	10950	1.7259	0.253	30.2	11931.8	9.0	0.3317	12.5

Table B.2: High-mach number study results from Bray (1998) parametric study. [Bray (1998)]

Appendix C

Implementation of Empirical Models with Source Term

The derivation will start from the Navier Stokes equation. Upper and lower case letters refer to undisturbed flow and induced velocities from the VGs, respectively. The velocity field and pressure field are decomposed in mean and fluctuation parts: $U_i = \bar{U}_i + U'_i + u_i$ and $P_i = \bar{P}_i + P'_i + p_i$.

In x-direction (in 2D domain), the convective terms equal to:

$$U \frac{\partial U}{\partial x} + V \frac{\partial U}{\partial y} = \frac{\partial UU}{\partial x} + \frac{\partial UV}{\partial y} \quad (\text{C.1})$$

Performing the decomposition mention before and Reynolds averaging, the convective terms can be written in the following form:

$$\begin{aligned} \text{convective} = & \frac{\partial}{\partial x} (\bar{U}\bar{U} + 2\overline{\bar{U}u} + 2\overline{\bar{U}'u} + \overline{uu} + \overline{U'U'}) + \\ & \frac{\partial}{\partial y} (\bar{U}\bar{V} + \overline{\bar{V}u} + \overline{U'V'} + \overline{V'u} + \overline{\bar{U}v} + \overline{U'v} + \overline{uv}) \end{aligned} \quad (\text{C.2})$$

And the x component of RANS as:

$$\frac{\partial \bar{U}}{\partial t} + \frac{\partial \bar{u}}{\partial t} + \text{convective} = -\frac{1}{\rho} \left(\frac{\partial \bar{P}_x}{\partial x} + \frac{\partial \bar{p}_x}{\partial x} \right) + \nu \left(\frac{\partial^2 \bar{U}}{\partial x^2} + \frac{\partial^2 \bar{u}}{\partial x^2} + \frac{\partial^2 \bar{U}}{\partial y^2} + \frac{\partial^2 \bar{u}}{\partial y^2} \right) \quad (\text{C.3})$$

Furthermore knowing that the induced velocities are steady, the terms $\overline{U'_j u_i}$ and $\overline{U'_i u_j}$ drop out. After some mathematical manipulation, the RANS equation can be written as:

$$\begin{aligned} \frac{\partial \bar{U}_i}{\partial t} + \frac{\partial \bar{u}_i}{\partial t} + \bar{U}_j \left(\frac{\partial \bar{U}_i}{\partial x_j} + \frac{\partial \bar{u}_i}{\partial x_j} \right) + u_i \left(\frac{\partial \bar{U}_j}{\partial x_j} + \frac{\partial \bar{u}_j}{\partial x_j} \right) + u_j \left(\frac{\partial \bar{U}_i}{\partial x_j} + \frac{\partial \bar{u}_i}{\partial x_j} \right) \\ = -\frac{1}{\rho} \left(\frac{\partial \bar{P}_x}{\partial x_i} + \frac{\partial \bar{p}_x}{\partial x_i} \right) + \nu \left(\frac{\partial^2 \bar{U}_i}{\partial x^2} + \frac{\partial^2 \bar{u}_i}{\partial x^2} \right) - \frac{\partial \overline{u'_i u'_j}}{\partial x_j} \end{aligned} \quad (\text{C.4})$$

As consequence, the additional source term - with the time derivative and VG pressure gradient terms neglected - is:

$$W_i = \bar{U}_j \left(\frac{\partial \bar{u}_i}{\partial x_j} \right) + \bar{u}_i \left(\frac{\partial \bar{U}_j}{\partial x_j} + \frac{\partial \bar{u}_j}{\partial x_j} \right) + u_j \left(\frac{\partial \bar{U}_i}{\partial x_j} + \frac{\partial \bar{u}_i}{\partial x_j} \right) - \nu \left(\frac{\partial^2 \bar{u}_i}{\partial x^2} \right) \quad (\text{C.5})$$

Appendix D

Induced Velocities Code

```
1 //=====
2 // Name      : InducedVelocities_FlatPlate.cpp
3 // Author    : Ana Sofia Ribeiro
4 //=====
5 #include <iostream>
6 #include <fstream>
7 #include <cmath>
8 #include <cstdlib>
9 #include <stdio.h>
10 #include <vector>
11 using namespace std;
12
13 #define INPUT_VG "./Input/VGs_input.txt"
14 #define INPUT_FIELD "./Input/U_input.txt"
15 #define OUTPUT "./postProcess/Velocity_BC.txt"
16 #define XI 0.29
17
18 //////////// HEADER ////////////
19 int k, i;
20
21 int Get_nVG(){ //read number of VGs: n
22     fstream myfile(INPUT_VG, std::ios_base::in);
23
24     int n;
25     string dummy;
26     while (getline(myfile, dummy))
27         myfile >> n >> dummy >> dummy >> dummy >> dummy >> dummy;
28     myfile.clear();
29     myfile.seekg(0, ios::beg);
30
31     return n;}
32
33 class VGgeo{ //read geometry of VGs and flow condition for each VG
34 private:
35     string dummy;
36 public:
```

```

37     vector<double> c, h, a, U_inf, BL, d, y_v; // chord [m], height[m], AoA [
           deg], U_inf[m/s], BL thickness [m], h/BL ratio [m], vortex lateral
           position
38
39     VGgeo(int N2){
40         fstream myfile(INPUT_VG, std::ios_base::in);
41
42         c.resize(N2); h.resize(N2); a.resize(N2);
43         U_inf.resize(N2); BL.resize(N2); d.resize(N2); y_v.resize(N2);
44
45         while (std::getline(myfile, dummy)){
46             myfile >> dummy >> c[i] >> h[i] >> a[i] >> U_inf[i] >> BL[i] >>
           y_v[i] ;
47             d[i]=h[i]/BL[i];
48             cout<<d[i]<<endl;
49             i++;
50         }
51     }
52 };
53
54 struct Coordinates{ //read cell centres coordinates of plane yz
55     int nline;
56     vector<double> coordY, coordZ;
57
58     Coordinates(){
59         nline=ReadNLines();
60
61         coordY.resize(nline);
62         coordZ.resize(nline);
63
64         ReadCoordinates();
65     }
66
67     int ReadNLines(){ //read number of cells
68         string dummy, line;
69         int n=0;
70
71         fstream domain(INPUT_FIELD, std::ios_base::in);
72         while (getline(domain, line)){n++;}
73
74         domain.clear();
75         domain.seekg(0, ios::beg);
76
77         return n;}
78
79     void ReadCoordinates(){ //read cell centres coordinates coordY[m] and
           coordZ[m]
80         double dummy2;
81
82         fstream domain(INPUT_FIELD, std::ios_base::in);
83         for(i=0; i<nline; i++){
84             domain >> dummy2 >> coordY[i] >> coordZ[i] >> dummy2 >> dummy2 >>
           dummy2;
85         }
86     }
87 };
88

```

```

89 class Vortex{ // calculate induced velocities of each vortex in each cell
    centre
90 private:
91     int n; // number of cells
92     double alpha, AR; // [rad], [-]
93     double zN, yN_im, zN_im; // y and z vortex and imaged vortex location
94     vector<double> dy, dz, dz_im;
95     vector<double> R2, R2_im, F, F_im;
96
97 public:
98     double chord, height, AoA, U_freestream, delta, yN; // [m], [m], [deg], [m
        /s], h/BL_thickness, [m]
99     double gamma, omega; //[m /s], [s^-1]
100     vector<double> Y, Z, v, w;
101
102 Vortex(int n1){
103     n=n1;
104     Y.resize(n); Z.resize(n); dy.resize(n); dz.resize(n); dz_im.resize(n);
105     R2.resize(n); R2_im.resize(n); F.resize(n); F_im.resize(n);
106     v.resize(n); w.resize(n);
107 }
108
109 void DegToRad(){ alpha = 2*M_PI*AoA/360;} //transform AoA to radians
110
111 void SetAspectRatio(){ AR = 8*height/(M_PI*chord);} //calculate Aspect
    Ratio
112
113 void SetCirculation() { //calculate circulation gamma [m^2/s]
114     float k1, k2, k3, k4;
115     k1 = 1.61; k2 = 0.48; k3 = 1.41; k4=1.00;
116     gamma = (k1*U_freestream*alpha*chord)/(1+k2/AR)*tanh(k3*pow(delta,k4))
        ;
117 }
118
119 void SetMaxVort() { //calculate peak vorticity [1/s]
120     double beta = 1 / (2*XI*XI*pow(1-exp(-0.5),2)) ;
121     omega = (pow(gamma,3)*pow(beta-1,2)) / (2*pow(M_PI,3)*pow(alpha*chord*
        height*U_freestream,2));
122 }
123
124 void SetVortexCoordinates() {yN_im = yN; zN = height; zN_im = -zN;}
125
126 void SetRadius(){ // calculate R and F of vortex and imaged vortex
127     for (i=0; i<n; i++){ //number of cells
128         dy[i] = Y[i]-yN;
129         dz[i] = Z[i]-zN;
130         dz_im[i] = Z[i]-zN_im;
131
132         R2[i]= dy[i]*dy[i] + dz[i]*dz[i]; // == R^2
133         R2_im[i] = dz_im[i]*dz_im[i] + dy[i]*dy[i]; // ==R^2 of imaged
            vortices
134
135         if (R2[i]<0.001*height*height)
136         {
137             R2[i] = 0.001*height*height;
138         }
139

```

```

140         F[i] = 1 - exp(-M_PI*omega*R2[i]/gamma);
141         F_im[i] = 1 - exp(-M_PI*omega*R2_im[i]/gamma);
142     }
143 }
144
145 void VGvelocities(){ // calculate induced velocities in each cell v and w
146     [m/s]
147     for(i=0; i<n;i++){
148         v[i] = -gamma*dz[i]*F[i]/(2*M_PI*R2[i]) + gamma*dz_im[i]*F_im[i]
149             ]/(2*M_PI*R2_im[i]);
150         w[i] = gamma*dy[i]*F[i]/(2*M_PI*R2[i]) - gamma*dy_im[i]*F_im[i]/(2*
151             M_PI*R2_im[i]);
152     }
153 }
154 };
155
156 struct VelocityField{ // sum induced velocities of neighbour vortices
157     vector<double> v, w;
158
159     VelocityField(int n2){
160         v.resize(n2); w.resize(n2);
161         for (int i=0; i<n2; i++){
162             v[i]=0; w[i]=0;
163         }
164     }
165 };
166
167 //////////////////////////////////////////////////////////////////// MAIN ////////////////////////////////////////////////////////////////////
168 int main() {
169     /// Definition of variables ///
170     const int N = Get_nVG();
171     VGgeo VG(N);
172     Coordinates Mesh;
173     vector<Vortex>Array;
174     VelocityField Vel(Mesh.nline);
175
176     /// Address inputs of Array ///
177     for (k=0; k<N; k++)
178     {
179         Array.push_back(Vortex(Mesh.nline));
180     }
181
182     for(k=0;k<N;k++){
183         for(i=0; i<Mesh.nline; i++){
184             Array[k].Y[i]=Mesh.coordY[i];
185             Array[k].Z[i]=Mesh.coordZ[i];
186         }
187         Array[k].chord = VG.c[k];
188         Array[k].height = VG.h[k];
189         Array[k].AoA = VG.a[k];
190         Array[k].U_freestream = VG.U_inf[k];
191         Array[k].delta = VG.d[k];
192         Array[k].yN = VG.y_v[k];
193     }
194
195     /// Calculate velocities of each VG ///
196     for (k=0; k<N; k++){

```

```
194     Array[k].DegToRad();
195     Array[k].SetAspectRatio();
196     Array[k].SetCirculation();
197     Array[k].SetMaxVort();
198     Array[k].SetVortexCoordinates();
199     Array[k].SetRadius();
200     Array[k].VGvelocities();
201 }
202
203
204     /// Calculate velocity field ///
205     for(k=0; k<N; k++){
206         for(i=0; i < Mesh.nline; i++){
207             Vel.v[i] = Vel.v[i] + Array[k].v[i];
208             Vel.w[i] = Vel.w[i] + Array[k].w[i];
209         }
210     }
211
212     FILE * fileBC;
213     fileBC = fopen (OUTPUT,"w");
214     fprintf(fileBC, "%d \n( \n", Mesh.nline);
215     for(i=0; i < Mesh.nline; i++){fprintf(fileBC," (0 %f %f)\n", Vel.v[i],
216         Vel.w[i]);}
217     fprintf(fileBC, ")");
218     return 0;}
```

Appendix E

myFixedJump Boundary Condition Code

E.1 *myJumpCyclic* Main

```
1  /*
   -----*\
2  ===== |
3  \\      / F i e l d      | OpenFOAM: The Open Source CFD Toolbox
4  \\      / O p e r a t i o n |
5  \\      / A n d           | Copyright (C) 2011-2012 OpenFOAM Foundation
6  \\      / M a n i p u l a t i o n |
7  -----*/
8
9  #include "myJumpCyclicFvPatchField.H" // line updated
10
11 // * * * * * Constructors * * * * * //
12 template<class Type>
13 Foam::myJumpCyclicFvPatchField<Type>::myJumpCyclicFvPatchField // line updated
14 (
15     const fvPatch& p,
16     const DimensionedField<Type, volMesh>& iF
17 )
18 :
19     cyclicFvPatchField<Type>(p, iF)
20 {}
21
22 template<class Type>
23 Foam::myJumpCyclicFvPatchField<Type>::myJumpCyclicFvPatchField // line updated
24 (
25     const myJumpCyclicFvPatchField<Type>& ptf,
26     const fvPatch& p,
27     const DimensionedField<Type, volMesh>& iF,
28     const fvPatchFieldMapper& mapper
29 )
30 :
31     cyclicFvPatchField<Type>(ptf, p, iF, mapper)
```

```

32 {}
33
34 template<class Type>
35 Foam::myJumpCyclicFvPatchField<Type>::myJumpCyclicFvPatchField // line updated
36 (
37     const fvPatch& p,
38     const DimensionedField<Type, volMesh>& iF,
39     const dictionary& dict
40 )
41 :
42     cyclicFvPatchField<Type>(p, iF, dict)
43 {
44     // Call this evaluation in derived classes
45     //this->evaluate(Pstream::blocking);
46 }
47
48 template<class Type>
49 Foam::myJumpCyclicFvPatchField<Type>::myJumpCyclicFvPatchField // line updated
50 (
51     const myJumpCyclicFvPatchField<Type>& ptf // line updated
52 :
53     cyclicFvPatchField<Type>(ptf)
54 {}
55
56 template<class Type>
57 Foam::myJumpCyclicFvPatchField<Type>::myJumpCyclicFvPatchField // line updated
58 (
59     const myJumpCyclicFvPatchField<Type>& ptf, // line updated
60     const DimensionedField<Type, volMesh>& iF
61 )
62 :
63     cyclicFvPatchField<Type>(ptf, iF)
64 {}
65
66 // * * * * * Member Functions * * * * * //
67 template<class Type>
68 Foam::tmp<Foam::Field<Type> >
69 Foam::myJumpCyclicFvPatchField<Type>::patchNeighbourField() const // line
    updated
70 {
71     const Field<Type>& iField = this->internalField();
72     const labelUList& nbrFaceCells =
73         this->cyclicPatch().neighbFvPatch().faceCells();
74
75     tmp<Field<Type> > tpnf(new Field<Type>(this->size()));
76     Field<Type>& pnf = tpnf();
77
78     Field<Type> jf(this->jump());
79     if (!this->cyclicPatch().owner()) {jf *= -1.0;}
80
81     if (this->doTransform()) {
82         forAll(*this, facei){
83             pnf[facei] = transform
84                 (
85                     this->forwardT()[0], iField[nbrFaceCells[facei]]
86                 ) - jf[facei];
87         }

```

```

88     }
89     else{
90         forAll(*this, facei){
91             pnf[facei] = iField[nbrFaceCells[facei]] - jf[facei];
92         }
93     }
94     return tpnf;
95 }
96
97 template<class Type>
98 void Foam::myJumpCyclicFvPatchField<Type>::updateInterfaceMatrix // line
    updated
99 (
100     Field<Type>& result,
101     const Field<Type>& psiInternal,
102     const scalarField& coeffs,
103     const direction cmpt, // line added
104     const Pstream::commsTypes
105 ) const
106 {
107     Field<Type> pnf(this->size());
108
109     const labelUList& nbrFaceCells =
110         this->cyclicPatch().neighbFvPatch().faceCells();
111
112     // only apply jump to original field
113     if (&psiInternal == &this->internalField()){
114         Field<Type> jf(this->jump());
115
116         if (!this->cyclicPatch().owner()){jf *= -1.0;}
117
118         forAll(*this, facei){pnf[facei] = psiInternal[nbrFaceCells[facei]] -
            jf[facei];}
119     }
120     else{
121         forAll(*this, facei){pnf[facei] = psiInternal[nbrFaceCells[facei]];}
122     }
123     // Transform according to the transformation tensors
124     this->transformCoupleField(pnf);
125     // Multiply the field by coefficients and add into the result
126     const labelUList& faceCells = this->cyclicPatch().faceCells();
127     forAll(faceCells, elemI){result[faceCells[elemI]] -= coeffs[elemI]*pnf[
        elemI];}
128 }

```

E.2 *myFixedJump* Main

```

1  /*-----*\
2  ===== |
3  \ \      /  F i e l d      | OpenFOAM: The Open Source CFD Toolbox
4  \ \      /  O p e r a t i o n  |
5  \ \      /  A n d           | Copyright (C) 2011-2012 OpenFOAM Foundation
6  \ \      /  M a n i p u l a t i o n  |
7  \*-----*/
8
9  #include "myFixedJumpFvPatchField.H"

```

```

10
11 // * * * * * Constructors * * * * *
12 //
13 template<class Type>
14 Foam::myFixedJumpFvPatchField<Type>::myFixedJumpFvPatchField // line updated
15 (
16     const fvPatch& p,
17     const DimensionedField<Type, volMesh>& iF
18 )
19 :
20     myJumpCyclicFvPatchField<Type>(p, iF), // line updated
21     jump_(this->size(), pTraits<Type>::zero)
22 {}
23
24 template<class Type>
25 Foam::myFixedJumpFvPatchField<Type>::myFixedJumpFvPatchField // line updated
26 (
27     const myFixedJumpFvPatchField<Type>& ptf, // line updated
28     const fvPatch& p,
29     const DimensionedField<Type, volMesh>& iF,
30     const fvPatchFieldMapper& mapper
31 )
32 :
33     myJumpCyclicFvPatchField<Type>(ptf, p, iF, mapper), // line updated
34     jump_(ptf.jump_, mapper)
35 {}
36
37 template<class Type>
38 Foam::myFixedJumpFvPatchField<Type>::myFixedJumpFvPatchField // line updated
39 (
40     const fvPatch& p,
41     const DimensionedField<Type, volMesh>& iF,
42     const dictionary& dict
43 )
44 :
45     myJumpCyclicFvPatchField<Type>(p, iF), // line updated
46     jump_(p.size(), pTraits<Type>::zero)
47 {
48     if (this->cyclicPatch().owner()){jump_ = Field<Type>("jump", dict, p.size
49         ());}
50     if (dict.found("value")) {
51         fvPatchField<Type>::operator=
52         (
53             Field<Type>("value", dict, p.size())
54         );
55     }
56     else{ this->evaluate(Pstream::blocking); }
57 }
58
59 template<class Type>
60 Foam::myFixedJumpFvPatchField<Type>::myFixedJumpFvPatchField // line updated
61 (
62     const myFixedJumpFvPatchField<Type>& ptf // line updated
63 )
64 :

```

```

65     myJumpCyclicFvPatchField<Type>(ptf),
66     jump_(ptf.jump_)
67 {}
68
69 template<class Type>
70 Foam::myFixedJumpFvPatchField<Type>::myFixedJumpFvPatchField // line updated
71 (
72     const myFixedJumpFvPatchField<Type>& ptf, // line updated
73     const DimensionedField<Type, volMesh>& iF
74 )
75 :
76     myJumpCyclicFvPatchField<Type>(ptf, iF), // line updated
77     jump_(ptf.jump_)
78 {}
79
80 // * * * * * Member Functions * * * * *
81 //
82 template<class Type>
83 Foam::tmp<Foam::Field<Type> > Foam::myFixedJumpFvPatchField<Type>::jump()
84     const // line updated
85 {
86     if (this->cyclicPatch().owner()){ return jump_;}
87     else{
88         return refCast<const myFixedJumpFvPatchField<Type> > // line updated
89             (
90                 this->neighbourPatchField()
91             ).jump();
92     }
93 }
94 template<class Type>
95 void Foam::myFixedJumpFvPatchField<Type>::autoMap // line updated
96 (
97     const fvPatchFieldMapper& m
98 )
99 {
100     myJumpCyclicFvPatchField<Type>::autoMap(m); // line updated
101     jump_.autoMap(m);
102 }
103
104 template<class Type>
105 void Foam::myFixedJumpFvPatchField<Type>::rmap // line updated
106 (
107     const fvPatchField<Type>& ptf,
108     const labelList& addr
109 )
110 {
111     myJumpCyclicFvPatchField<Type>::rmap(ptf, addr); // line updated
112
113     const myFixedJumpFvPatchField<Type>& tiptf = // line updated
114         refCast<const myFixedJumpFvPatchField<Type> >(ptf);
115     jump_.rmap(tiptf.jump_, addr);
116 }
117
118 template<class Type>
119 void Foam::myFixedJumpFvPatchField<Type>::write(Ostream& os) const // line

```

```
    updated
120 {
121     fvPatchField<Type>::write(os);
122     os.writeKeyword("patchType") << this->interfaceFieldType()
123         << token::END_STATEMENT << nl;
124
125     if (this->cyclicPatch().owner())
126     {
127         jump_.writeEntry("jump", os);
128     }
129
130     this->writeEntry("value", os);
131 }
```